Sukkur IBA Journal of Emerging Technologies (SJET) is the bi-annual research journal published by **Sukkur IBA University**, Pakistan. **SJET** is dedicated to serve as a key resource to provide applied engineering research associated with the Electrical, Electronics and innovations in Energy at the global scale. This Journal publishes manuscripts which are well written by highlighting development in emerging technologies. This Journal covers all branches of Engineering, Science & Emerging Technologies.

Disclaimer: The research material expressed in **Sukkur IBA Journal of Emerging Technologies (SJET)** is sole contribution of the authors. The research contribution of the authors does not reflect the management, advisory board, the editorial board, **Sukkur IBA University** press and the organization to which the authors are affiliated. Manuscripts published in **SJET** shall be processed through double-blind peer-reviewed by the two experts of field. The identities of the experts/reviewers shall remain anonymous to the authors. The Journal shall be published two issues in a year. Neither the **Sukkur IBA University** nor the **SJET** shall be responsible for errors or any consequences highlighted by the reader. The errors and deficiencies in terms of research in manuscript can directly be reported to the authors.

Mission Statement

The mission of **Sukkur IBA Journal of Emerging Technologies (SJET)** is to provide a premier interdisciplinary platform to researchers, scientists and practitioners from the field of engineering in particular, electrical, electronics, renewable and emerging engineering fields for dissemination of their finding and to contribute in the knowledge domain.

Aims & Objectives

Sukkur IBA Journal of Emerging Technologies (SJET) will publish and encourage the submission of critically reviewed manuscripts on the cutting-edge research in the field of emerging engineering technologies.

The objectives of **SJET** are:

1. To bring new engineering ideas, research and findings on a single platform.
2. To integrate interdisciplinary research for technological sustainable solution.
3. To provide scholarly platform to connect academia and industries for socio-economic development.

Research Themes

The research focused on but not limited to following core thematic areas:

Renewable Energy Sources and Storage:

- Solar energy system fabrication and construction of advanced fuel cell technology
- Designing and analyzing smart hydro and wind energy systems
- Developing systems for biomass and bio-fuels
- Energy management and storage
- Energy devices and materials
- Energy harvesting for wireless and body sensor networks
- Energy efficiency and policies
- Energy devices and materials

Power Systems and Smart Grids:

- Power Quality Issues and solutions
- Micro grid systems and their Integration Problems

- Design control and management
- Energy management and Environmental issues
- Hybrid power system
- Distributed and co-generation systems
- Power market and power system economics

Electrical Machines and Adjustable Speed Drives:

- AC and DC machines and drives
- Sensor-less control
- Piezo and electrostatic actuators
- Machine design and equipment training
- Maintenance and fault diagnosis
- Bearing less driving technologies

Power Electronics and its Application:

- Hard-switching and soft-switching static converters
- Multi-level and matrix converters
- Emerging topologies
- Simulation and control power converters
- Power factor correctors
- Active filters and total harmonics distortions analysis
- Optoelectronics and photonic devices
- Power semiconductors, passive components, and packaging technologies
- Switch-mode power supplies and automotive
- Applications of power electronics in home appliance

High Voltage Engineering and Insulation Technology:

- Micro-electromechanical system (MEMS)
- Power Integrated circuits (PIC)
- Power Engineering related Technologies
- Power system stability and control
- Power system transient modeling, simulation and analysis
- Electromagnetic transient programs (EMTP)
- HVDC and FACTS applications

Nanomaterials/Nanotechnology:

- Sensors and Actuators
- Electronic Thin Films
- Nanogenerators
- Nanomaterials

- Nanotechnology optoelectronic sensors
- magnetic sensors
- thermal sensors
- mechanical sensors

Communication and Signal Processing:

- Communication & signal processing
- Radio frequency systems, microwave and antenna design
- Analog and mixed signal circuits
- Filter designing
- Satellite communication, mobile communication
- Cognitive and software design radio
- Analog and Mixed Signal Circuits

Biomedical Electronics:

- Energy-efficient wireless body sensor networks
- Wireless power/energy transfer in e-health applications
- Green and battery-friendly wireless medical networks
- Renewable energy and energy harvesting for wireless and body sensor networks
- Telemedicine and medical IoT
- Medical video transmission
- Energy management for medical health applications
- Role of 5G in medical health applications

Thermal and complex fluid dynamics:

- Active and passive techniques for fluid flow manipulation

- Fluid flow process for industrial equipment's
- Modeling of working fluids
- Experimental fluid dynamics
- Multifunctional heat exchangers/chemical reactors
- Energy efficient combustion
- Environmental fluid flows

Materials and their processing

- Piezoelectric materials
- Polymers, metal oxides
- III, V and II, VI semiconductors
- Thick and thin films
- Optical glass fibers
- Amorphous
- Polycrystalline monocrystalline silicon, nanomaterials
- Synthesis of nanomaterials, composite materials
- Functional material
- Electronic thin films and integrated devices
- Engineering materials
- Solid and structural mechanics

Patron's Message

Sukkur IBA University has been imparting education with its core values merit, quality and excellence since its inception. Sukkur IBA University has achieved numerous milestones in a very short span of time that hardly any other university has achieved in the history of Pakistan. The institute continuously being ranked as one of the best Institute in Pakistan by Higher Education Commission (HEC). The distinct service of Sukkur IBA University is to serve rural areas of Sindh and also underprivileged areas of other provinces of Pakistan. Sukkur IBA University is committed to serve targeted youth of Pakistan who is suffering from poverty and deprived of equal opportunity to seek quality education. Sukkur IBA University is successfully undertaking its mission and objectives that lead Pakistan towards socio-economic prosperity.

In continuation of endeavors to touch new horizon in the field of Engineering and Emerging Technologies, Sukkur IBA University publishes an international referred journal. Sukkur IBA University believes that research is an integral part of modern learnings ad development. **Sukkur IBA Journal of Emerging Technologies (SJET)** is the modest effort to contribute and promote the research environment within the university and Pakistan as a whole. SJET is a peer-reviewed and multidisciplinary research journal to publish findings and results of the latest and innovative research in the fields. Following the tradition of Sukkur IBA University, SJET is also aimed at achieving international recognition and high impact research publication in the near future.

Prof. Nisar Ahmed Siddiqui
Sitara-e-Imtiaz
Vice Chancellor
Sukkur IBA University
Patron **SJET**

Editorial

Dear Readers,

It is immense pleasure to present you the Third issue of Sukkur IBA Journal of Emerging Technologies (SJET). Sukkur IBA University firmly believes in research environment and has provided a platform for the intellectuals and researchers to share knowledge and new findings on emerging trends in various research areas to solve the difficult technical problems related to the technological advancements in response to the demands of the times. The SJET provided interdisciplinary platform to researchers' community to collaborate, co-innovate and instigate efforts to break the technological barriers. This journal provides the opportunity to gain and present authentic and insightful scientific & technological information on the latest advances in the field of emerging technologies.

The SJET provides invaluable source of information and enables the interested researchers to access the original information they are seeking. The manuscripts submitted in SJET have been followed by double-blind peer-review process, which addresses key issues in the field of emerging engineering technologies. The SJET has endorsed highly standards which are prerequisite for publishing high quality research work. This journal manifests into eco-system for the academician and engineers work together in the pursuit of excellence & innovation, that is why the editorial board of SJET is comprises of academic and industrial researchers from various advanced countries. The journal has been recognized by Higher Education Commission (HEC) Pakistan in "Y" category. It has adopted Open access policy without charging any publication fees that will certainly increase the readership by providing free access to a wider audience.

On behalf of the SJET, I welcome the submissions for upcoming issue (Volume-3, Issue-2, July–December, 2020) and looking forward to receive your valuable feedback.

I hope this journal will make a difference in our perspective and choice of research.

Sincerely,

Dr. Saeed Ahmed Khan
Chief Editor
SJET

Advisory Board

Contents

Experimental based Comparative Analysis and Characteristics of DC Series Motor by using Different Techniques

Mohsin Ali Koondhar[1], Ali Asif Malak[1], Masood Ali Koondhar[1], Irfan Ali Channa[2]

Abstract:

In this paper, distinct techniques of speed controlling of a Direct Current (DC) motor and its characteristics are discussed. The Direct Current (DC) motor has a wide range of speed control, which can be used in robots, drilling, cutting, and household applications due to affordable cost and low complexity of control configuration for speed and torque control. As DC Motors are considered as the best type of motors, in view of the speed control and speed regulation, numerous approaches are available to control the motor rotational speed. DC series motor control by using a resistive controller with and without a Programmable Logic Controller (PLC) is proposed. The motor voltage can be changed by inserting a resistor in series with DC motor. In this paper, through an experimental work armature resistive drive control technology and motor control PLC technology is used to control motor speed. PLC is used to control the resistance of the motor, thereby reducing driving voltage to change the speed. The results confirm the authentic efficiency of the proposed method of controlling motor speed.

Keywords: *DC Series Motor, PLC, Torque, Resistive controller.*

1. Introduction

The DC drives are used in rolling, wine winders, cranes, paper mills, machine tools, printing press, and textile mills, etc. DC motors have irregular essentials and used largely in uncertain speed. DC motor can produce immense origin torque and it is still achievable to gain speed control by the immense range [1]. DC Motors have variable characteristics and are used extensively in variable speed drives. DC motor can provide a high starting torque and it is also possible to obtain speed control over a wide range [2].

Generally, DC motor is used in several applications like robotics and domestic appliances due to affordable cost and low complexity of control configuration for speed and torque control [3]. DC Motors are considered as the best type of motors, in view of the speed control and speed regulation. Numerous approaches are available to control the motor rotational speed and armature voltage control is one method among these methods [4, 6].

The DC machine by a DC power source for determining the inductance in a DC machine disables some difficulties related to traditional methods using AC source [7, 8].

[1] Department of Electrical Engineering, Quaid-e-Awam University of Engineering, Science and Technology Nawabshah, Pakistan
[2] Department of Automation, Beijing University of Chemical Technology, Beijing China
Corresponding Author: engr.mohsinkoondhar@quest.edu.pk

DC machines are versatile energy conversion devices. These can be used for loads of high starting torques and to meet loads of high accelerating and decelerating torques [9]. For DC motors, the armature and field current are the same because the connection between them is standard [10, 11]. Armature voltage/armature control methods can be used to control the speed of dc motor [12, 13].

2. Conventional Controllers

Speed control of a motor escape intended to replace speed render to the demand of the workload connected with the motor. This preserve if done by mechanical expedients, such as by using stepped simple machines.

Nevertheless, speed control by the electrical way has greater advantages over mechanical. In many applications, DC motor is preferred over other types of motors because DC Motors offer easy speed control.

DC Motor Speed control methods depend upon,

a. Armature Control Method and
b. Armature Voltage Control Method [14].

2.1 Armature Control Method

It can apply during speeds where loading speed is not required. Supply voltage usually invariable, by place a flexible rheostat in series with armature circuit, the voltage across armature may change shown in figure1.

To decrease the armature speed potential difference beyond armature is dropped by increasing the value of resistance in the controller. For load-torque, speed is closely comparative to potential difference over the armature [15].

Armature resistance control is simple for small motors while it wastes energy and unusable with large motors [16].
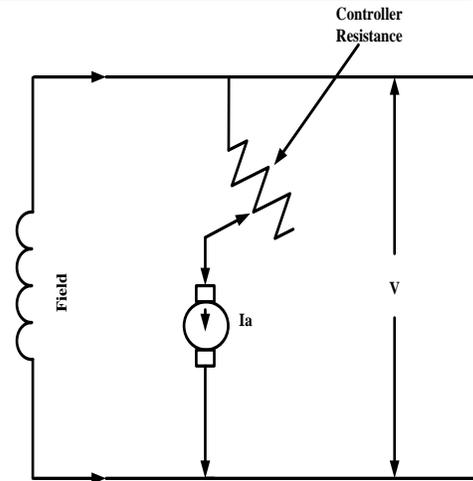
Fig 1: Armature Control Method

2.2 Armature Voltage Control Method

The speed of armature-controlled DC motor is controlled by armature voltage V_a and utilizes a constant field current shown in figure 2.
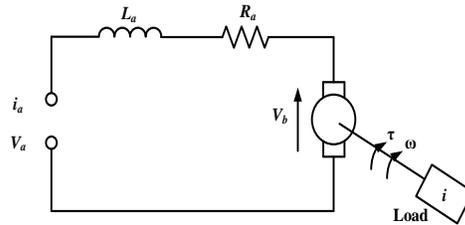
Fig 2: Armature Voltage Control Method

The armature controlled can be expressed by equations as:

$$I\omega = -b.\omega + K_t\, i_a T_L \qquad (1)$$

$$V_a - V_b = \text{La}\,\frac{dia}{dt} + R_a.i_a \qquad (2)$$

Where

$$V_b = K_b \cdot \omega$$

In the state-space form, the equation of DC Motor is:

$$\frac{d}{dt}\begin{bmatrix} \omega \\ i_a \end{bmatrix} = \begin{bmatrix} -\dfrac{b}{I} & \dfrac{K_t}{I} \\ -\dfrac{R_a}{L_a} & -\dfrac{K_b}{L_a} \end{bmatrix} \begin{Bmatrix} \omega \\ i_a \end{Bmatrix} + \begin{bmatrix} 0 \\ \dfrac{1}{L_a} \end{bmatrix} \cdot V_a + \begin{bmatrix} -\dfrac{1}{I} \\ 0 \end{bmatrix} \cdot T_L \quad (3)$$

3. Programmable Logic Controller

DC motors are one of the devices that can be connected and controlled by PLC [17]. The PLC-based control system is a microprocessor-based controller. In this, a memory specifically programmable memory is used to store the instructions and various functions. Presently Programmable Logic Controller is vastly used in industry [6]. The PLC is a functional computer employed in the machines where the control and operation of completion manner [18, 19]. It is the function of the programmable retention, accumulation guidance, and finishing including ON and OFF shown in figure 4.

Figure 3 shows the basic arrangement of PLC incorporated within the trainer. There are 20 I/O connectors, from which 10 for input and 10 for output, and a voltage stabilizer is used to maintain the required voltage.
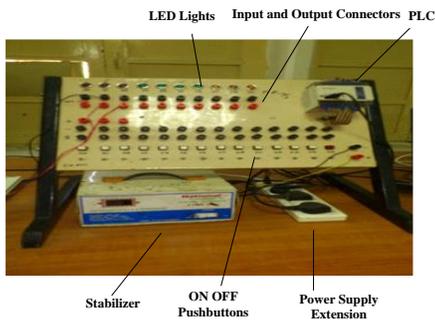
Fig 3: PLC

4. PLC Ladder Diagram

For ease of programming, the programmable controller is advanced by adopting existing relay ladder design and expressions to take as program logics, necessary to control the machine or process. A relay ladder diagram is shown in figure 6.
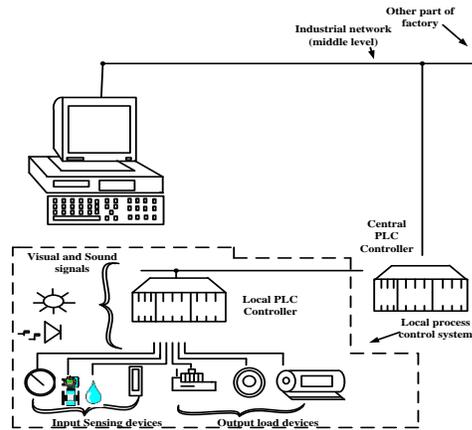
Fig 4: PLC Layout
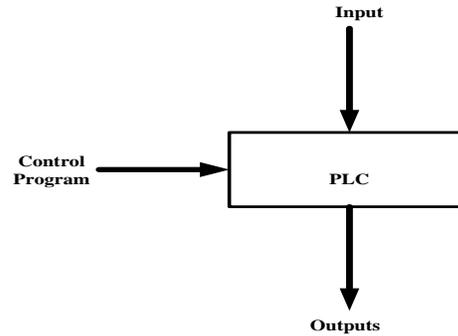
Fig 5: PLC as a Control Action
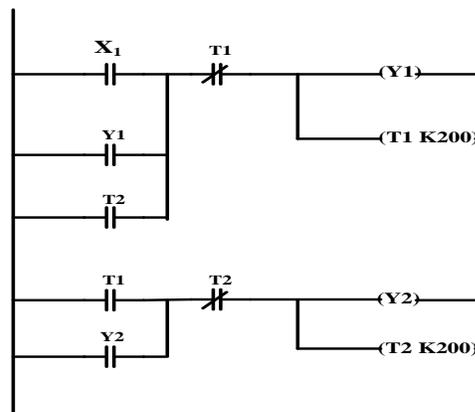
Fig 6: Ladder Diagram of a PLC

4.1 DC Motor Characteristics with Armature Controller

The characteristic of the motor means the determination relationship between speed, power, and current without load. Figure 7 shows the experimental setup of the dc series motor with the Armature controller.

Fig 7: Experimental setup of DC Series Motor with Armature Controller

4.1.1 Torque vs. speed characteristics of DC Motor with Armature Controller

The characteristic result of torque vs. speed of dc series motor is presented in Table 1 and graphically present shown in figure 8. In this table there are different levels of supply voltages are supplied and different torque are applied as a load from 0 Nm to 1 Nm in equal of 1 step respectively in order to observe the effectiveness of torque on the speed of DC Motor. It is clearly mentioned in the table that if the value of torque increased from 0.1 Nm to 1 Nm than the speed of DC Motor decreased

Figure 8 illustrates that as supply voltages raises from 30 to 50 voltages the speed of DC series motor is increased but as torque increases simultaneously the speed of dc series motor decreases.

Table 1: Toque Speed Characteristics with Armature Controller

Torque (N-M)	V=30 v	V=35 v	V=40 v	V=45 v	V=50 v
	Armature Controller				
	Speed (RPM)	Speed (RPM)	Speed (RPM)	Speed (RPM)	Speed (RPM)
0	1125	1440	1750	1980	2280
0.1	1065	1380	1690	1930	2265
0.2	1034	1336	1620	1890	2110
0.3	1000	1278	1555	1850	2080
0.4	968	1240	1510	1740	1960
0.5	924	1210	1470	1680	1910
0.6	886	1170	1400	1580	1703
0.7	868	1135	1340	1500	1680
0.8	852	1090	1290	1430	1660
0.9	809	1030	1280	1370	1600
1	770	1008	1222	1340	1530

Torque-Speed Characteristics of DC Series Motor
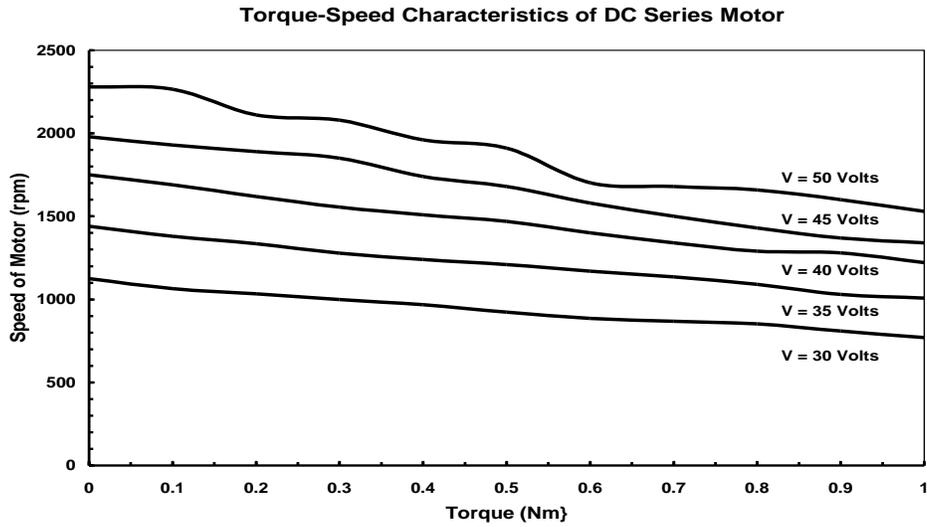
Fig 8: Torque vs. Speed characteristics of DC Series Motor

4.1.2 Torque vs. Current characteristics of DC Series Motor with Armature Controller

Result of torque and current characteristic of DC series motor presented in table 2 and graphically present in figure 9. In this table there are different levels of supply voltages are supplied and different torque are applied as a load from 0 Nm to 1 Nm in equal of 1 step respectively in order to observe the effectiveness torque on the speed of DC Motor. Clearly mention in the table that if the value of torque varies from 0.1 N-m to 1 N-m than the speed of DC Motor decreased.

Table 2: Torque Current characteristics DC Series Motor

Torque (N-M)	V=30V	V=35V	V=40V	V=45 V	V=50V
	Armature Controller				
	Current (A)	Current (A)	Current (A)	Current (A)	Current (A)
0	0.8	0.7	0.7	0.7	0.7
0.1	0.8	0.8	0.8	0.8	0.8
0.2	0.8	0.8	0.8	0.8	0.8
0.3	0.8	0.9	0.9	0.9	0.8
0.4	0.9	0.9	0.9	0.9	0.9
0.5	0.9	0.9	0.9	0.9	0.9
0.6	0.9	0.9	0.9	0.9	0.9
0.7	1	1	1	1	1
0.8	1	1	1	1	1
0.9	1	1	1	1	1
1	1	1	1	1	1

Torque-Current Characteristics of DC Series Motor
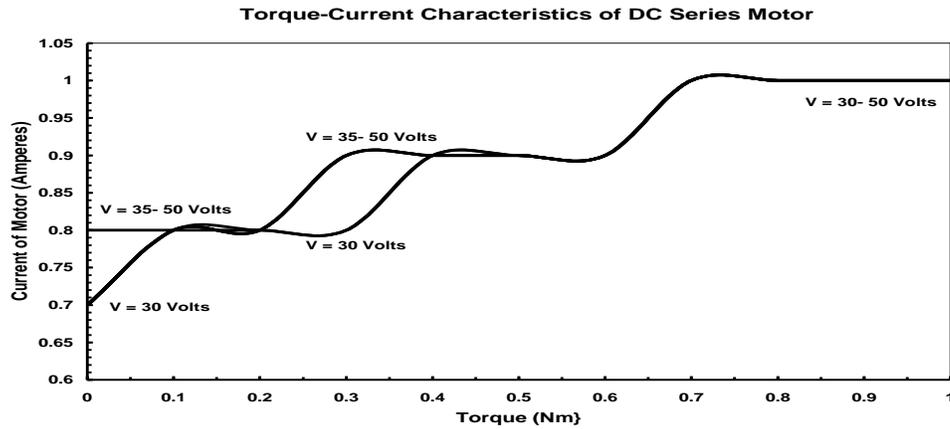
Fig 9: Torque vs. Current characteristics of DC Series Motor

4.1.3 Torque vs. Power characteristics of DC Series Motor with Armature Controller

The characteristic result of the torque and power of DC Series Motor is presented in table 3 and graphically present shown in figure 10. In this table there are different levels of supply voltages are supplied and different torque are applied as a load from 0 Nm to 1 Nm in equal of 1 step respectively to observe the effectiveness of torque on the speed of DC Motor. Here clearly mention in the table that if the value of torque increased from 0.1 Nm to 1 Nm than the speed of DC Motor decreased.

Table 3 Torque Power characteristics DC Series Motor

Torque (N-M)	V=30 V	V=35 V	V=40 V	V=45 V	V=50 V
	Armature Controller				
	Power (Watt)	Power (Watt)	Power (Watt)	Power (Watt)	Power (Watt)
0	24	24.5	28	31.5	35
0.1	24	28	32	36	40
0.2	24	28	32	36	40
0.3	24	31.5	36	40.5	40
0.4	27	31.5	36	40.5	45
0.5	27	31.5	36	40.5	45
0.6	27	31.5	36	40.5	45
0.7	30	35	40	45	50
0.8	30	35	40	45	50
0.9	30	35	40	45	50
1	30	35	40	45	50
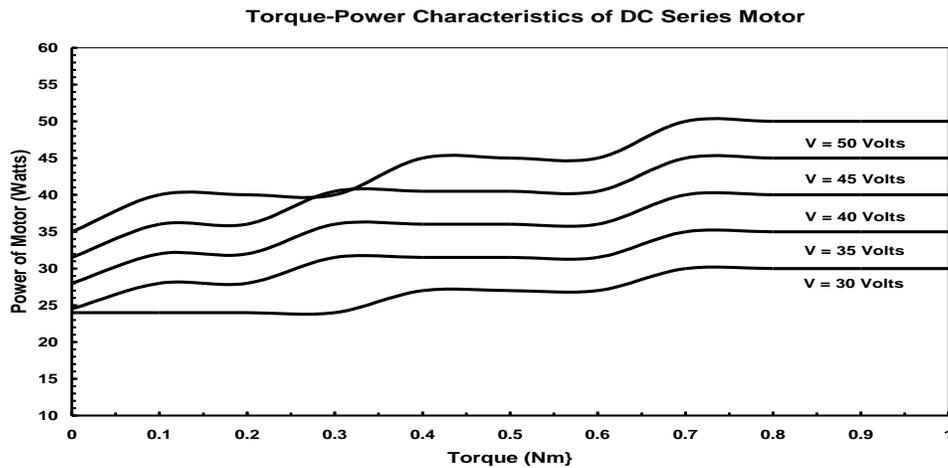
Fig 10: Torque Power characteristics of DC Series Motor

4.2 Experimental structure of DC Series Motor with PLC

`Experimental setup is illustrated in figure 11.
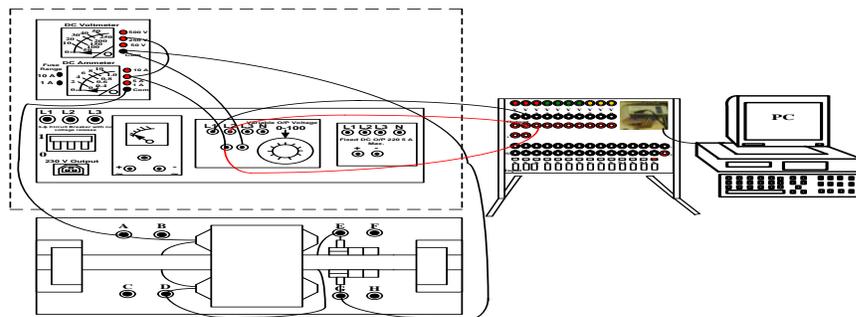
Fig 11: Experimental structure of DC Series Motor with PLC

4.2.1 DC Motor Torque vs. speed characteristics with PLC

The characteristic result of torque vs. speed of DC series motor is presented in Table 4 and graphically present shown in figure 12. In this table there are different levels of supply voltages are supplied and different torque are applied as a load from 0 Nm to 1 Nm in equal of 1 step respectively to observe the effectiveness of torque on the speed of DC Motor. It's clearly mentioned in the table that if the value of torque increased from 0.1 Nm to 1 Nm than the speed of dc motor decreased.

Table 4: DC Series Motor Torque vs. Speed characteristics with PLC

Torque (N-M)	V=30 v	V=35 v	V=40 v	V=45 v	V=50 v
	With PLC				
	Speed (RPM)	Speed (RPM)	Speed (RPM)	Speed (RPM)	Speed (RPM)
0	1000	1200	1530	1736	1940
0.1	982	1150	1520	1690	1700
0.2	950	1130	1480	1650	1680
0.3	880	1070	1320	1470	1590
0.4	870	1060	1300	1460	1580
0.5	850	978	1150	1290	1400
0.6	800	950	1140	1230	1380
0.7	670	900	1040	1200	1250
0.8	650	833	1000	1100	1230
0.9	630	820	935	1060	1220
1	594	800	900	980	1150
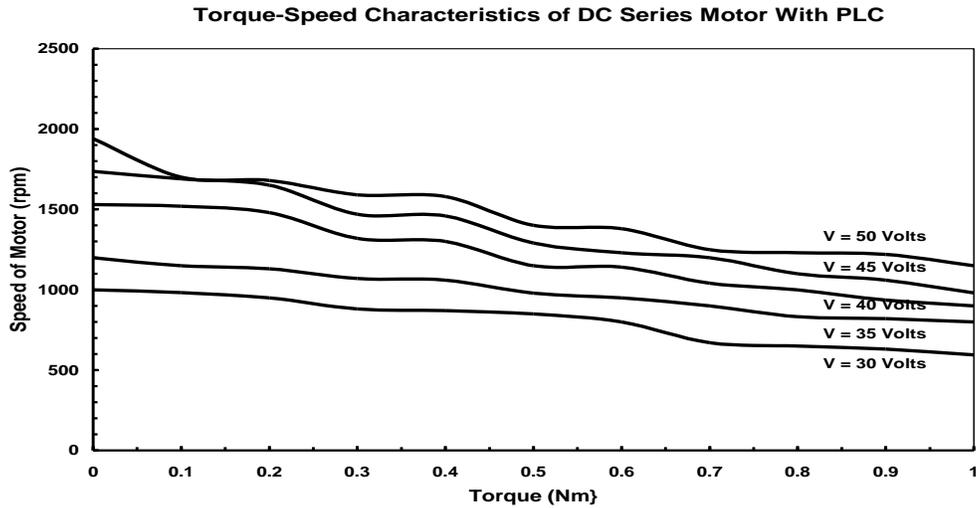
Fig 12: DC Series Motor Torque vs. Speed characteristics with PLC [5]

Torque vs. current characteristics of DC Series Motor with PLC

The characteristic result of torque and current of DC series motor is presented in table 5 and graphically present shown in figure 13. In this table there are different levels of supply voltages are supplied and different torque are applied as a load from 0 Nm to 1 Nm in equal of 1 step respectively to observe the effectiveness of torque on the speed of DC Motor. It is clearly mentioned in the table that if the value of torque varies from 0.1 Nm to 1 Nm than the speed of DC motor decreased.

Table 5: DC Series Motor Torque Current characteristics with PLC

Torque (N -M)	V =30 v	V =35 v	V =40 v	V =45 v	V =50 v
			With PLC		
	Current (A)	Current (A)	Current (A)	Current (A)	Current (A)
0	0.8	0.8	0.8	0.9	0.9
0.1	0.9	0.9	0.9	0.9	0.9
0.2	0.9	0.9	0.9	0.9	0.9
0.3	0.9	0.9	0.9	0.9	0.9
0.4	0.9	0.9	0.9	0.9	0.9
0.5	1	1	1.1	1.1	1.1
0.6	1.2	1	1.1	1.1	1.1
0.7	1.2	1.2	1.2	1.2	1.2
0.8	1.2	1.2	1.2	1.2	1.3
0.9	1.2	1.2	1.2	1.2	1.3
1	1.3	1.3	1.3	1.3	1.3
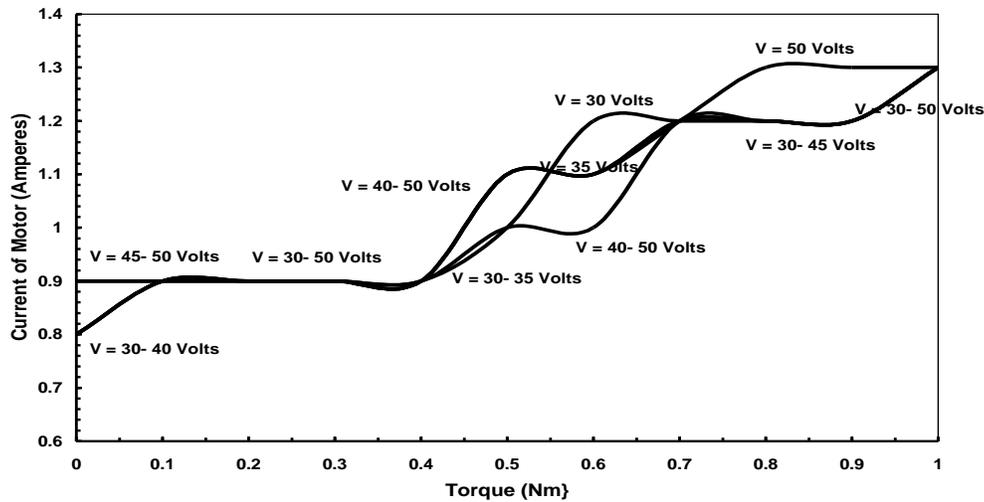
Fig 13: DC series Motor Torque vs. Current characteristics of with PLC

4.2.2 DC Series Motor Torque power characteristics with PLC

Characteristic result of torque power of DC series motor presented in table 6 and graphically present in figure 14. In this table respectively to observe the effectiveness of torque on the speed of DC Motor. It is clearly mentioned in the table that if the value of torque increased from 0.1 Nm to 1 Nm than the speed of DC motor decreased

Table 6 Torque Power characteristics DC Series Motor with PLC

Torque (N-M)	V=30V	V=35V	V=40 V	V=45 V	V=50 V
	With PLC				
	Power (Watt)	Power (Watt)	Power (Watt)	Power (Watt)	Power (Watt)
0	24	28	32	40.5	45
0.1	27	31.5	36	40.5	45
0.2	27	31.5	36	40.5	45
0.3	27	31.5	36	40.5	45
0.4	27	31.5	36	40.5	45
0.5	30	35	44	49.5	55
0.6	36	35	44	49.5	55
0.7	36	42	48	54	60
0.8	36	42	48	54	65
0.9	36	42	48	54	65
1	39	45.5	52	58.5	65
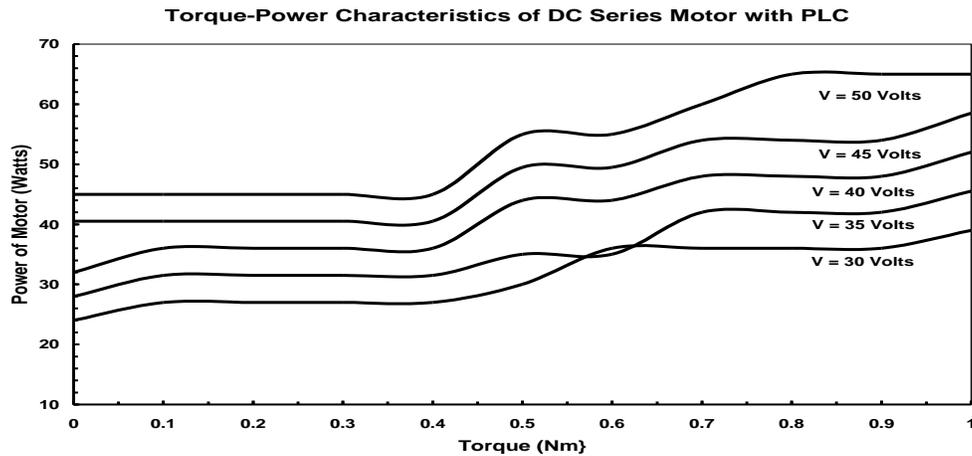
Fig14: DC Series Motor Torque vs. Power characteristics with PLC

Table 7 Comparison of Torque Speed characteristics DC Series Motor PLC with Armature Controller

Torque (N.m)	Speed (rpm)									
	V = 30v		V = 35v		V = 40v		V = 45v		V = 50v	
	Without PLC	With PLC	Without PLC	With PLC	Without PLC	With PLC	Without PLC	With PLC	Without PLC	With PLC
0	1125	1000	1440	1200	1750	1530	1980	1736	2280	1940
0.1	1065	982	1380	1150	1690	1520	1930	1690	2265	1700
0.2	1034	950	1336	1130	1620	1480	1890	1650	2110	1680
0.3	1000	880	1278	1070	1555	1320	1850	1470	2080	1590
0.4	968	870	1240	1060	1510	1300	1740	1460	1960	1580
0.5	924	850	1210	978	1470	1150	1680	1290	1910	1400
0.6	886	800	1170	950	1400	1140	1580	1230	1703	1380
0.7	868	670	1135	900	1340	1040	1500	1200	1680	1250
0.8	852	650	1090	833	1290	1000	1430	1100	1660	1230
0.9	809	630	1030	820	1280	935	1370	1060	1600	1220
1	770	594	1008	800	1222	900	1340	980	1530	1150

4.3 Characteristics comparison of DC Series Motor with PLC and Armature Controller

A comparison between PLC and armature controller here is presented.

4.3.1 Comparison Torque vs. speed characteristics of DC Series Motor with PLC and Armature Controller

A comparison between torque and speed are shown in table 7 and graphically represented in figure 15.
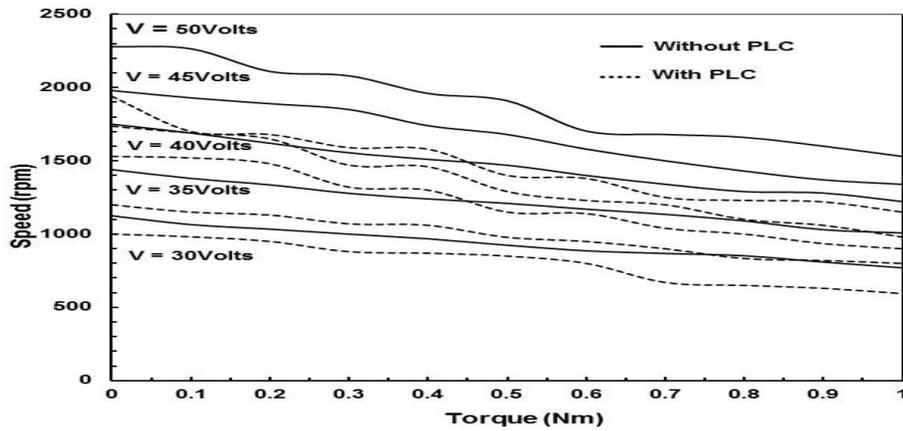
Fig 15: Graphically representation of Torque and Speed of DC Series motor with PLC and Armature controller [5].

4.3.2 Characteristics Comparison of Torque vs. current of DC Series Motor with PLC and Armature Controller

Comparison between torque and current are shown in table 8 and graphically represented in figure 16.

Table 8 Comparison of Torque Current characteristics DC Series Motor PLC with Armature Controller

Torque (NM)	Current (Ampere)									
	V =30v		V =35v		V =40v		V =45v		V =50v	
	Without PLC	With PLC	Without PLC	With PLC	Without PLC	With PLC	Without PLC	With PLC	Without PLC	With PLC
0	0.8	0.8	0.7	0.8	0.7	0.8	0.7	0.9	0.7	0.9
0.1	0.8	0.9	0.8	0.9	0.8	0.9	0.8	0.9	0.8	0.9
0.2	0.8	0.9	0.8	0.9	0.8	0.9	0.8	0.9	0.8	0.9
0.3	0.8	0.9	0.9	0.9	0.9	0.9	0.9	0.9	0.8	0.9
0.4	0.9	0.9	0.9	0.9	0.9	0.9	0.9	0.9	0.9	0.9
0.5	0.9	1	0.9	1	0.9	1.1	0.9	1.1	0.9	1.1
0.6	0.9	1.2	0.9	1	0.9	1.1	0.9	1.1	0.9	1.1
0.7	1	1.2	1	1.2	1	1.2	1	1.2	1	1.2
0.8	1	1.2	1	1.2	1	1.2	1	1.2	1	1.3
0.9	1	1.2	1	1.2	1	1.2	1	1.2	1	1.3
1	1	1.3	1	1.3	1	1.3	1	1.3	1	1.3
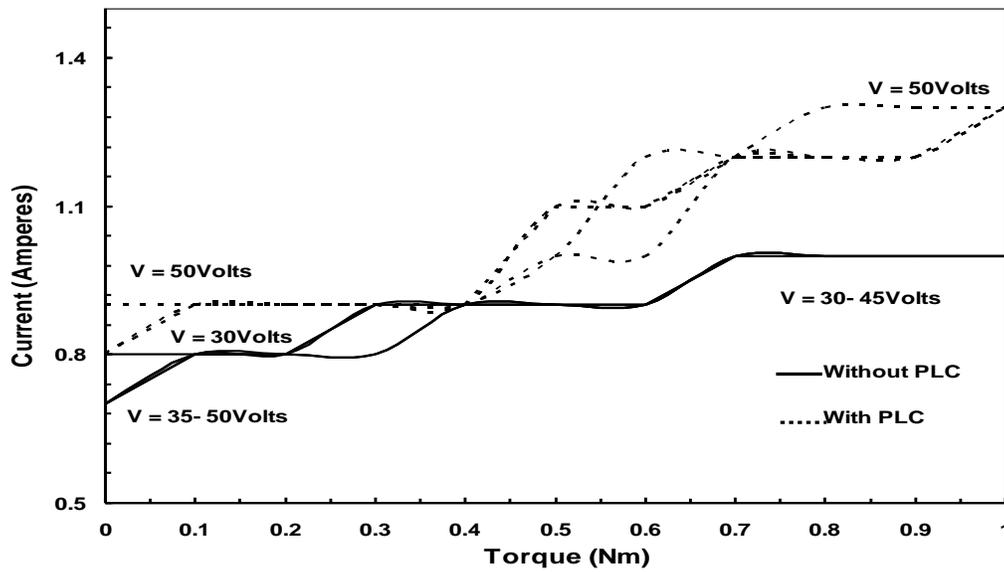
Fig 16: Graphically representation of Torque and Current of DC Series motor with PLC and Armature controller

4.3.3 Comparison Torque power characteristics of DC Series Motor with PLC and Armature Controller

Comparison between torque and current are shown in table 9 and graphically represented in figure 17.

Table 9 Comparison of Torque Power characteristics DC Series Motor PLC with Armature Controller

Torque (N- M)	Power									
	V =30v		V =35v		V =40v		V =45v		V =50v	
	Without PLC	With PLC	Without PLC	With PLC	Without PLC	With PLC	Without PLC	With PLC	Without PLC	With PLC
0	24	24	24.5	28	28	32	31.5	40.5	35	45
0.1	24	27	28	31.5	32	36	36	40.5	40	45
0.2	24	27	28	31.5	32	36	36	40.5	40	45
0.3	24	27	31.5	31.5	36	36	40.5	40.5	40	45
0.4	27	27	31.5	31.5	36	36	40.5	40.5	45	45
0.5	27	30	31.5	35	36	44	40.5	49.5	45	55
0.6	27	36	31.5	35	36	44	40.5	49.5	45	55
0.7	30	36	35	42	40	48	45	54	50	60
0.8	30	36	35	42	40	48	45	54	50	65
0.9	30	36	35	42	40	48	45	54	50	65
1	30	39	35	45.5	40	52	45	58.5	50	65
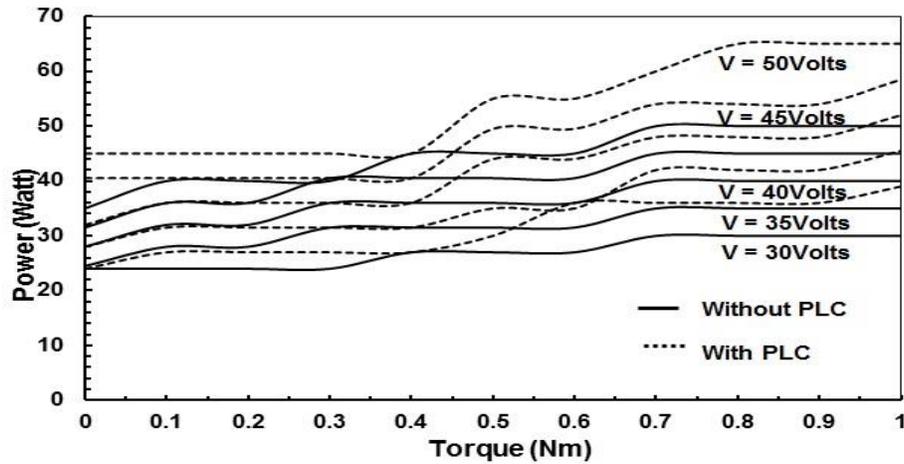
Fig 17: Graphically representation of Torque and Power of DC Series motor with PLC and Armature controller.

Figure 17 represents the relationship between power with respect to torque with and without PLC. At different voltages from 30 to 50 V as torque gradually increases from 0 NM to 1 NM power is increased.

5 Conclusion and Future Work

In this paper, the characteristics results of DC Series Motor have been obtained by using different controller techniques such as PLC and Armature controllers. In the above results and discussion, it can be easily understood that the best results are obtained by using PLC as compare to the armature controller.

By this research work, speed and torque of DC Motor can be controlled for laboratories and industrial applications.

This work can be further enhanced in the future in the following ways.
- It can be applied in industry.
- It is also used in an educational institute.
- An adaptive controller can be used for Motor control.
- Combined controlling techniques with PLC can be used to observe torque vs. speed characteristics.
- Matlab based Motor can be simulated for power drives and medical appliances.

References

[1] P. Malviya and M. Dubey, 2015, "Speed control of DC Motor a Review", International Journal of Engineering Sciences and Research Technology, 4(8), pages 298-305.

[2] N. Tripathi, R. Singh and R. yadav, **2015**, "Analysis of Speed Control of DC Motor –A review study", International Research Journal of Engineering and Technology, 2(8).

[3] S. B. Kumar, M. H. Ali and A. Sinha, **2014**, "Design and Simulation of Speed Control of DC Motor by Artificial Neural Network Technique", International Journal of Scientific and Research Publications, 4(7).

[4] M. A. Koondhar, A. K. Junejo, A. S. Saand, and M. U. Keerio, **2016**, "Speed Control of DC Series Motor with Conventional and PLC Techniques", International Journal of Information Technology and Electrical Engineering, 4(5) , pages 21-26.

[5] Koondhar, M.A, "Speed and Torque control of DC Series Motor by using PLC", Master Thesis, **2016**.

[6] V. Naveen and T. B. Isha, **2017** " A low cost speed estimation technique for closed loop control of BLDC motor drive", IEEE International Conference on Circuit, Power and Computing Technologies (ICCPCT), April 2017, pages 1-5.

[7] S. S. Keream, K.G. Mohammed and M.S. Ibrahim, **2018**, "Analysis Study In Principles of Operation of DC Machine", Journal of Advance Research in Dynamical and Control Systems, 10(2), pages 2323-2329.

[8] N. Chuang, T. J. Gale, and R. A. Langman, **2016**, "Developing measuring inductance strategies on a direct current machine using a DC source with magnetic saturation", International Journal of Circuit Theory and Applications, 44, pages 1094-1111.

[9] D. Rajesh and D. Ravikumar, S.K.Bharadwaj and B. K. S. Vastav, **2016**, "Design and Control of Digital DC Drives in Steel Rolling Mills", IEEE International Conference on Inventive Computing Technologies, 3, pages 1-5.

[10] H. T. H. Thabet and M. A. Oasim, **2016**, "Measurement of a DC Series Motor Torque Based on PLC Techniques" Kufa Journal of Engineering, 7(1), pages 93-103.

[11] N. K. Nambisan and B. N. Sarkar, **2014**, "Study of speed control of DC series motor using DC chopper", International Journal of Advanced Research in Electrical, Electronics and Instrumentation Engineering, 3(8), pages 11116-11123.

[12] A. Mohammad and S. B. Billah, **2015**, "Analysis of speed control of series DC motor using diverter and observation of speed saturation point", International Conference on Electrical Engineering and Information Communication Technology, May 2015, pages 1-4.

[13] Mehta, V. K., and Mehta, R. (**2008**). Principle of electrical Machines. S. Chand.

[14] R. Rudra and R. Banerjee, **2017**, " Modeling and Simulation of DC Motor Speed Regulation by Field Current Control Using MATLAB", International Journal of Computer Electrical Engineering, 2(9), pages 502-512.

[15] B. L. Theraja and A. K. Theraja, **2017**, Textbook of Electrical Technology Volume I, In SI System of Units. S. Chand, **2017**.

[16] H. F. Frayyeh, M. A. Mukhlif, A.M. Abbood and S. S. Keream, **2019**, "Speed control of direct current motor using Mechanical Characteristics", Journal of Southwest Jiaotong University, 54(4).

[17] M.S. Saleh, K. G. Mohammed, Z.S. Al-Sagar and A. Z. Sameen, **2018**, "Design and Implementation of PLC-Based Monitoring and Sequence Controller System", Journal of Advance Research in Dynamical and Control Systems, 10(2), pages 2281-2289.

[18] J. R. Monfared, M. Fazeli and Y. Lotfi, **2015**, "Design and PLC implementation for speed control of DC Motor using Fuzzy Logic", Journal of Electrical andComputer Engineering Innovations, 3(2), pages 71-75.

[19] L. Guo P. Pecen, 2008, "Design projects in a programmable logic controller (PLC) course in electrical engineering technology", In American Society for Engineering Education, 1(10), pages 1-10.

[20] K. Venkateswarlu and C. Chengaiah, **2014**, "Comparative study on DC motor speed control using various controllers", Global Journal of Research In Engineering.

[21] S. Sharma, S. S. Oberoi and S. Nair, **2014**, "Speed Control Method OF DC series motor", International Journal of Innovative Research in Technology, 1(6), pages 1450-1453.

Facile synthesis and characterization of mesoporous titanium oxide nanoparticles for ethanol sensing properties

Altaf Hussain Shar[1], Muhammad Nazim Lakhan[1], Jingyuan Liu[1], Mukhtiar Ahmed[1], Muhammad Basit Chandio[2], Ahmer Hussain Shah[3], Abdul Hanan[1], Irfan Ali[4], Jun Wang[1]

Abstract:

Mesoporous TiO_2 nanoparticles were successfully synthesized via solvothermal. The morphology and crystal structure was characterized by UV–vis spectrum (UV-Vis), Fourier Transform Infrared (FTIR) spectroscopy, X-ray diffraction (XRD), Scanning electron microscopy (SEM) and transmission electron microscopy (TEM).   All the observations confirmed that the as-fabricated mesoporous TiO_2 nanoparticles were successfully synthesized with surface Plasmon resonance peak between a range of 250-350 nm and its pattern meets with the JCPDS Standard (card No. 21-1272). TEM confirmed the mesoporous structure morphology and shows the incredible gas sensing performance due to their large accessible surface area. Furthermore, the as-prepared TiO_2 nanoparticles exhibited more rapid response/recovery and higher sensitivity towards ethanol at 180°C distinguished with isopropyl alcohol and methanol. In addition, it can be affirmed that the synthesized mesoporous TiO_2 nanoparticles are a promising applicant for fabricating high-performance ethanol gas sensor in real-time monitoring.

Keywords*: Gas sensor; mesoporous; nanotechnology; TiO_2; ethanol sensing.*

1. Introduction

Currently, atmospheric environmental protection is considered as a concerning issue because of the emission of harmful gas molecules and due to the rapid development in modern industries. To mitigate this, the detection of toxic gases is extremely essential for the excellence of the environment and human health [1]. Vapor sensors based on ethanol are widely usable sensors owing to their unique properties in chemical and biomedical industries and also for the analysis of breath [2]. High sensitivity, minimum

[1]Key Laboratory of Superlight Material and Surface Technology, Ministry of Education, Harbin Engineering University, PR People's Republic of China.

[2]College of Mechanical and Electrical Engineering, Harbin Engineering University, People's Republic of China

[3]Department of Textile Engineering, Balochistan University of Information Technology, Engineering and Management Sciences, Quetta, Pakistan

[4]College of Chemical Engineering, Beijing University of Chemical Technology, People's Republic of China

Corresponding Author: altafshar12@gmail.com

operating temperature, and less recovery time with short responses are ideal features in ethanol vapor (EV) sensors. Therefore, EV sensors and their functional materials research attracted huge attention by scientists for the development of high-performance EV sensors.

Nowadays, many sensing mechanisms and technologies have been employed for volatile organic compounds (VOCs) detection including thermal conductivity, catalyst, electrochemical, chemi-resistors types, mechanical and optical [3]. Among them, chemi-resistors based sensors are mostly preferable and economical devices with the existence of transuding platforms and acceptor materials and are broadly accepted because of their high potential application and long-term stability [4].

The gas sensing material is considered an important parameter for the selection of gas sensors. Among many, metal oxide semiconductors (MOSs) nanomaterials have attained some significant attention and considered promising material due to advantages such as; easy fabrication, fast response and recovery time, low operating cost, minimum power consumption, and minimum size with excellent chemical stability [5]. Mesoporous semiconducting metal oxides have been extensively used as the chemi-resistive based gas sensors due to their outstanding properties such as high surface area, large pores volume, high interconnection, long-term stability, high electron conductivity and enhanced sensing performance [6]. Among other metal oxides, Titanium dioxide (TiO_2) with wide-bandgap (3.4 eV) MOSs are considered as promising material Because of its distinctive properties includes chemical stability, excellent sensor performance, low cost, high activity, non-toxicity and abundance [7], and is used in various applications including batteries [8], photocatalysis, water splitting, solar cells, gas sensors, and biological application [9]. TiO_2

attracts much attention in the field of gas sensors [10]. In comparison with some common MOSs gas sensors operated on high temperatures, TiO_2 is favorable owing to higher sensitivity, fast response, long-term stability, and easily detectable gas at low temperatures. Various structures of TiO_2 used for ethanol detection have been reported, such as nanoparticles and nanoflowers [11, 12]. However, pristine TiO_2 is not widely investigated due to they are some drawbacks including low sensitivity, slow response-recovery time and limited specific area [13]. To solve these problems, many researchers committed to enhance the performance of TiO_2 based sensors to modify morphology of TiO_2 surface and nanostructure, as they are key factors that influence gas sensing performance [14]. Particularly, mesoporous TiO_2 nanostructures have a large specific surface area which provides numerous active sites facilitating more oxygen to be adsorbed at the surface and it also allows gas molecules to easily penetrate and adsorb on the surface of sensing materials for the improvement of response recovery time and detection limit [15]. Much research has still to be made for the development of mesoporous sensing materials having properties such as high sensitivity, minimum operating temperature, short response with less recovery time, easy fabrication and environmental flexibility.

Herein, a novel ethanol vapor based sensor on mesoporous TiO_2 nanoparticles has been successfully synthesized via solvothermal methods. The as-fabricated mesoporous TiO_2 material microstructure properties were characterized by FTIR, UV-Vis, XRD, SEM and TEM. Furthermore, Gas sensing properties such as operating temperature, response to concentration, selectivity, response and recovery time were evaluated.

2. Materials and method

2.1. Synthesis mesoporous TiO2 nanoparticles:

All the chemicals we used in this experiment are of analytical grade and used directly without any further purification prior to usage. Mesoporous TiO_2 nanoparticles are prepared by an environmentally friendly and one-step Solvothermal route. In a typical process, first 20 ml of deionized water (DW) and 40ml isopropyl alcohol were mixed together using magnetic stirrer until a homogeneous solution formed. Then, 6.0 g of titanium sulfate (Ti $(SO_4)2$) was added under strong stirring till a uniform solution achieved. Afterward, the aqueous solution was transferred into 100 ml Teflon-lined stainless steel autoclave and heated at 90˚C for 12 h. Later, as-prepared TiO_2 were centrifuged, rinsed and overnight dried at 90˚C. Finally, the dried powder was calcined in tube furnace at 300°C for 2 h in atmospheric air at a rate of 5 °C/min.

2.2. Characterization

UV-Vis absorption spectra were calculated by using a TU-1901 dual-beam UV-Vis spectrophotometer. The FTIR spectrum of mesoporous nanoparticles was collected on KBr plates cast using a Perkin Elmer Spectrum 100 FTIR spectrometer. The crystal structure was investigated by XRD system with Cu K1 radiation (= 0.15406 nm). The surface morphology of catalyst was observed with SEM (JOEL JSM − 6480A) operated at a 20kv of driving voltage while TEM images were acquired by using an FEI TECNNI G2 instrument. The gas sensing measurements were tested by a commercial NMDOG multi-functional accuracy sensor analysis tester (manufactured in Changsha city, China) at room temperature.

2.3. Fabrication and measurement of the sensor

In a typical process, the as-prepared sensing material was fully grinded by adding a small amount of ethanol to form slurry, and then pasted it onto the ceramic tube and then heated at 60°C for 2 h to evaporate the ethanol and kept in air for one day to improve the stability of the sensing materials layer. The operating temperature was controlled by providing the heating current through the Ni-Cr, resistor heating wire inserted into the ceramic tube. Sensing properties of the gas sensor were measured by a commercial NMDOG Multifunctional Precision Sensor Analysis Instrument (Changsha Dingchen Scientific Instrument Co, Ltd, Hunan, China). For measurement, the saturated target vapor in corresponding amounts was injected into a closed 10 L chamber by a micro-syringe to obtain the different concentrations of analytes. After fully mixed with atmospheric air, the sensor was put into the chamber to measure its performance. When the response on the display reached constant value, the sensor was taken out to atmospheric air. The response of the sensor is defined as the S=Rg/Ra, where Rg is the resistance of the sensor in target gas and Ra is the resistance of the sensor in air.

The response/ recovery time is defined as time spent by the sensor to achieve 90% of the total resistance change.

3. Results and Discussion

3.1. UV-Visible spectrum

The UV-Vis absorption spectrum of mesoporous TiO_2 nanoparticles is shown in Fig. 1. UV-Vis spectrum of TiO_2 sharp edge 250-350 nm showing mesoporous TiO_2 nanoparticles absorbs light from the ultraviolet region at room temperature displaying a good absorption band in the UV region [16].
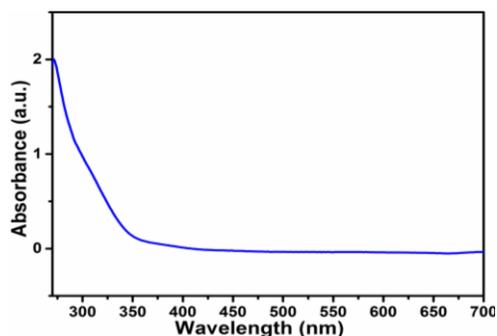
Fig 1. The UV-Visible spectrum of mesoporous titanium dioxide nanoparticles.

3.2. FTIR analysis

FTIR spectroscopy was used to characterize the proper surface functional groups responsible for the synthesis of mesoporous TiO_2 nanoparticles as shown in Fig. 2. The intensive absorption peaks were characterized by a number of characteristic bands occurring at 3744 cm^{-1}, 3648 cm^{-1}, 2917 cm^{-1}, 2853 cm^{-1}, 1741 cm^{-1}, 1585 cm^{-1}, 1376 cm^{-1} and 1118 cm^{-1}. The characteristic peaks were noticed between 3700 cm^{-1} and 3500 cm^{-1} were related to TiO_2 product as well as small intensity peak at 1650 cm^{-1} was showing stretching and bending vibrations of hydroxyl groups on the surface of TiO_2 nanoparticles. Additionally, another absorption peaks situated at 2917 and 2853 cm^{-1} were assigned to the asymmetric and symmetric stretch vibrations of CH_2 groups, 1740 cm^{-1} represents the stretching of C=O aldehydes group, 1586 cm^{-1} (C-C) stretches in the aromatic ring, 1420 cm^{-1} (CH groups) and 1118 cm^{-1} (C=O stretching vibrations). The obtained peaks in spectra confirm the formation of final TiO_2 products [17].

3.3. XRD analysis

XRD pattern confirms the composition and crystal structure of as-synthesized TiO_2 nanoparticles. Materials were characterized in a range of 10-90. Fig. 3 depicted the XRD patterns of the obtained anatase TiO_2 sample. All the diffraction peaks located at 2θ = 25.2, 37.8, 48.0, 53.9, 55.0, 62.7, 68.7, 70.3 and 75.0 could be indexed to (101), (004), (200),

(105), (211), (204), (116), (220) and (215) planes of anatase$TiO2$, respectively. The peaks of the anatase TiO_2 phase are of (JCPDS card No. 21-1272) standard. No characteristic peaks of impurity phases were observed in the XRD pattern and sharp diffraction peaks indicated good crystallinity. The grain size of mesoporous TiO_2 nanoparticles was calculated using the Scherrer formula [18].

$$D= (k\lambda / (\beta cos\theta)$$

Where D is average crystallite size, λ is the wavelength of Cu Kα (0.154 nm), k is a shape factor which is 0.9, β is measured from the full width at half maximum (FWHM) in radian and θ is Bragg angle it is obtained by dividing 2 the 2θ value of corresponding diffraction peak. The mean crystallite sizes of mesoporous TiO_2 nanoparticles were found in the ranges of 17-24 nm as shown in table 1.
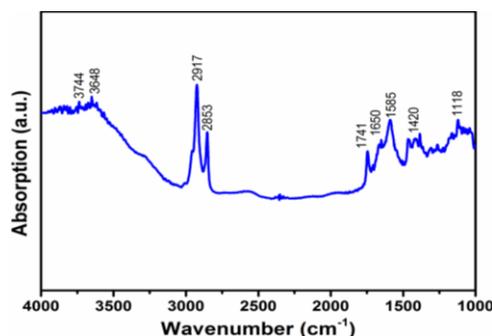

Fig 2. FTIR analysis of mesoporous TiO_2 nanoparticles.

Table 1. Particle size calculation from the XRD pattern.

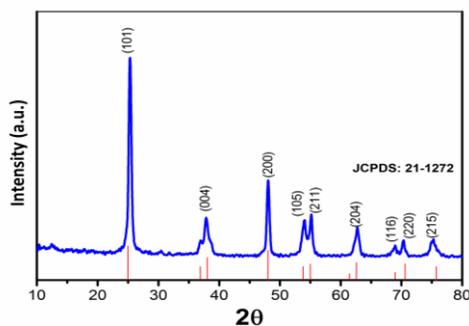| Lattice plane	Peak Position (degree)	FWHM (degree)	Particle size (nm)
(101)	25.2	0.47	17.3
(004)	37.8	0.57	17.8
(200)	48.0	0.40	18.4
(211)	55.0	0.37	19.0
(215)	75.0	0.20	48.5

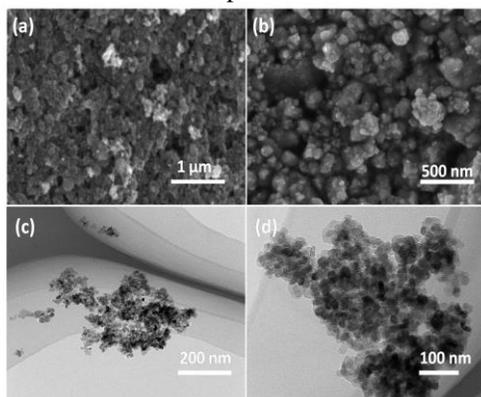Fig 3. XRD patterns of mesoporous TiO$_2$ nanoparticles

Fig 4. (a-b) SEM images of mesoporous TiO2 nanoparticles and TEM (c-d).

3.4. Morphology and structure analysis

The morphology of the as-synthesized mesoporous TiO$_2$ nanoparticles sample was investigated by SEM. Fig. 4a depicted that as-obtained mesoporous TiO$_2$ nanoparticles were adhered to by many small size mesoporous particles that are densely distributed inside and outside of the substrate surface. Fig. 4b showed that the fine nanoparticles are assembled on the mesoporous surface of TiO$_2$ pores were agglomerated to form large particles (lumps) and the shape of nanoparticles is irregular with their average sizes range around 20-200 nm.

The microstructure of mesoporous TiO$_2$ nanoparticles was further investigated by the TEM technique. Fig. 4c revealed that the

higher degree of mesoporous structure and also large number of pores appeared on the surface of the as-prepared mesoporous TiO$_2$ nanoparticles. Fig. 4d showed the HRTEM images of mesoporous TiO$_2$ nanoparticles from there we could be observed that the shape of particles is irregular and their average size ranges 20-70 nm. TEM results are correlated with SEM results.

3.5. Gas Sensing Properties

The porous structure plays a vital role in determining the sensing properties by affecting the diffusion of test gases toward sensing material surface [19]. The operating temperature of the sensor is significantly influenced by MOSs based sensors. Therefore, the gas sensing performance of the mesoporous TiO$_2$ nanoparticles to 100 ppm ethanol gas was examined. Fig. 5a revealed the response of the sensor toward 100 ppm ethanol at an operating temperature from 100°C to 220°C. it is found that the response increased with the initial operating temperature, and reached the maximum value at about 180 °C, afterward the response decreased with further increment in temperature then the existence of an optimal temperature was observed, which is finally taken as 180°C with the strongest response value of the sensor based on TiO$_2$ is 5.2 at 180 °C. The selectivity is a crucial parameter for the gas sensor to evaluate the sensing performances of gas sensors for their practical application. Thus, the selectivity test of the sensor was investigated by exposing several kinds of common gases including ethanol, isopropyl alcohol, and methanol tested with a concentration of 100 ppm at the same temperature of 180 °C and the results are shown in a bar graph as shown in Fig. 5b. Clearly, it can be observed that the sensor-based mesoporous TiO$_2$ nanoparticles exhibited a much higher response to ethanol in comparison to any other gases at the same concentration. The response and recovery time also plays a significant role in the

practical detection of detrimental gases. Fig. 6 showed a dynamic curve of mesoporous TiO_2 nanoparticles response and recovery towards 100 ppm ethanol gas at 180°C was plotted. The result affirms that the resistance of the sensor instantly changes when the sensor was exposed to targeted gases, and later reached a steady state. The response and recovery time of the sensor to ethanol was within 25 s and the recovery time was 15 s, respectively.
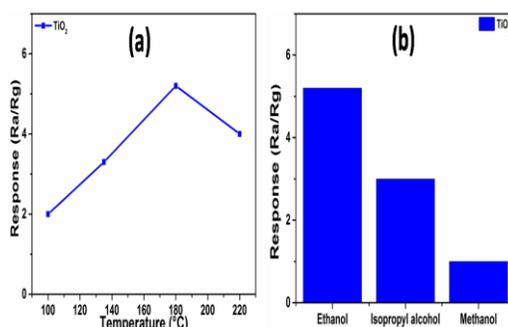

Fig 5. (a) Response of the different mesoporous TiO2nanoparticles versus operating temperature to 100 ppm acetone (b) Selectivity of mesoporous TiO_2 nanoparticles towards 100 ppm of various gases.
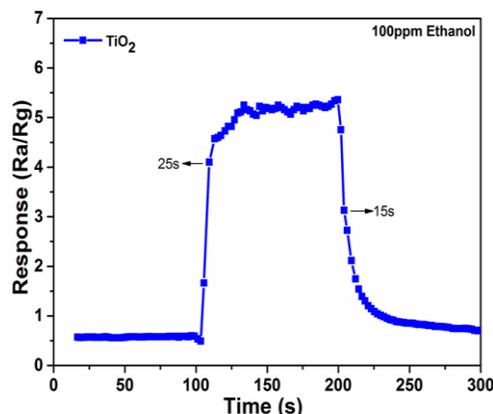

Fig 6. The response-recovery dynamic curve of mesoporous TiO_2 nanoparticles to 100 ppm ethanol at 180°C.

4. Conclusion

We have successfully prepared mesoporous TiO_2 nanoparticles by a simple and low cost solvo thermal method under the calcinations temperature at 300°C. The as-obtained sample was characterized by various analytic techniques and their gas sensing properties were examined. It is found that the mesoporous structure of TiO_2 nanoparticles exhibits high surface area and large pore volume and showed a better performance of ethanol sensing towards 100 ppm at 180°C with fast response and recovery times. The enhancements of gas sensing properties were ascribed to the distinctive porous structure.

References

[1]. N. T.A.Thu, N.D. Cuong, L.C. Nguyen, D.Q. Khieu, P.C. Nam, N.V. Toan, C.M. Hung, N.V. Hieu, Fe2O3 nanoporous network fabricated from Fe3O4/reduced graphene oxide for high-performance ethanol gas sensor, Sensors and Actuators B: Chemical, Vol. 255, 2018, pp. 3275-3283.

[2]. D.R. Miller, S.A. Akbar, P.A. Morris, Nanoscale metal oxide-based heterojunctions for gas sensing: A review, Sensors, and Actuators B: Chemical, Vol, 204, 2014, pp. 250-272.

[3]. T. Yuan, Z. Li, W. Zhang, Z. Xue, X. Wang, Z. Ma, Y. Fan, J. Xu, Y. Wu, Highly sensitive ethanol gas sensor based on ultrathin nanosheets assembled

Bi2WO6 with composite phase, Science Bulletin, Vol. 64, 2019, pp. 595-602.

[4]. M. Tonezzer, L.T.T. Dang, H.Q. Tran, S. Iannotta, Multiselective visual gas sensor using nickel oxide nanowires as chemiresistor, Sensors, and Actuators B: Chemical, Vol. 255, 2018.

[5]. A. Dey, Semiconductor metal oxide gas sensors: A review, Materials Science and Engineering: B, Vol. 229, 2018, pp. 206-217.

[6]. N.D. Hoa, S.A. El-Safty, Highly sensitive and selective volatile organic compound gas sensors based on mesoporous nanocomposite monoliths, Analytical Methods, Vol. 3, 2011, pp. 1948–1956.

[7]. R. Wilson, C. Simion, C. Blackman, C. Carmalt, A. Stanoiu, F. Di Maggio, J. Covington, The Effect of Film Thickness on the Gas Sensing Properties of Ultra-Thin TiO2 Films Deposited by Atomic Layer Deposition, Sensors, Vol. 18, 2018, pp. 735.

[8]. M.V. Reddy, G.V. Subba Rao, B.V.R. Chowdari, Metal Oxides and Oxysalts as Anode Materials for Li Ion Batteries, Chemical Reviews, Vol. 113, 2013.

[9]. A. Bertuna, E. Comini, N. Poli, D. Zappa, G. Sberveglieri, Titanium Dioxide Nanostructures Chemical Sensor, Procedia Engineering, Vol. 168, 2016, pp. 313-316.

[10]. C. Wang, Y. Li, P. Qiu, L. Duan, W. Bi, Y. Chen, D. Guo, Y. Liu, W. Luo, Y. Deng, Controllable synthesis of highly crystallized mesoporous TiO2/WO3 heterojunctions for acetone gas sensing, Chinese Chemical Letters, (2019).

[11]. S. Nasirian, H. Milani Moghaddam, Hydrogen gas sensing based on polyaniline/anatase titania nanocomposite, International Journal of Hydrogen Energy, Vol. 39, 2014, pp. 630-642.

[12]. A. H. Shar, M. N. Lakhan, J. Wang, M. Ahmed, K. T. Alali, R. Ahmed, I. Ali, A. Q. Dayo, facile synthesis and characterization of selenium nanoparticles by the hydrothermal approach, Digest Journal of Nanomaterials and Biostructures, Vol. 14, 2019, pp. 867-872.

[13]. J. Zhang, X. Liu, G. Neri, N. Pinna, Nanostructured Materials for Room-Temperature Gas Sensors, Advanced Materials, Vol. 28, 2016, pp. 795-831.

[14]. S. Zhang, P. Song, Z. Yang, Q. Wang, Facile hydrothermal synthesis of mesoporous In 2 O 3 nanoparticles with superior formaldehyde-sensing properties, Physica E: Low-dimensional Systems and Nanostructures, Vol. 97, 2018, pp. 38-44.

[15]. S. Liu, Z. Wang, H. Zhao, T. Fei, T. Zhang, Ordered mesoporous Co3O4 for high-performance toluene sensing, Sensors and Actuators B: Chemical, Vol. 197, 2014, pp. 342-349.

[16]. B. Durairaj, T. Xavier, S. Muthu, fungal generated titanium dioxide nanopartilces for uv protective and bacterial resistant fabrication, International Journal of Engineering Science and Technology (IJEST), Vol. 6, 2014, pp. 621-625.

[17]. G. Rajakumar, A. A. Rahuman, S. M. Roopan, V. G. Khanna, G. Elango, C. Kamaraj, A. A. Zahir, K. Velayutham, Fungus-mediated biosynthesis and characterization of TiO(2) nanoparticles and their activity against pathogenic bacteria, Spectrochim Acta A Mol Biomol Spectrosc, Vol. 91, 2012,

[18]. F. T. L. Muniz, M. A. R. Miranda, C. M. D. Santos, J. M. Sasaki, The Scherrer equation and the dynamical theory of X-ray diffraction, Vol. 72, 2016, pp. 1-6.

[19]. Z. Wen, L. Zhu, Y. Li, Z. Zhang, Z. Ye, Mesoporous Co3O4 nanoneedle arrays for high-performance gas sensor, Sensors and Actuators B: Chemical, Vol. 203, 2014, pp. 873-879.

Illicium verum as a green source for the synthesis of silver nanoparticles and investigation of antidiatom activity against Paeodactylum Tricornutum

Muhammad Nazim Lakhan [1], Rongrong Chen [1], Altaf Hussain Shar [1], Kishore Chand [1], Muhammad Basit Chandio[2] , Ahmer Hussain Shah[3], Mukhtiar Ahmed [1], Rizwan Ahmed[4] , Jun Wang [1]

Abstract:

Biological fouling has caused a lot of concern in marine industries due to the attachment of microorganisms including bacteria, algae, and diatoms on a marine surface to create a biofilm. Biofouling causes negative impacts on the marine industry such as an increase in weights of hulls, low speed, and high fuel consumption. In the recent past, nanoparticles have attracted a lot of attention in the fields of material science, chemistry, and biology owing to their rare biological properties. Silver nanoparticles (AgNPs) have been long known for its strong toxicity against a wide range of microorganisms. Herein, we synthesized the AgNPs via a green synthesis approach known for its benefits such as one-pot, inexpensive, and eco-friendly; by using Illicium verum (IV) extract as a demoting and sustaining agent. Further, characterization tests of obtained AgNPs-IV were investigated including Ultraviolet-visible spectroscopy (UV-Vis), Fourier-transform infrared spectroscopy (FTIR), X-Ray Diffraction (XRD), Scanning electron microscopy (SEM), Transmission electron microscopy (TEM) and Atomic force microscopy (AFM). The UV-Vis result confirmed the AgNPs-IV formation with its surface Plasmon resonance peak. FTIR was tested to investigate the bio-functional groups liable for the AgNPs-IV synthesis. XRD peaks also meet with the standard of AgNPs (JCPDS: 41-1402). SEM, TEM, and AFM analysis of AgNPs-IV showed the hexagonal structure with 14.56 nm mean size. The cell growth of diatom on 5th day with blank sample suspension was 2.308 (Cell 10^5 number/mL), while for AgNPs-IV sample suspension was 0.19 (Cell 10^5 number/mL). The green synthesized AgNPs-IV showed excellent antidiatom activity against *Paeodactylum Tricornutum (P. Tricornutum)* marine diatom.

Keywords*: Nanotechnology; silver nanoparticles; illicium verum; synthesis; characterization.*

---

[1]Key Laboratory of Superlight Material and Surface Technology, Ministry of Education, Harbin Engineering University, People's Republic of China

[2]College of Mechanical and Electrical Engineering, Harbin Engineering University, People's Republic of China

[3]Department of Textile Engineering, Balochistan University of Information Technology, Engineering and Management Sciences, Quetta, Pakistan

[4]School of Chemical Engineering, Dalian University of Technology, People's Republic of China
Corresponding Author; nazimlakhan@gmail.com

1. Introduction

Biological fouling is the accumulation of algae, plants, and microorganisms on marine surfaces immersed in seawater. Antifouling is the ability of specifically designed materials to prevent biofouling by various numbers of microorganisms such as algae, fungi, and diatoms. Development of eco-friendly and facile green synthesis of metallic nanoparticles (having size < 100 nm) has attained huge attention in recent days due to their ample areas of biological applications including antibacterial, diagnostics, and drug delivery systems [1-3]. Metallic nanoparticles possess chemical and physical properties including a surface area to volume ratio and exhibit strong antibacterial property [4-5]. Among the others, silver has received extreme importance due to its strong toxicity against microorganisms. Currently, silver nanoparticles (AgNPs) are considered as rich particles with their applications in various areas including antimicrobial and antioxidant properties [6-8]. There are several approaches to AgNPs synthesis such as thermal decomposition, microwave irradiation, electrochemical, and biological. Among them, the biological method has many benefits such as simple, less cost, and eco-friendly for large scale applications that do not use toxic chemicals, high temperature, and pressure [9]. Interestingly, AgNPs can be synthesized by using enzymes, proteins, microorganisms, and plant materials. Plant extract synthesis is considered as an efficient approach than chemical and microbial synthesis because plant works as demoting and sustaining agent in the preparation of AgNPs and the particles formed are more stable with different shapes and sizes. Herein, we have used northeast Vietnam and southwest China evergreen tree plant fruit Illicium verum, also known as "Chinese star anise" as a demoting and sustaining agent. Star anise has been used in China for flavoring and medicine purposes for over three thousand years. It has been widely used in the medicines system and contains the principal constituent Anethole which possesses antiviral, antibacterial, antifungal, and antioxidant activity.

In this study, the AgNPs-IV synthesized via a green approach using an extract of IV as a demoting and sustaining agent. The as-prepared AgNPs-IV were characterized by different techniques such as UV-Vis, FTIR, XRD, SEM-EDX, TEM, and AFM. Furthermore, this is the first report of AgNPs-IV and its antidiatom activity against marine diatom *P. tricornutum* in the marine environment.
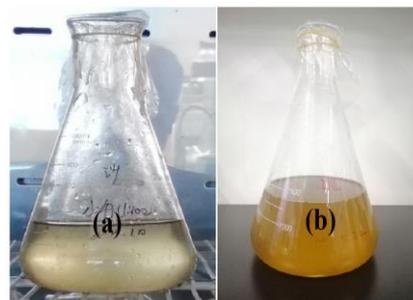

Fig. 1. (a) Blank and (b) P. tricornutum diatom growth solution

2. Materials and Method

2.1. Materials

The fresh plant Illicium verum (IV) fruit was obtained from the local market of Harbin, China, and grinded in powder form. The silver nitrate (AgNO$_3$) and ethanol (C$_2$H$_6$O) were received from Tianjing Chemical Co., China. Distilled water was used to wash the equipment and later dried in the oven. Materials used in the synthesis process were of analytical grade.

2.2. Preparation of Plant extract

0.5 g of IV powder was weighted and dissolved with 400 ml of Milli-Q water and then the solution was boiled at 60°C for 20 min to obtain its aqueous extract. After cooling at room temperature the IV extract was filtered via Whatman No.1 and stored in the refrigerator at 4°C for further experimental study.

2.3. Biosynthesis of AgNPs-IV with Illicium verum extract

For the green synthesis of AgNPs-IV, the solution of 1 molarity was obtained by dissolving weighed amount of AgNO$_3$ in 400 ml of distilled (DI) water under

sonication. Then the as-prepared 80 ml of extract IV was added in $AgNO_3$ aqueous solution drop by drop for reduction of Ag^+ into Ag^0 under the continuous magnetic stirring. The mixed solution was placed in a dark environment for 24 hrs to minimize the photoactivation of $AgNO_3$. After the successful synthesis of the AgNPs-IV solution, AgNPs-IV was centrifuged and washed two times for 15 min at 8000 rpm with DI water. Later, the as-obtained AgNPs-IV was placed in a vacuum oven overnight at 60°C and collected for further characterization and antidiatom activity.

2.4. Characterization

The absorption spectrum of the synthesized AgNPs-IV was investigated by UV-Vis spectrophotometer TU-1901 dual-beam in the range of 200-800 nm. FTIR analysis was carried out using a Perkin Elmer spectrum 100 FTIR spectrometer in the wave number range of 4000-500 cm^{-1} to identify the chemical constituents liable for the successful preparation of AgNPs-IV. XRD pattern was examined to check the nature of the as-obtained samples by using Rigaku TTR at 40 kV and 150 mA within 2θ area between 10-90° with intensity Cu-Ka radiation (λ=0.15406 nm). The morphology of as-obtained AgNPs-IV was viewed by the SEM instrument (JOEL, JSM-6480A) operated at a 20KV of the driving voltage. Element and composition analysis of the powdered AgNPs-IV was conducted using a JEOL's EDX detector attached to the SEM machine. The size of as-obtained AgNPs-IV was observed by TEM using an FEI TECHNI G2 instrument. The topography of AgNPs-IV was investigated by AFM using a Keysight equipment Model 5500. The average mean size of nanoparticles was measured by Nano Measurer Software.

2.5. Antidiatom Analysis

The algae *P. Tricornutum* were examined for the anti-diatom test to check the antifouling performance of AgNPs-IV. The algal stock solution of *P. Tricornutum* was received from Xiamen University-CCMA and it was growth in F/2 medium with a 12/12 light, dark cycle of fluorescent

illumination at 2000 lux and growth sample solutions were shaken daily twice a day. Blank sample and green synthesized AgNPs-IV (5mL) solution was poured in the algal solution at the bottom of the aquarium with at least 1×10^5 algal cells per mL and blank substrate was placed in both beakers to confirm the morphology of surface after 5 days' immersion, later the beakers were placed in an incubator [10]. The diatom settling assay of blank and AgNPs-IV samples was recorded on an Optical microscope.
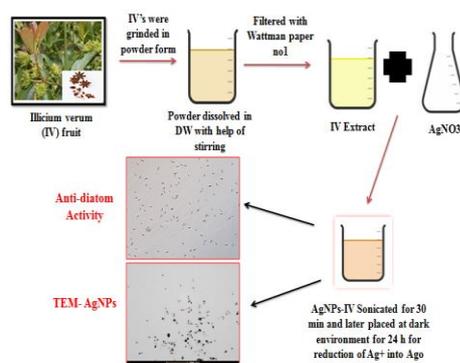

Fig. 2. Schematic route of AgNPs formation using plant extract of illicium verum (IV).

3. Results and discussion

The successful synthesis of AgNPs-IV was observed on UV-Vis spectrum through the color formation. The color of the $AgNO_3$/Illicium verum extract mixture turned from light to dark brown indicates the successful formation of AgNPs-IV. The dark brown color appeared due to the excitation of surface plasmon resonance (SPR) effect. Further, the formation of the AgNPs-IV was observed by the SPR absorption band at 425 nm in the UV–Vis region as depicted in Fig. 3 [11].

Further, AgNPs-IV were characterized by FTIR spectra to analyze the functional groups liable for demoting and sustaining of Ag nanoparticles as depicted in Fig. 4. The FTIR spectrum shows different main peaks at 581, 1118, 1634, 2357, and 3459 cm^{-1}. The peak appeared in the spectrum at 1634 cm^{-1} clearly shows the stretching vibration of C=O and indicating the formation of

AgNPs-IV and capped with the biofunctional groups [12]. The peak at 2357 cm^{-1} and 1157 cm^{-1} represents the O-H and C-O stretching. The peak at 581 cm^{-1} indicates the existence of alkaloids. The peak at 3459 cm^{-1} was assigned to NH stretching vibration of amide group and aromatic rings [13].
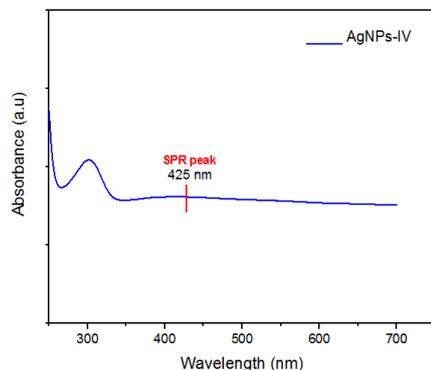

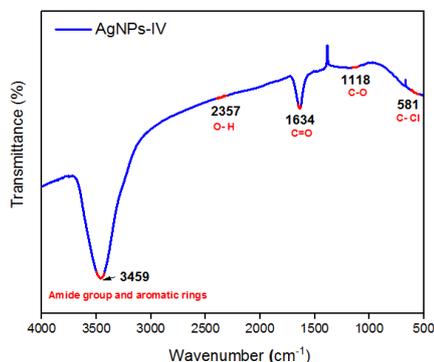Fig. 3. UV-Vis Spectrum of AgNPs-IV.

Fig. 4. FTIR Spectrum of AgNPs-IV.

The XRD pattern of AgNPs-IV is displayed in Fig. 5. Several different diffraction peaks were observed at 2θ of approximately 35.89°, 37.04°, 51.68°, 55.07°, 59.13°, 67.52° and 76.08° corresponding to reflections from the (004), (101), (104), (006), (105), (112) and (008) crystallographic planes of AgNPs-IV, respectively, and confirming the hexagonal structure of silver (JCPDS, No. 41-1402) [14,15].
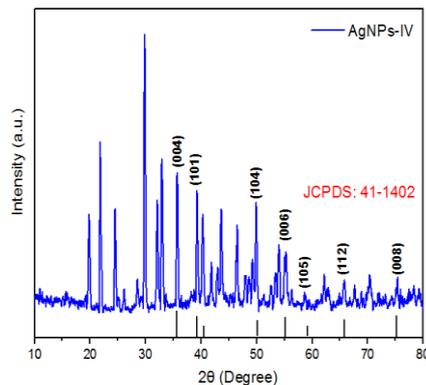

Fig. 5. XRD Pattern of AgNPs-IV.

The morphology of the as-obtained AgNPs-IV was observed by SEM as shown in Fig. 6(a). It was seen that the larger particles are also formed with smaller particles which indicates the aggregation in Ag particles and the evaporation of solvent while sampling preparation [16]. The EDX spectrum of AgNPs-IV showed strong signal at 3 keV [17]. In Fig. 6(b), the peak for Cl was observed due to the presence of plant extract, while the peak of Cu was due to the carbon grid that was used during sample preparation.

The morphology and size of the AgNPs-IV were examined by TEM and AFM. The obtained TEM result illustrated that silver nanoparticles are readily oxidized due to the functional compounds present in the plant extract and successfully formed with hexagonal in shape as depicted in Fig. 7(a) [18-19]. In Fig. 7(b), the measured average mean size of nanoparticles was 14.56 nm obtained through Nano Measurer software using the TEM image. The dark shades on the surface of nanoparticles revealed the presence of plant extract. The AFM image in Fig. 7(c) showed that the particles are formed with little aggregation and marked lines showing the line size of particles at different positions. The particle size curve was obtained through NanoScope Analysis software as shown in Fig. 7(d). The AFM analysis has similarities with the TEM and SEM results.
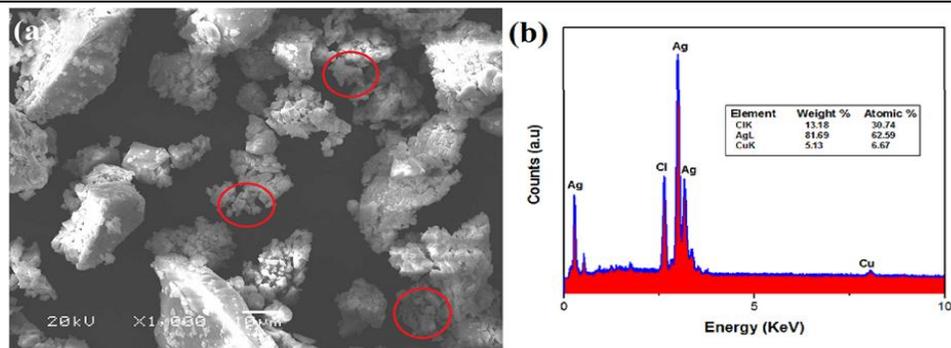
Fig 6. Scanning electron microscopy image of AgNPs-IV (a), EDX Spectrum of AgNPs-IV (b).
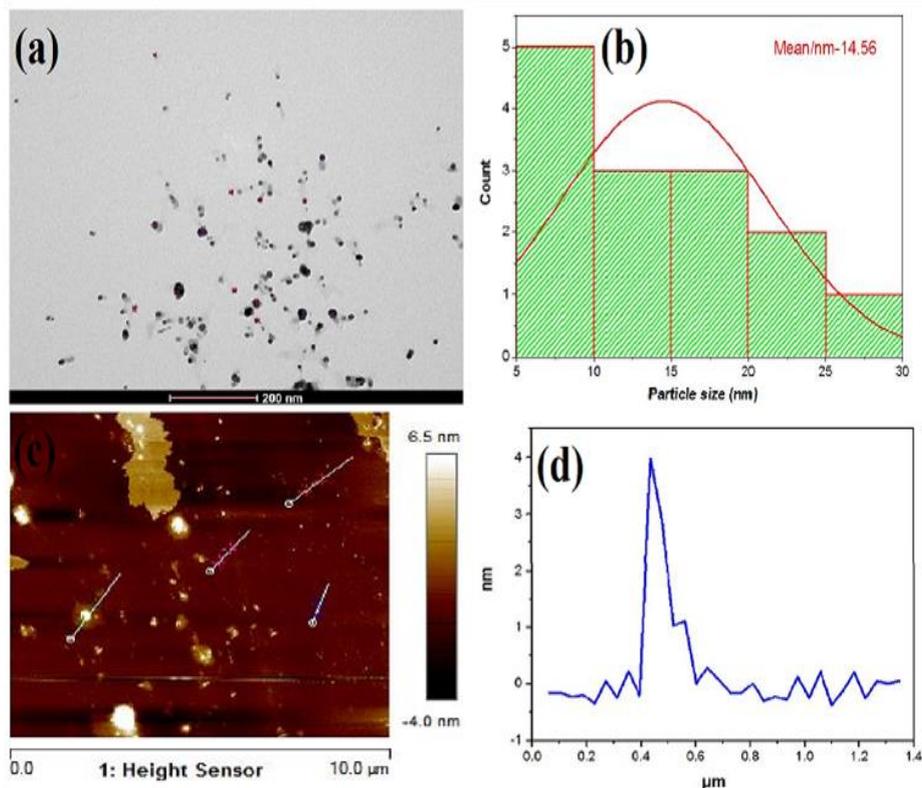
Fig. 7. Transmission electron microscopy image at 200 nm (a), particle size distribution through TEM image (b), atomic force microscopy image (c), and Particle size obtained through AFM image (d) of AgNPs-I

Diatoms are microscopic algae that grow on manmade surfaces present in the seawater. Biofouling develops due to the attachment of diatoms, bacteria, and other microorganisms on the surfaces in seawater. The anti-settling test of diatom was analyzed to check the antifouling performance of the blank sample and AgNPs-IV. Therefore, herein, the *P. tricornutum* diatom was tested to check the biofouling attachemnt. The inhibition growth effect of AgNPs-IV was observed in the *P. tricornutum* suspension [10]. From the anti-settling analysis, it was seen that

the more algae cells were found on a blank sample, while AgNPs IV surface was attached with the no algae cells after 5 days' immersion as shown in Fig. 8(a-d). The diatom attachment was checked in suspension sample by an optical microscope attached with the cell count chamber haemocytometer. Fig. 9 showed

the cell number of diatoms in the *P. tricornutum* suspension on day 1 and after cultivation for 5 days. The absorbance of diatoms was less for AgNPs-IV sample, which was observed on Uv-Vis spectroscopy at 600 nm in algae solution, while for blank samples; its absorbance was almost the same after five days' period.
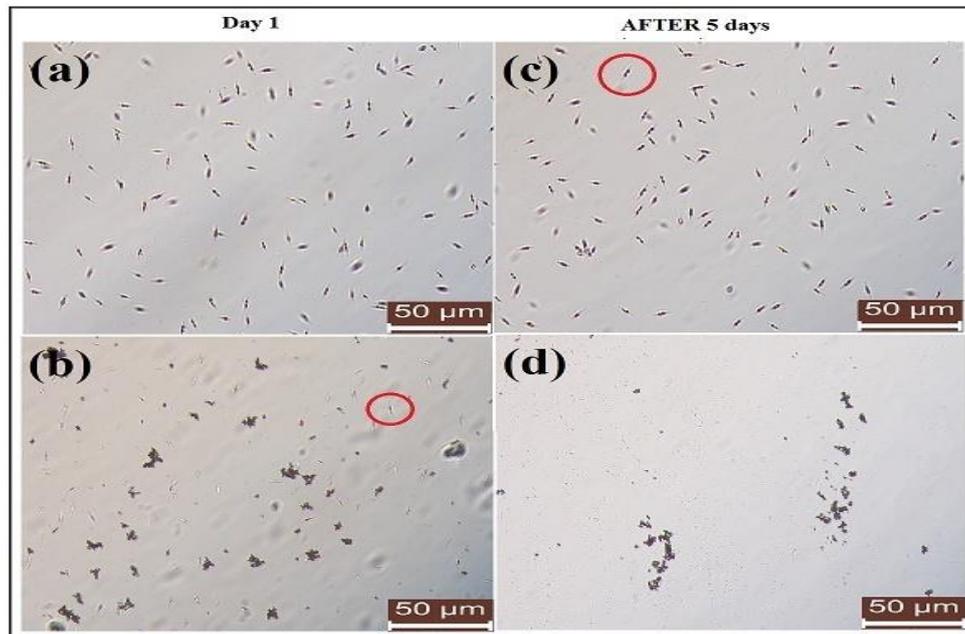

Fig. 8. Antidiatom activity of blank sample on (a) day 1, (c) day 5, and AgNPs-IV 5ml sample on (b) day 1 and (d) day 5.
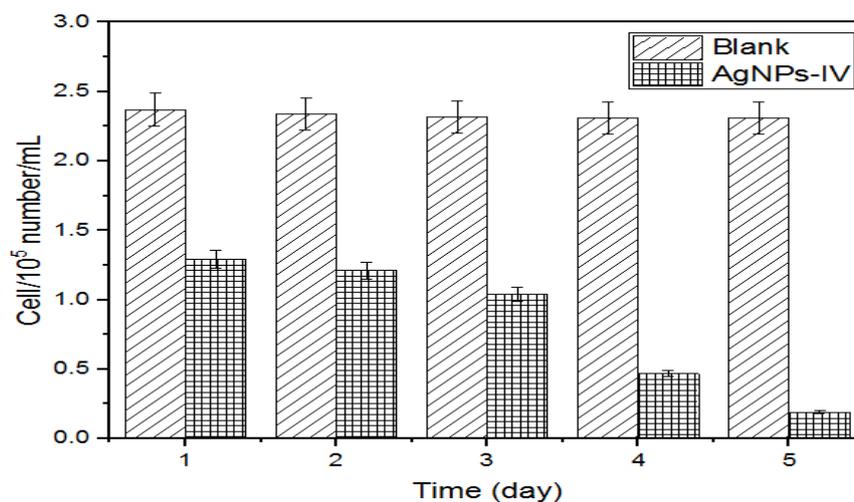

Fig. 9. The cell number of diatoms (P. tricornutum) in the solutions with blank and AgNPs-IV samples. Each point is the average of three readings

4. Conclusion

In this article, we presented a green route for the synthesis of the silver nanoparticles from Illicium verum extract. The amount of plant extract plays a vital role in the preparation of well-dispersed and small size nanoparticles and also acts as a reducing and stabilizing agent. The method employed here is one-pot, simple, inexpensive, and eco-friendly. The results confirm the uniform formation of small size nanoparticles with a hexagonal shape. The green synthesized AgNPs-IV showed excellent antidiatom activity against *Paeodactylum Tricornutum* diatom. In this regard, we can affirm that the AgNPs prepared by the green approach could be a potential tool in the near future to combat biofouling on manmade surfaces in seawater.

References

[1]. E. Pavitra, , B. Dariya, G. Srivani, S.M Kang, A. Alam, P.R Sudhir, M. A Kamald, G. S.R Raju, Y.K Han, B. V K. S Lakkakula, G. P Nagarajui, Y. S. Huh, Engineered nanoparticles for imaging and drug delivery in colorectal cancer, Seminars in cancer Biology, 2019, pp. 1-14.

[2]. S. Ahmed, M. Ahmad, B. L. Swami, S. Ikram, A review on plants extract mediated synthesis of silver nanoparticles for antimicrobial applications: A green expertis, J Adv Res, Vol. 7, 2016, pp. 17-28.

[3]. H. Chandra, P. Kumari, E. Bontempi, S. Yadav, Medicinal plants: Treasure trove for green synthesis of metallic nanoparticles and their biomedical applications, Biocatalysis and Agricultural Biotechnology, 2020, pp. 1-47.

[4]. R. Dadi, R. Azouani, M. Traore, C. Mielcarek, A. Kanaev, Antibacterial activity of ZnO and CuO nanoparticles against gram positive and gram negative strains, Material Science & Engineering C, Vol. 104, 2019, pp. 1-9.

[5]. S. Kheiri, X. Liu, M. Thompson, Nanoparticles at biointerfaces: Antibacterial activity and nanotoxicology, Colloids and Surfaces B: Biointerfaces, 2019, pp. 1-43.

[6]. A. Chatterjee, S. Khatua, K. Acharya , J. Sarkar, A green approach for the synthesis of antimicrobial bio- surfactant silver nanoparticles by using a fern, Digest Journal of Nanomaterials and Biostructures, Vol. 14, 2019, pp. 479-490.

[7]. M. C. Biswas, B. J. Tiimob, W. Abdela, S. Jeelani, V. K. Rangari, Nano silica-carbon-silver ternary hybrid induced antimicrobial composite films for food packaging application, Food Packgaing and Shelf Life, Vol. 19, 2019, pp. 104-113.

[8]. P. Senthilkumar, G. Yaswant, S. Kavitha, E. Chandramohan, G. Kowsalya, R. Vijay, B. Sudhagar, D. S. R. S. Kumar, Preparation and characterization of hybrid chitosan-silver nanoparticles (Chi-Ag NPs); A potential antibacterial agent, International Journal of Biological Macromolecules, Vol. 141, 2019, pp. 290-297.

[9]. R. G. Saratale, I. Karuppusamy, G. D. Saratale, A. Pugazhendhi, G. Kumar, Y Park, G. S. Ghodake, R. N. Bharagava, J. R. Banu, H. S. Shin, A comprehensive review on green nanomaterials using biological systems: Recent perception and their future applications, Colloids and Surfaces B: Biointerfaces, Vol. 170, 2018, pp. 20-35.

[10]. R. Chen, Y. Li, M. Yan, X. Sun, H. Han, J. Li, J. Wang, L. Liu, K. Takahashi, Synthesis of hybrid zinc/silyl acrylate copolymers and their surface properties in the microfouling stage, RSC Advances, Vol. 6, 2016, pp. 13858-13866.

[11]. P. Das, K. Ghosal, N. K. Jana, A. Mukherjee, P. Basak, Green synthesis and characterization of silver nanoparticles using belladonna mother tincture and its efficacy as a potential antibacterial and anti-inflammatory agent, Materials Chemistry and Physics, Vol. 228, 2019, pp. 310-317.

[12]. B. Kumar, K. Smita, L. Cumbal , A. Debut, Green synthesis of silver nanoparticles using Andean blackberry fruit extract, Saudi J Biol Sci, Vol. 24, 2017, pp. 45-50.

[13]. R. Mythili, T. Selvankumar, S. Kamala-Kannan, C. Sudhakar, F. Ameen, A. Al-Sabri, K. Selvam, M. Govarthanan, H. Kim, Utilization of market vegetable waste for silver nanoparticle synthesis and its antibacterial activity, Materials Letters, Vol. 225, 2018, pp. 101-104.

[14]. K. Rajathi and A. Rajendran, Antimicrobial activity of silver nanoparticles from substituted and unsubstituted imidazolium ionic liquids, International Journal of Pharmaceutical Sciences Research, Vol. 8, 2017, pp. 4335-4340.

[15]. F. A. Sheikha, M. A. Kanjwal, H. Kim, D. R. Pandeya, S. T. Hong, H. Y. Kim, Fabrication of titanium oxide nanofibers containing silver nanoparticles, Journal of Ceramic Processing Research, Vol. 11, 2010, pp. 685-691.

[16]. A. H. Shar, M. N. Lakhan, J.Wang, M.Ahmed, K.T. Alali, R. Ahmed, I. Ali, A. Q. Dayo, Facile synthesis and characterization of selenium nanoparticles by the hydrothermal approach, Digest Journal of Nanomaterials and Biostructures, Vol. 14, 2019, pp. 867-872.

[17]. B. Mahitha, B. D. P. Raju, G. R. Dillip, C. M. Reddy, K. Mallikarjuna, L. Manoj, S. Priyanka, K. J. Raon, J. Sushma, Biosynthesis, characterization and antimicrobial studies of AgNPs extract from Bacopa monniera whole plant, Digest Journal of Nanomaterials and Biostructures, Vol. 6, 2011, pp. 135- 142.

[18]. S. Zoha, M. Ahmad, S. J. A. Zaidi, M. N. Ashiq, W. Ahmad, T. J. Park, M. A. Basit, ZnO-based mutable Ag2S/Ag2O multilayered architectures for organic dye degradation and inhibition of E. coli and B. subtilis, Journal of Photochemistry & Photobiology, A: Chemistry, 2020, pp. 1-27.

[19]. K. Chand, M. I. Abro, U. Aftab, A. H. Shah, M. N. Lakhan, D. Cao, G. Mehdi, A. M. Ali Mohamed, Green synthesis characterization and antimicrobial activity against Staphylococcus aureus of silver nanoparticles using extracts of neem, onion and tomato, RSC Advances, Vol. 9, 2019, pp. 17002-17015.

Mini Hydel Power Generation From Over Head Tanks Using Pelton Turbine

Basit Ali[1], Abdul Attayyab Khan[1], Kiran Khalid[1], M. Israr[1], Madiha Nazim[1]

Abstract:

The electricity demand is increasing day by day all over the world. A lot of efforts are made to make the buildings productive and self-sustainable. Due to this fact it is proposed to get energy from overhead water tanks. Following this approach, a 20 m high water tank is considered, water in the pipeline rotates a mini-hydro turbine. The purpose of this scheme is to generate power using low cost mini hydro turbine having negligible environmental effects. The experimental setup of this idea consists of a mini-hydro turbine having a diameter of 0.21 m which is coupled with a dc generator via a chain-gear mechanism to obtain desired rotation. The sensor box is designed to monitor the technical parameters. The calculations and theoretical concepts are presented using basic theory and equations of fluid mechanics and turbo-mechanics, outputs are validated using mathematical and experimental results. This system can replace the ordinary backup units for power generation as it will not consume the power of the existing system for charging batteries.

Keywords: *Pelton turbine, Power generation, Green energy, low head, Hydropower.*

1. Introduction

Energy resources of the world are mainly divided into two categories fossil fuels resources and renewable resources. Renewable resources have the advantage of providing free of cost energy without major environmental effect e.g. solar, wind, biomass, and hydro energy, etc. Hydropower represents a great source of producing a handsome amount of energy as compared to fossil fuels [1]. 16.4% generation of the world's power is generated from hydropower plants. Among all the renewable resources the energy of water is more cost-effective. The report of the international journal on hydropower shows that 23% to 63% of countries extracting hydropower for electricity generation [2], [3]. Hydropower plants at a low scale and domestic scale are known as a major resource of renewable energy today. They have more capacity than other renewable resources. Mini-hydel power plants are capable of generating a maximum power up to 5 KW. Mini-hydel power plants are useful in remote areas where a small amount of electricity is required such as for small lightening bulbs, radio or television, etc. This system has low maintenance and installation cost. The mechanism of mini-hydel power plants is the same as dams, the overhead tank acts as a reservoir to store the water and a mini turbine is used to convert the energy of flowing water to rotational energy. The mini hydel power plant is a solution to extract hydropower from an overhead water

---

[1] Department of Electrical Engineering, Bahria University Karachi Campus Karachi, Pakistan
Corresponding Author: basitali_91@yahoo.com

tank to ful fill the power demand at the domestic level. If such plants are installed on overhead tanks than these plants can generate a good amount of electricity along with that it lowers the burden on the distribution network to contribute to the economy of the country. A comparative study is for rural areas using small turbines discussed [4]. Small projects for irrigation discussed in [5]. In previous studies, the specific overhead hydel source is not used for the domestic generation of electricity.

A turbine is a form of machine that converts turning energy from a liquid that is selected through a system of the rotor into operating effort or energy. Rapidly moving fluid (liquids or gases) Strikes the turbine's blades. When the water strikes the runner of the turbine energy of flowing water is transformed into mechanical rotational energy, along with that generator is coupled with the turbine. When the runner rotates the energy produced from the shaft rotation is collected by a generator that converts the rotating mechanical energy to electrical energy. The reaction machine generates the torque by low pressure and weight of water and the impulse machines require high velocity of jet and high pressure to generate the torque. Due to this fact it required casing [6].

The selection of a suitable turbine is very important for setting up a new project. Large scale electrical energy production mostly depends on the uses of turbines. For domestic production, small turbines can be installed which can perform work under low pressure of water. It also has very low maintenance as compared to other large units of the turbine.

2. Methodology

2.1. Hydro Turbine

The hydro turbine is a type of machine that transforms the kinetic energy of the fluid to moving energy. Hydraulic turbine has a row of blades exactly fitted to the rotating shaft. When liquid, mostly water passes through the hydraulic turbine it hits the buckets and makes

the shaft rotate. While flowing liquid (water) through the hydraulic turbine the pressure and velocity of the liquid (water) is reduced, the effect of this parameter results in the development of torque and rotation of the turbine give the perfect output.

Hydropower turbines are divided into two main categories; impulse and reaction turbine as in Fig. 1. Each turbine of these types is used for a certain range of values of head and flow rates of water. The reaction turbine is mostly used for those sites having low higher flow and head. A reaction turbine produces power by the combination of pressure and flow of water. In reaction turbine runner is placed directly in the water flowing over the blades rather than striking each individually.

Impulse turbines mostly used because of low flow and high head. The impulse turbine discharges to atmospheric pressure to rotate the runner with the use of the velocity of the water. Flowing of water strikes every bucket on the runner. No section on the lower side of the turbine and the water flows out the bottom. Reaction turbines are mostly used for those sites having higher flow and low head. A reaction turbine produces power by the combination of pressure and flow of water [7].
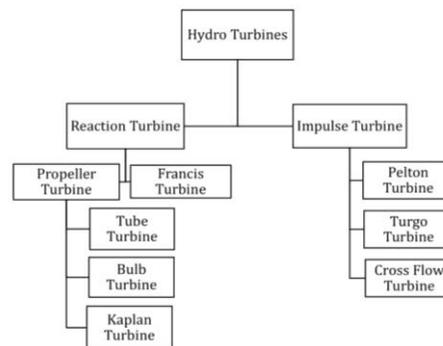

Fig 1: Types of Hydro Turbine

2.2. Turbine Selection

The turbine is directly linked with generator pulleys, gears, and belts. Speed of generator depends on the belt [8][3], the performance of the mini-hydro system

depends on water and the efficiency of turbine wheel pelton turbine is one of the most commonly used impulse turbines. Pelton turbines are suitable in case of high heat. Kinetic energy is only available at the inlet of the turbine. The main parts of the Pelton turbine are nozzle, bucket and runner, casing, and breaking jet. The velocity of the water jet is doubled as compared to buckets and according to the obtained head of water. Fig. 2 shows the structure of Pelton turbine.

Fig 2: Pelton Turbine

2.3.   Generator Selection

Synchronous and induction generators are being used in different types of generation plants and are available in a single and three-phase system [8]. DC generator is used for the establishment of this prototype. DC generator converts mechanical energy into electrical energy. To convert a DC generator into a DC motor no change in construction is required and the same for the motor to the generator, for this reason, we can say that it is a DC machine. So, a self-excited dc generator is a good choice for this system. Fig 3 shows the dc generator used in the experiment.

Fig 3: DC Generator

2.4.   Chain Gears

The dc generator required 452 RPM to give maximum output. The RPM of the turbine was not much enough to reach the requirement of the dc generator. To increase the RPM the gear mechanism is introduced in the system. The chain gear system was introduced to a couple of generators with the turbine. The pulley with more number of teeth was coupled with the turbine shaft and pulley with less number of teeth was coupled with the generator shaft to more RPM at the generator shaft as shown in Fig. 4.
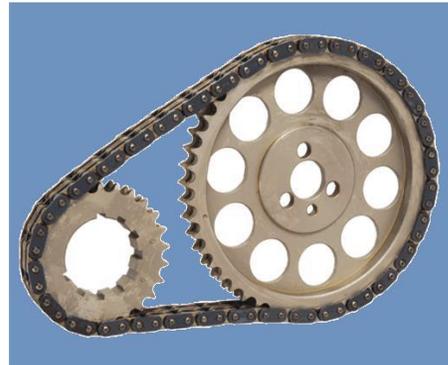

Fig 4: Chain Gears

2.5. Electronic Circuit

2.5.1   Charge Controller:

The charge controller is a circuit which is used for the battery charging purpose. The power generated from the generator is not constant it depends upon the flow of water and the RPM of the turbine. So, to charge the battery from this type of power we need a

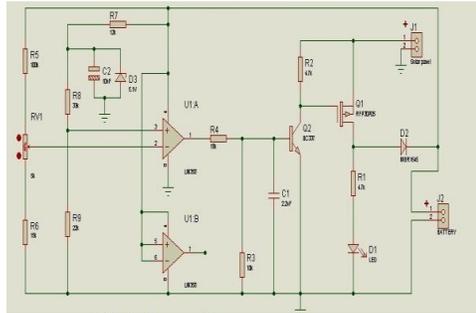charging circuit. Fig. 5 shows the circuit diagram of the charge controller.

Fig 5: Charge controller

2.5.2   *Inverter*

The system generated output was useful for only DC devices. The output of the dc generator was not useful for the AC devices. So, to make it useful for all devices an electronics circuit is involved. The inverter is an electronic circuit that converts the DC power into AC power. There are two options in the system both AC and DC now the output of the generator can be used for both types of devices. The inverter circuit involves a number of a transistor for the switching purpose. A step-up transformer is used in the circuit to increase the voltage from 12 V to 220 V which are useful for domestic usage.

2.6 Sensors

There are five sensors used in this prototype for measuring different parameters.

RPM sensor is used to measure the rrotation of the turbine. It is designed with Arduino and LCD is used for the display. Flow sensor is used to measure the flow rate of the water. It installed just before the inlet of the turbine. A vibration sensor is used to measure the vibration of the system. It is installed at the turbine assembly.

A Bourdon tube type pressure gauge is used to monitor the pressure of the water. It installed just before the flow sensor. Water level indicator is used to monitor the level of water. Three LEDs are used to indicate the level of water. It is installed in the water storage tank.

3. Working

The energy of the flowing water through the pipeline is utilized to move the runner of the turbine. The pressure provided to the turbine is very small, due to this impulse turbine will be more suitable hence the Pelton turbine is selected for this design. After entrance from the overhead of the tank into the inlet of the casing, the nozzle is attached to the casing to improve the velocity. High-pressure water than hits the cups followed by exit pipe connected through the tap. A display box depicted in Fig. 6 is used to show the readings of the different parameters (i-e) (flow meter, RPM sensor, Vibration sensor, and Current sensor).

Fig 6: Hardware setup

The working of Pelton turbine Fig. 7 consists of four main parts that are nozzle, buckets and runner, casing, and the last one are breaking jet. The high speed of water flow through the penstock and water jet emerging in the nozzles hit the buckets of the runner. The generator is connected to the shaft of the runner that converts the moving energy into electrical energy and the arrangement of the nozzle is set to the close of penstock which

helps to accelerate water and flow of water with prohibitive speed and greater velocity and eject atmospheric pressure. When the water hits the buckets it divides the bucket into two half and then the turbine starts to rotate. The water jet velocity is double as compared with the velocity of the bucket. The buckets of the turbine are mounted on the circular path with equal spacing. Due to this, the runner rotates at a very high speed. The energy of jet will decrease in the form of kinetic energy because the jet changes its direction due to the spherical shape of buckets and produce U-rotation and waterfall into the tailrace.

Fig 7: Pelton Turbine in the casing

4. Results

A Pelton Turbine was designed by using basic turbine formulae [9]. Complete calculations of all the parameters are depicted in Table I. There is the direct relation between the hydropower, flow of water (Q), Head (H), gravitational force (g) overall efficiency (no) where, H = 20 m;

$$P = Q * H * g * no \qquad (1)$$

Where overall efficiency is directly related to the mechanical efficiency (nm), hydraulic efficiency (nh), and volumetric efficiency (nv).

$$no = nh * nm * nz \qquad (2)$$

The number of buckets is the main part of the designing of the Pelton wheel. The diameter of each bucket is 0.21 m, the total number of buckets is 24. Each bucket mounted together with shaft and used to increase the ability of the turbine to move with good speed and give smooth rotation [10][11][12]. Where C is the coefficient of velocity that varies from 0.97 to 0.99. N is the speed of the turbine in revolution/minute (RPM) which is 800. Specific speed ratio (f) that varies between 0.43 and 0.48. The designed buckets of the Pelton Turbine are depicted in Fig. 8. Table 1 shows the complete parameter calculations of the system.

Table 1: System parameters

S.no	System parameter	Calculations
1	Flow rate (Q)	0.0022 m³/s
2	Velocity of water v_1	19.50 m/s
3	Velocity of cup (u)	8.77 m/s
4	Diameter of turbine	0.21 m
5	Diameter of jet (d)	0.012 m
6	Jet ratio (m)	17.5
7	Number of buckets (z)	24
8	Length of buckets	2.76 cm
9	Breadth of buckets	3.36 cm
10	Depth of buckets	0.72 cm
11	Hydraulic efficiency	0.98
12	Volumetric efficiency	0.9
13	Rotor power	0.3851 KW
14	Mechanical efficiency	0.9
15	Overall efficiency	0.8
16	Power	0.348 KW
17	Specific speed	11.158

Fig 8. Buckets of Pelton Turbine

5. Conclusion

Hydropower is the main natural and clean resource of renewable energy. The best thing about hydropower is that it is free of cost with minimal environmental effects. This prototype used mini hydel technology we can produce free of cost energy which can be stored in the battery. Hydro-power is always being a main and important part of electricity generation. By this mini hydel generation domestic model, we can generate power up to 0.348 kW which can be increased by increasing the flow rate of water. The system can be enhanced and can be used in tall buildings and municipality overhead water tanks. A sensor box is attached which monitors different parameters of the whole system.

References

[1] Adhau, S. P., R. M. Moharil, and P. G. Adhau. "Mini-hydro power generation on existing irrigation projects: Case study of Indian sites." *Renewable and Sustainable Energy Reviews* 16.7 (2012): 4785-4795.

[2] Paish, Oliver. "Small hydro power: technology and current status." *Renewable and sustainable energy reviews* 6.6 (2002): 537-556.

[3] Saket, R. K. "Design, development and reliability evaluation of micro hydro power generation system based on municipal waste water." *2008 IEEE Canada Electric Power Conference*. IEEE, 2008.

[4] Adhau, S. P. "A comparative study of micro hydro power schemes promoting self sustained rural areas." *2009 International Conference on Sustainable Power Generation and Supply*. IEEE, 2009.

[5] Adhau, S. P., R. M. Moharil, and P. G. Adhau. "Mini-hydro power generation on existing irrigation projects: Case study of Indian sites." *Renewable and Sustainable Energy Reviews* 16.7 (2012): 4785-4795.

[6] MMSRS, Bhargav, S. P. Anbuudayasankar, and K. Balaji. "Power generation by high head water in a building using micro hydro turbine—a greener approach." *Environmental Science and Pollution Research* 23.10 (2016): 9381-9390.

[7] Nag, P. K. *Power plant engineering*. Tata McGraw-Hill Education, 2002.

[8] Kothari, D. P., K. C. Singal, and Rakesh Ranjan. *Renewable energy sources and emerging technologies*. PHI Learning Pvt. Ltd., 2011.

[9] Yahya, Ahmad Khusairee, Wan Noraishah Wan Abdul Munim, and Zulkifli Othman. "Pico-hydro power generation using dual pelton turbines and single generator." *2014 IEEE 8th International Power Engineering and Optimization Conference (PEOCO2014)*. IEEE, 2014.

[10] Cobb, Bryan R., and Kendra V. Sharp. "Impulse (Turgo and Pelton) turbine performance characteristics and their impact on pico-hydro installations." *Renewable Energy* 50 (2013): 959-964.

[11] Ali, Basit, et al. "Portable Solar Powered DC Pumping System Using Pump jack and MPPT." *2019 2nd International Conference on Computing, Mathematics and Engineering Technologies (iCoMET)*. IEEE, 2019.

[12] Ali, Basit, and Imran Siddique. "Distribution system loss reduction by automatic transformer load balancing." *2017 International Multi-topic Conference (INMIC)*. IEEE, 2017.

[13] Ali, Basit, A. A. Khan, and Imran Siddique. "Analysis of distribution system losses due to harmonics in IESCO." *2018 IEEE International Conference on Information and Automation for Sustainability (ICIAfS)*. IEEE, 2018.

A System Analysis Approach to Visual Object Tracking

Obaid Ahmed Khan[1], Ahmed Saeed[1]

Abstract:

In the modern-day study of system behavior and analysis, understanding the response of how the system will behave in a certain condition is considered vital. Thus, keeping object behavior as the primary objective and object detection as a core instrument this project intends to identify the object and track the motion of the desired object. This paper provides an overview of how a closed-loop control-based system was designed using a camera as visual input. The video signal is analyzed to detect distinct color and shape similarities to the desired object. Based on a high similarity index the Raspberry Pi controller generates a pulse width modulation signal to regulate the angular position of the rotary actuator to align the camera frame of view according to a desired object's position. Post system design experimentation results and potential realized system faults are expressed within the conclusion.

Keywords: *Computer Vision, Object tracking, closed-loop control system, System Analysis.*

1. Introduction:

Computer vision analysis of object characteristics and their behavior has always been a topic that has found a lot of success in the scientific community. The first studies date back all the way to the 1700s when electronic devices started getting more powerful. It was during this era the fundamental basics of how we can analyze objects were understood through applications in the field of medicine [1] [2].

While this was an amazing feat these techniques could not be applied towards the field of object detection due to the lack of computing power required for such a task. While the technology was not ready yet many techniques for detection of object characteristics were being studied [3]. Soon specialized computing devices were put into practice that allowed users to process images and apply pattern recognition techniques [4].

The implementation of these techniques meant that users can improve the previously existing techniques and algorithms to design better and more robust applications. One of these applications was the amalgamation of the control theory and computer vision. This led to many applications towards military, road control, and filmography [5] [6].

Application of this amalgamation between control theory and computer vision has been most prevalent in the field of automation. One such application of this technology in the automation is object tracking. Object tracking is the tracking of a specific object possessing desired characteristics using movable visual sensors. This concept of tracking objects through vision is not rather new with it being a crucial part of human development for years and with most infants having developed this ability soon after birth [7].

[1] DHA Suffa Univeristy Karachi, Pakistan
Corresponding Author: Obaid_10@live.com

2. State of the art

Research in the area of computer vision is quite dense with a lot of studies conducted towards efficient algorithm techniques. Some of these notable techniques can be consulted in [8]. This documentation analyzed the vast literature of computer vision and only the most well-established techniques were pondered on that have been physically realized. Based on an in-depth analysis of the literature it was found that there is a lack of quality of quantitative work towards the application of computer vision in the field of automation and control.

Some note-worthy efforts that have been made were either with a fixed viewpoint [9] or if the viewpoint was movable the system lacked an essential effort towards the incorporation of an efficient automation control strategy [10]. To overcome the issues plaguing object detection the system was designed with a control systems point of view.

3. Methodology

The ability to analyze objects visually and take actions accordingly are the features of smart controlling and when it is being developed for computing devices it needs to be developed in two steps. The first being object detection which involves the identification of the desired target and the second is object tracking, where the system reacts to the visual data.

A. Object Detection

The first step for object tracking is object detection or the ability to detect a specific object. In [11] the basic technique of object detection is considered using Color Threshold Method in which a basic array of RGB code is set, after which the code is compared with each individual pixel within the frame processing the image into binary setting white to the RGB code threshold and black to other code converting the image into a black and white image sending the required colors code to the processor.

This is further improved upon [12] by involving canny edge detection for the detection of edges by convolving a raw unprocessed image with a Gaussian filter resulting in a blurry image with no noticeable noise.

B. Object Tracking

To track the object, a basic control structure that would enable the controller to efficiently control the position of the system was designed. In this regard, an error reduction technique is used. Since the object tracking is based on error reduction so the error is the difference between the center of the screen frame and the center of the object. The setpoint i.e. object center was calculated using Hough transform [13] whereas, the process variable is the frame center which is calculated by dividing the screen resolution into half.

The error is calculated in terms of the pixels' difference. So, in order to calculate the center of the screen measure the screen resolution, the screen used in this experiment is 720x1280p and divide the pixels into half to get the center of the screen which is (640,360).
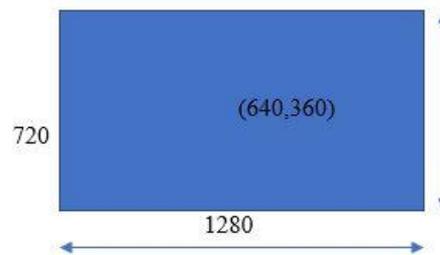

Fig 1: Frame of Reference

$$DutyCycle\% = \big((x * On\ Time) + bias\big) * Time\ interval$$

Where,
On-Time = Total pulse duration for servo movement between 0-180 degrees in ms.

bias = The minimum pulse duration required for the servo to become active in ms.

Time interval = Time in ms.

x = the calculated ratio between time intervals and pulse width for achieving the desired angle.
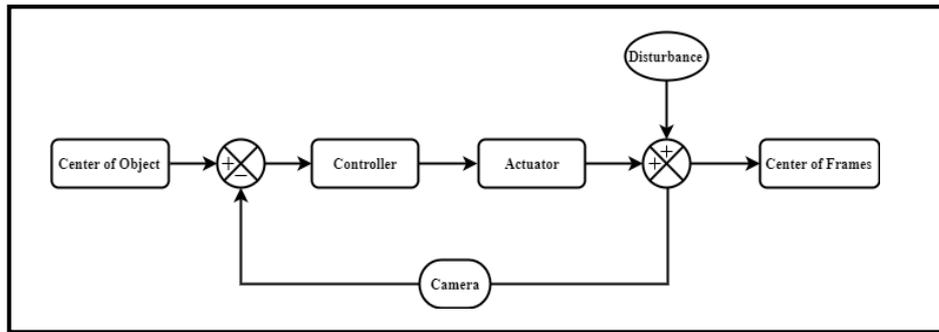
Fig 2: Block Diagram of Control System

4. System modeling

A. Control System

The basic control structure could not be directly employed without the system model. To understand the system, model the hardware specifications were initially explored.

Based on hardware specifications (Given in table 1) it was speculated that the most appropriate control structure for the system would be a proportional controller design.

Table 1: Servo motor specifications

Weight (g)	9
Torque (KG)	1.8
Speed (Sec/60deg)	0.1
Dead bandwidth	1 us
Temperature range	0 C – 55 C
Operating voltage	4.8 V
Stall torque	1.8kg/cm
Dimension	23 x 12.2 x 29mm
Gear type	POM gear set

To test the hypothesis of the desired control, structure a system response analysis was conducted:

• System Response Analysis

To record the input-output data, an excitation signal is sent through the system. Using this data, a plant model is built, and based on plant model accuracy the system model is tuned to achieve a quick and stable response. After analyzing system response data, it was realized that a second-order model was the most appropriate for the system. Exploring the previous hypothesis merits of each controller design were compared which led to the use of P controller, compared to PD and PID controllers the system response using a proportional controller is much faster which is a major requirement of the system design [14]

In P controller the P is proportional to the value generated of the error between setpoint and process variable.

P controller is used in the first-order system by optimizing the transient behavior by reducing the steady-state error of the system. The gain K is inversely proportional to the steady-state error, as one of them increases the other decreases and vice versa. This controller is only applicable when the steady-state error is in the applicable range.
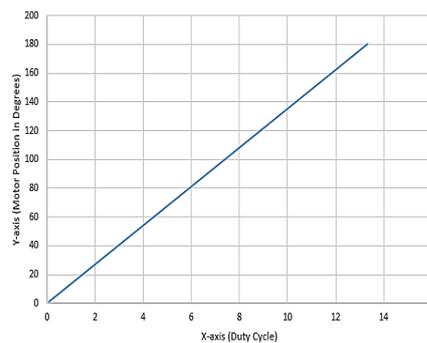
B. System identification

Fig 3: graph plotted between Duty cycle and Position

The slope of the graph measured is 13.53.

$$G(s) = \frac{\Delta y}{\Delta x}$$
$$\frac{d\theta}{dx} = 13.53$$

Where $y(x) = (position)$; x = % Duty cycle;

The Laplace transform equation of the system was modeled as,

$$\mathcal{L}[y(x)](s) = \frac{13.53x(s)}{s}$$

Assuming $y(0) = 0$ initially

$$y(s) = \frac{13.53x(s)}{s^2}$$
$$y(x) = c1 + 13.53x$$

5. Algorithm

The algorithm initiates the camera draws a new frame and scans the surrounding for the desired object. Depending on the yaw motor movement the algorithm decides whether to turn right or left. The program goes into tracking state when the desired object is the detected and after feature extraction proceeds with tracking of the object. The frame is updated in real-time tracking objects' current position.
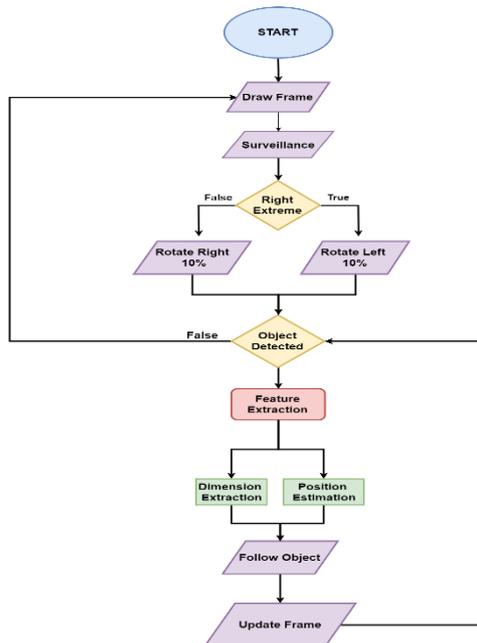

Fig 4: Algorithm flow chart

A. Experimentation

The experiment included the physical model implantation of the above mention algorithm and constructed a system consisting of a raspberry pi 3 model B and two high fidelity servo motors with a specified control structure. The first motor acted as the yaw rotational motor and the other acted as the pitch rotational motor. Then a webcam was installed on the top of the pitch rotational servo motor and a series of trials were conducted using an object.

B. Calibration

The object was placed first directly in front of the system to identify if any bias errors are present so that these can be calibrated out of the final working model. The system showed no presence of any bias error and would remain constantly stuck with the center of the view frame locked at the calculated cylinder center but with small bias.

C. Sensitivity Analysis

The object was then moved to identify whether the algorithm adapts to the input change, at small error values the system would quickly adapt to the change and reposition the view frame to the correct value with negligible error. The problem arose when the system was presented very high.
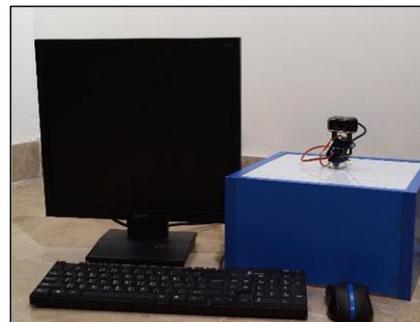

Fig 5: Hardware

6. Results

The object detection method proposed in [11] was further improved upon by using color thresholding in combination with canny edge detection to find a similarity between the camera image and the desired

object. This technique led to the object being detected and tracked very accurately. Table 2 shows the optimal timing of the system:

Table 2: Optimal timing of the system

Timing		Time is taken
T 0	The system turns on and Scans the environment	0 - ∞
T1	Object detected by the system	20 milli-second
T2	Object Tracked with 5% threshold error	4.5 seconds
T3	Object tracked with high accuracy	1 second
T4	An object within steady-state	800 Milli-seconds
T5	System readjusts due to proportional control	1.5 seconds

*Note: Time between T0 and T1 could an infinite amount of time and depends on when the object is introduced in the system. Please see Figure 8 for an example of the object detected at 0.3 Seconds.

The methodology described in [11] does lend well to the rapid detection of the object. However, this approach lacks a fundamental feature in distinguishing between different objects with the same color code which results in false object detection. Additionally, the design methodology [12] based on canny edge detection focuses on the outer boundary of the object but it can only provide the approximation between similar size objects and fails to extract different features. Whereas, the present paper proposes the solution for object detection using a colour threshold in combination with the Canny edge detection methodology to bridge the

flaws inherited with the two techniques. On the other hand, object tracking using the error reduction method is efficient and consumes low processing power. Although there are some minor fluctuations in tracking between error calculation and actual execution, it can be easily removed by introducing deadtime once the error is less than the desired accuracy.
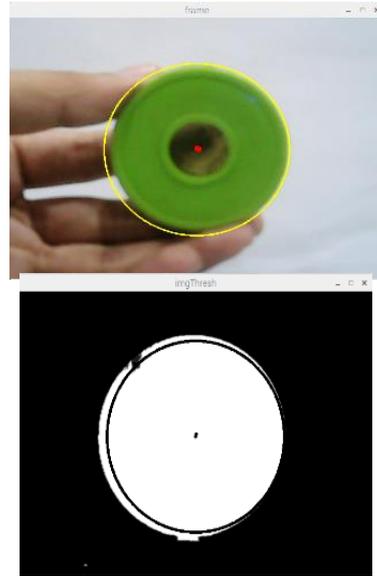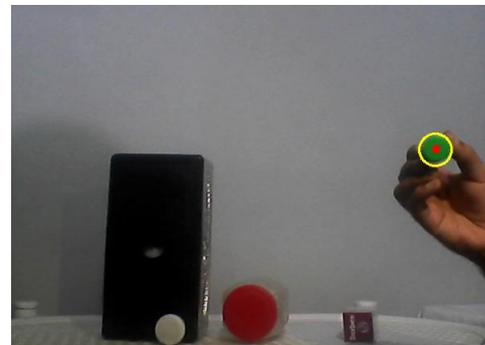

Fig 6: Object Detection &Tracking

Fig 7: Testing with different objects

Figure 8 shows error plotting with respect to time which shows that error reduces as the camera approaches towards the desired set point.
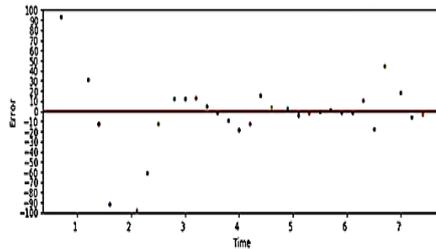
Fig 8: Error plotting

7. Conclusion & Future Work

The algorithm was then rewritten to include the change and based on further evaluation it was found that most of the sensitivity errors were resolved and the bias was also seemingly removed. The system now with the object even at the farthest end of the view frame could centralize the frame of view of the camera to the object's position in under 11 milliseconds and could track it smoothly.

A problem that was realized during the system implementation was that when the object was static the system would slightly move and reposition itself due to a refresh of the system cache.

This issue was fixed by inserting an additional condition in the algorithm when switched off the control actuation whenever the error accumulation of the last 5 values is lower than 0.5.

Some areas for further research are:

- Instead of involving the condition of switching off the control actuation, the error could be minimized further but without a severe increase in tracking time. This would require an effort towards optimization of the system by techniques such as branch and bound method.

- The control structure was based on a P controller with a 3-point model but in order to achieve the best results a higher polynomial data analysis is required. This would be investigated to further improve the system's performance.

References

[1] M. Forouzanfar, N. Forghani, and M. Teshnehlab, "Parameter optimization of improved fuzzy c-means clustering algorithm for brain MR image segmentation", Engineering Applications of Artificial Intelligence, vol. 23, no. 2, pp. 160-168, 2010. Available: 10.1016/j.engappai.2009.10.002..

[2] "A New Perspective of Wavelet-Based Image Denoising Using Different Wavelet Thresholding", International Journal of Science and Research (IJSR), vol. 5, no. 8, pp. 1504-1509, 2016. Available: 10.21275/art20161212.

[3] R. Jarvis, "Special feature: An interactive minicomputer laboratory for graphics, image processing, and pattern recognition", Computer, vol. 7, no. 10, pp. 49-60, 1974. Available: 10.1109/mc.1974.6323334.

[4] F.Schlag, A. C.Sanderson, C. P. Neuman, and F. C. Wimberly, "Implementation of Automatic Focusing Algorithms for a Computer Vision System with Camera Control", Robotics Institute, 1983. [Accessed 25 July 2019].

[5] E. Dickmanns and A. Zapp, "A Curvature-based Scheme for Improving Road Vehicle Guidance by Computer Vision", Mobile Robots I, 1987. Available: 10.1117/12.937795 [Accessed 25 July 2019].

[6] W. Miller, "Real-time application of neural networks for sensor-based control of robots with vision", IEEE Transactions on Systems, Man, and Cybernetics, vol. 19, no. 4, pp. 825-831, 1989. Available: 10.1109/21.35345 [Accessed 25 July 2019].

[7] M. Moore, R. Borton and B. Darby, "Visual tracking in young infants: Evidence for object identity or object permanence?", Journal of Experimental Child Psychology, vol. 25, no. 2, pp. 183-198, 1978. Available: 10.1016/0022-0965(78)90076-0 [Accessed 25 July 2019]

[8] R. Jain, R. Kasturi and B. Schunck, Machine vision. New York: McGraw-Hill, 1995.

[9] B. Shao and H. Xin, "A real-time computer vision assessment and control of thermal comfort for group-housed pigs", Computers and Electronics in Agriculture, vol. 62, no. 1, pp. 15-21, 2008. Available:

10.1016/j.compag.2007.09.006 [Accessed 24 July 2019].

[10] D. Lee and Y. Park, "Vision-based remote control system by motion detection and open finger counting," in IEEE Transactions on Consumer Electronics, vol. 55, no. 4, pp. 2308-2313, November 2009.

[11] S. Jayati Singh, "Object Detection by Color Threshold Method," *International Journal of Advanced Research in Computer and Communication Engineering,* vol. 4, no. 10, pp. 354-356, 2015

[12] J. Canny, "A Computational Approach to Edge Detection," *IEEE Transactions on Pattern Analysis and Machine Intelligence,* Vols. PAMI-8, no. 6, pp. 679 - 698, 1986

[13] M. Rizon and et al., "Object detection using circular Hough transform," *American Journal of Applied Sciences,* vol. 2, pp. 1606-1609, 2005.

[14] K Smriti Rao and Ravi Mishra, "Comparative study of P, PI and PID controller for speed control of VSI-fed induction motor" International Journal of Engineering Development and Research, vol. no 2, pp 2740-2744, IJEDR1402230, 2014.

[15] Onkar R. Kirpan and et al., "Object Detection on Raspberry Pi," International Journal of Engineering Science and Computing, vol. 7, no.3, pp. 5360-5362, 2017

[16] Vijayalaxmi, et al, "OBJECT DETECTION AND TRACKING USING IMAGE PROCESSING," Global Journal of Advanced Engineering Technologies, Special issue (CTCNSF), pp. 113-115, 2014.

[17] B. Dinesh, "Understanding and Design of an Arduino-based PID Controller," Research Master Thesis, Physics and Applied Physics, *Virginia Commonwealth Univ.,* VA., 2016

[18] Katsuhiko Ogata, "PID Controllers and Modified PID Controllers," in Modern Control Engineering, Prentice Hall, fifth edition, pp. 567-647, 2010.

[19] D.Chris, "Github," Github,Inc., 10 October 2015. [Online]. Available: https://github.com/MicrocontrollersAndMore/Raspberry_pi_2_and_OpenCV_3_Tutorial_Part_1. [Accessed 13 September 2017].

[20] R.Adrian, "pyimagesearch," 14 September 2015. [Online].Available: https://ww.pyimagesearch.com/2015/09/14/ball-tracking-with-opencv/. [Accessed 17 October 2017].

An ERP Based Blood Donation Management System for Hospital and Donor

Ghulam Muhammad[1], Hamza Asif[1], Farrukh Abbas[1], Imran Memon[1], Hadiqua Fazal[1]

Abstract:

The objective of this paper is to develop a mobile blood donation management system application. This paper an android based application development technique by using an ERP model database management system. The techniques involve using mobile development IDEs and adequate APIs to have desired functionalities. There are two main mobile developing platforms present in the world iOS and Android. We have developed our application on Android OS. Different applications were surveyed and used to explore the presently available features to the end-user. After trials and research, the outline was made to what extent should go and developed. As the system is developed for hospitals and donors, the hospital puts a request for blood groups on the application. The system then finds nearby users online with the requested blood groups, if anybody required for his / her relative he or she can use this application for find donors who are available or offline with full information of donor if donor or user is interested in donation then he has done to the requester. Users' locations are tracked in real-time. If the users proceed to the hospital, the tracking shows if they are coming or not.

Keywords: *Android GUI, ERP Model, Hospital model, Donor model*

1.Introduction:

Nowadays, health technologies are developing rapidly. Incurable diseases are cured with the latest technology and medical research. With the rapidly developing technologies, medical professionals must cope up with changing trends and technologies. These technologies require fast response from professionals [1,2,3,4].

Such technology is a blood donation management system. A system that is capable of catering multiple users at a time. Hospital operations which include surgeries, transplantations, and medical processes, require a blood supply to facilitate patients undergoing those processes [5,6,7,8]. A blood donation management system can manage information of users, track their arrival to hospitals, informs about users online on the system with the registration of authentic user cell number and hospital related information based on google map location [9,10,11].

2. Problem Statement

Blood arrangements are uncertain. People who committed to donate often change their plan to donate. As a result of the survey done, we found that conventional apps just register users and donors [12,13,14]. The user puts requests and donors reply to those requests on the application. It is then not guaranteed

[1] Department of Computer Science, Bahria University Karachi, Pakistan
Corresponding Author: ghulammuhammad.bukc@bahria.edu.pk

Table 1. Comparison of Applications

Applications on playstore

APPS	Sms code	User Profile	User profile related services	User contact details	Limitation Factor of 3 months	Availability Nation wide	Availability Internationally	Location Provision
Blood Community		✓	✓	✓				
Blood Bank Pakistan	✓	✓	✓	✓	✓	✓		
Blood Donors		✓	✓	✓		✓		
Hayaat		✓	✓	✓		✓		
LIFE	✓	✓	✓	✓			✓	
Revive						✓		
Tahiri Blood Bank	✓	✓	✓	✓				
Life Saver		✓		✓				✓

Our Blood Donation Management Application

FEATURE	YES/NO
SMS code verification	YES
User Profile	YES
Profile related Services	YES
User Contact Details	YES
Limitation Factor of 3 months	YES
International Availability	NO
Location Provision	YES

whether the commitment done between the user and donor is fulfilled or not. On further analysis it was found that this posed some of the problems which were the following:

1) Either the user is authentic or not. Is he/she really having the need for blood?

2) Criminals can misuse the application. Invite people to donate and then loot them.

3) Donors show their will to donate on the application but do not proceed for donation hence wasting the time of users.

3. Related Work

We surveyed 8 mobile blood donation management applications that are currently being used. All the applications have most of the features in common mentioned below. We will discuss some of them in this section

These features include user registration through SMS verification, user profile, profile related services, real-time tracking, user personal information, limitation factor, availability countrywide, availability internationally, and location provision [15,16,17,18]. Table 1 shows the comparison

of present applications that we surveyed. This provides a bird's eye view on application features. Indicating what they are capable of and whatnot.

As we can see the comparison in the below table, there is no application with all features. Our aim and objective are to not only cover these deficiencies but to develop with more features.

After the survey and research, the architecture of two side applications was selected. The hospital will have its own application while donors will have their own application. This is discussed separately in the subsections below.

3.1. User Side App (Hospital)

Applications first module, which is the main module, is the user's (HOSPITALS) side application. Hospitals will use the app so that the donors have trust and they know they are in safe hands. Any person in need of blood will contact the hospital. The hospital will generate requests on the app [19]. The app will find online donors first. If there are no online users, then it will no offline donors [20]

3.2. Donor side application

The donor side application will allow registering donors. Put their personal information in their accounts. They will be tracked in real-time if they are proceeding to donate or not so that hospital can arrange alternatives.

4. Methodology

The design and methodology section cover system architecture use case diagram and UML diagram. The system architecture comprises of the main architecture in which we have a user application to which other entities are sending and receiving data. It features a firebase cloud messaging, a firebase database, and ASP.net web services [21,22].

Next, a use case diagram shows how actually the architecture is working between the donors and the hospital. It shows both online and offline case. Please refer to Fig. 1 for further understanding.
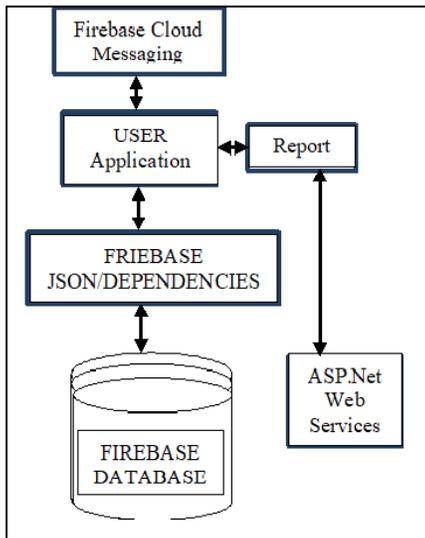

Fig. 1: System Design

The Fig. 2 Use Case Diagram explains the workflow of donors and hospitals. At the donor end, the request is received. The donor can accept or reject the request. On the hospital end, searching for a donor is being done on two occasions. One is when the donor is online. If the donor is online, the request is generated. If the donor is offline, an SMS broadcast is done.
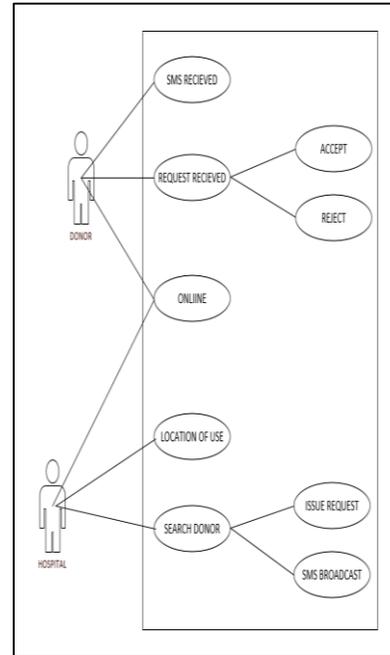

Fig 2: Use Case Diagram

Finally, we have the system UML diagram Fig. 3 which shows the data flow between the classes and entities of the application. Fig. 4 shows donors and their history data flow and Fig. 5 shows the requested functionality that how to request sent from hospital to donor, in this application hospitals register themselves to help patients by providing them donor successfully and save their lives. Many donors donate their blood without any required money they will arrive or reach at hospitals donate blood either match or unmatched group, then hospital blood bank provides blood to patients instead of an unmatched group. By using this application donor are free from any fraud or misuse of blood, the hospital is responsible to manage this type of activity to handle and control.
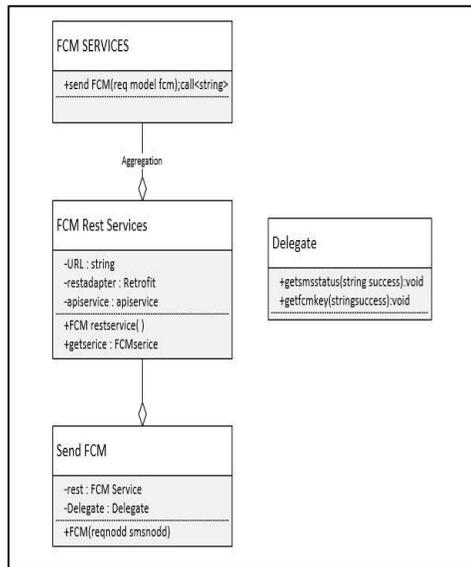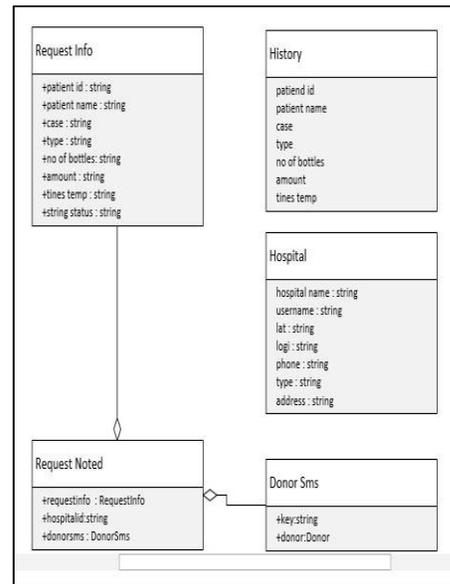
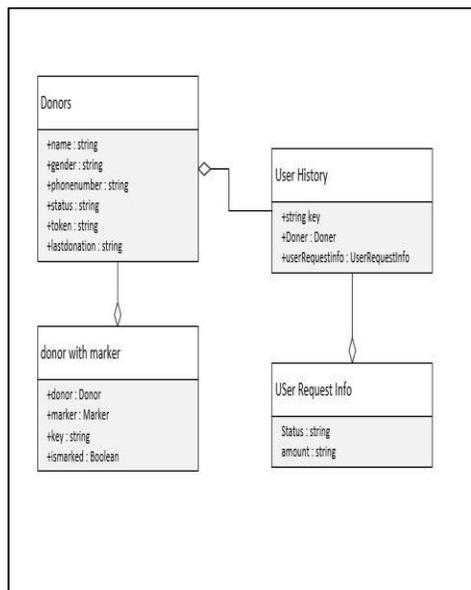Fig 3: UML Diagram

Fig 5: Request Functionality

Fig 4: Donors Data

In Fig. 6 represent the graphical user interface of the hospital where hospital management or hospital blood bank control this application and this application could be registered by multiple hospitals because patients are everywhere and the donor could reach over there in case of emergency, in this regard employee of the hospital do connect patients and donor via this application where patients could get benefit from it.

Fig. 7 about the user interface of the patient where the patient himself or his/her relative or friend can register after registration a unique ID will be generated for the user which will be sent to the donor when request sent from patient/user, in this portal patient must link with the concerned hospital where he/she is admitted because in this application donor will reach a destination which is the hospital,

Fig. 8 define the blood group matching mechanism where donor always confusing about matching that his/her donation goes to

the right patient or submitted in blood bank instead of unmatched blood group, sometimes patient relative don't know that which blood group is required in case of O+ and O- blood group, because these types of blood group are very less in humans and very difficult to get it from friends or family, so in critical conditions, it will help in this blood group matching that who can provide either same or cross blood or replaced from the blood bank. When the donor agreed and accept request from the sender then it can be located that how much far from the hospital, in Fig. 9 focus on donors' availability that how many donors are available nearly or far from the hospital. If a donor is not available, then we had done another solution that it could be found through offline request where the user inputs his cell number but forget to ON mobile data or may not available online then send a message through his cell number when he will online then check his status on google map Fig. 10 that where is he either he will be reach at a hospital within time or not or decline him and find another donor.

Fig.11 shows the request portal which is sent by the patient or from hospital blood bank reception to the donor.

In Fig.12, the complete message sent to the donor where the amount shows that you have requested for the amount and complete data of a patient with hospital name is there, at the end we design a Blood Bank user interface portal which is in Fig. 13. If the patient relative or any friend is not available, the hospital is responsible for this patient, in this case the blood bank send request to donors for donate blood and pay for it. As surveyed in many hospitals we get that many blood banks done earlier if patient is in critical condition after successfully patient is recovered then ADD amount in Patient Bills.
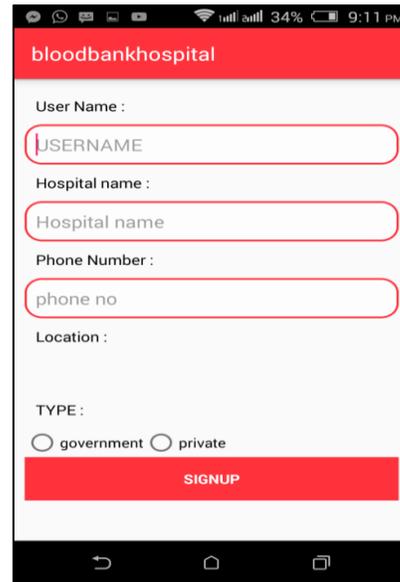

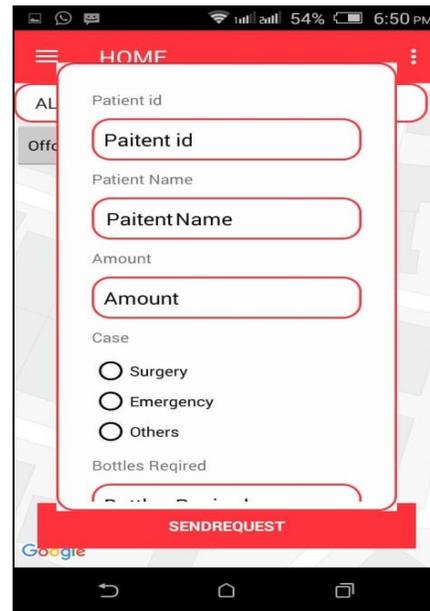Fig. 6. The graphical user interface of Blood Bank of Hospital

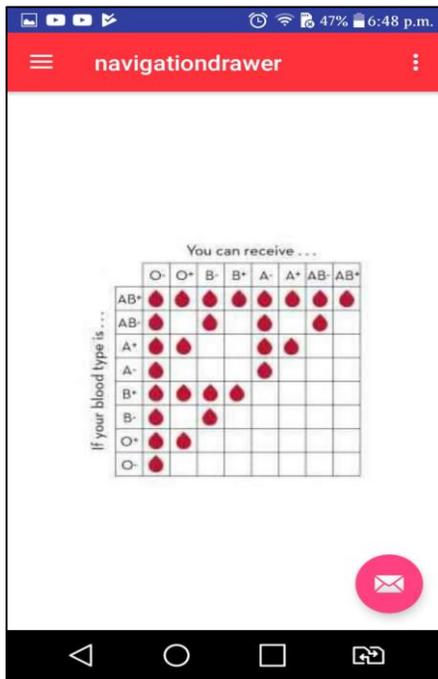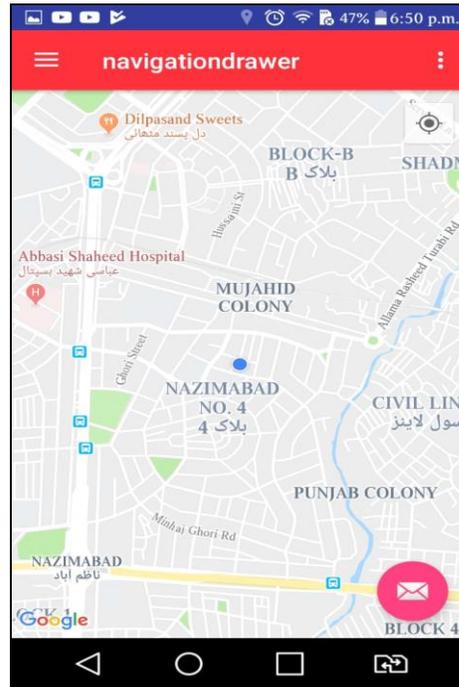Fig 7. The graphical user interface of Patient

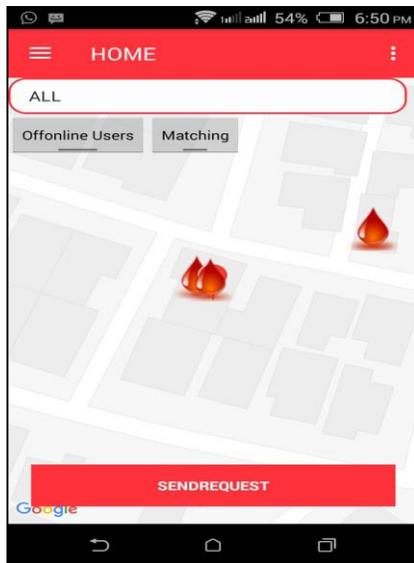Fig 8. Blood Group Matching

Fig 10. Location of Donor
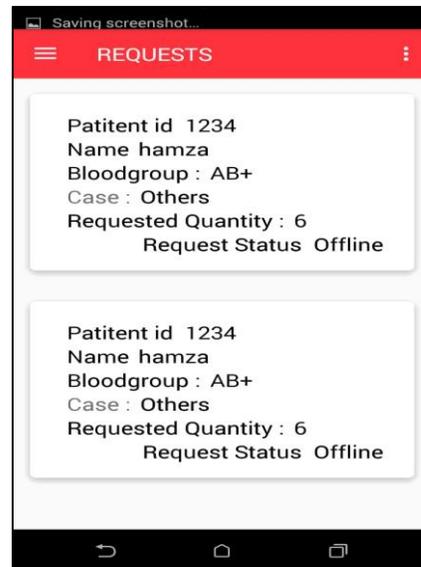

Fig 9. Availability of Donors
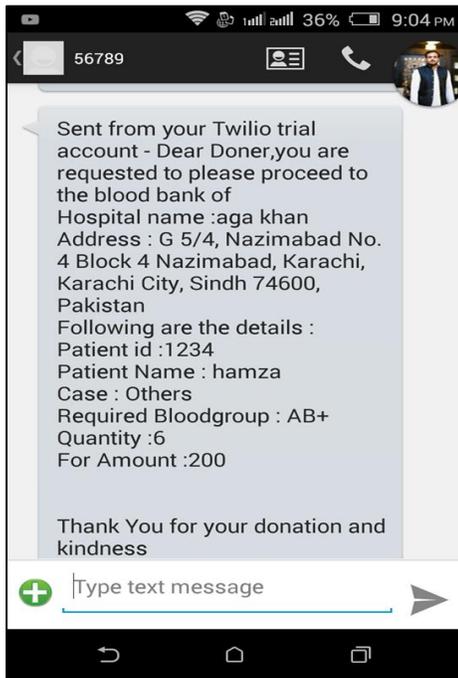
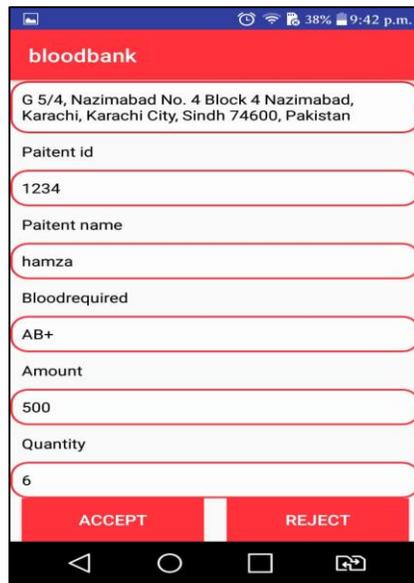

Fig 11. Request Portal

Fig 12. Message sent to the Donor

Fig 13. Blood Bank User Interface

5. Implementation

The implementation of the features is covered in this section of the report. The distinctive features include notification SMS broadcasting, firebase cloud messaging, Google maps for hospital and donor, donor history, dismissal of request, request generation by hospital, User account verification by SMS code. The code sections are written here for an understanding of the functionality of the application.

5.1. Notification SMS Broadcasting

```
[HttpPost]
  public async Task<string> sendsms(smsmodel
                      sms)
{
var data = new historydetails();
string abc = string.Empty
var sid =
"AC08036fa1e7d2e8fdf63e2ad27cd35613";
var token =
"aa68be533a2b6cd8b39da25ada9057b5";
TwilioClient.Init(sid, token);
string addess = string.Empty;
var firebase1 = new
FirebaseClient("https://bloodbank-
fd858.firebaseio.com/Hospital/");
var data1 = await
firebase1.Child(sms.info.hospitalid).OnceSingle
Async<hospital>();
requestinfo req = sms.info;
var firebase2 = new
FirebaseClient("https://bloodbank-
fd858.firebaseio.com/");
var postinfo = await
firebase2.Child("history").PostAsync(sms.info);
string key = postinfo.Key;
var firebase3 = new
FirebaseClient("https://bloodbank-
fd858.firebaseio.com/Hospital/" +
sms.info.hospitalid + "/history");
await firebase3.Child(key).PutAsync("true");
foreach (var i in sms.donerssms)
{
abc = sms.info.No_of_bottels;
var to = new
PhoneNumber(i.doners.phonenumber);
var from = new
PhoneNumber("+16182241163");
var message = MessageResource.Create(
to: to,
```

```
from: from,
body: "Dear Doner,you are requested to please
proceed to the blood bank of \n" +
"Hospital name :" +data1.Hospitalname+ "\n" +
"Address : "+data1.Address+"\n" +
"Following are the details :\n" +
"Patient id :" + sms.info.Patentid + "\n" +
"Patient Name : " + sms.info.Patentname + "\n" +
"Case : " + sms.info.Case + "\n" +
"Required Bloodgroup : " + sms.info.Type + "\n"
+
"Quantity :" + sms.info.No_of_bottels + "\n" +
"For Amount :" + sms.info.Amount + "\n\n\n" +
"Thank You for your donation and kindness"
);
var firebase5 = new
FirebaseClient("https://bloodbank-
fd858.firebaseio.com/history/" + key);
await firebase5.Child(i.key).PutAsync(true);
var firebase4 = new
FirebaseClient("https://bloodbank-
fd858.firebaseio.com/Doners/" + i.key +
"/history");
await firebase4.Child(key).PutAsync(data);
var firebase6 = new
FirebaseClient("https://bloodbank-
fd858.firebaseio.com/history/" + key + "/users/");
await firebase6.Child(i.key).PutAsync(true);
}
return key;
}
```

5.2.   Firebase Cloud Messaging

```
[HttpPost]
    public async Task<string> FCM(smsmodel
sms)
    {

        var data1 = new List<string>();
        foreach (var i in sms.donerssms)
        {

            data1.Add(i.doners.Token);
        }
        var firebase1 = new
FirebaseClient("https://bloodbank-
fd858.firebaseio.com/");
        var postinfo = await
firebase1.Child("history").PostAsync(sms.info);
        string key = postinfo.Key;
        var data = new FCMpayload
        {
            Hospitalid = sms.info.hospitalid,
```

```
            Historyid = key
        };

        using (var sender = new
Sender("AAAA9w1UOgA:APA91bEoW5yV9aj
q8MZVnKiKUNEwpiIsPXeulOtjEch2BkGQBzb
HNBOSlVyxyl7e2_ZuFXYJaSX5DCzo007EsUtI
pjipKv6OlbU3DA6dcbsxy4L3mzobNZp92ivN60
wtGPE48KaXb33S"))
        {
            var message = new Message
            {
                RegistrationIds = data1,
                Data = data,
                Notification = new Notification
                {
                    Title = "REQUEST FOR
BLOOD",
                    Body = "Blood requied" +
sms.info.Type,
                    ClickAction =
"com.example.hamzaa.bloodbank.getinfo",
                    Sound =
"TYPE_NOTIFICATION"
                }
            };
            var result = await
sender.SendAsync(message);
            string response =
result.MessageResponse.Success.ToString();
            if (response == "1")
            {
                var firebase2 = new
FirebaseClient("https://bloodbank-
fd858.firebaseio.com/Hospital/" +
sms.info.hospitalid + "/history");
                await
firebase2.Child(key).PutAsync(true);
                var firebase3 = new
FirebaseClient("https://bloodbank-
fd858.firebaseio.com/Hospital/" +
sms.info.hospitalid + "/ongoingrequest");
                await
firebase3.Child(key).PutAsync(true);
            }

            return key;
        }
    }
    public async Task<string> FCMnear(string
token,string name)
using (var sender = new
Sender("AAAA9w1UOgA:APA91bEoW5yV9aj
```

q8MZVnKiKUNEwpiIsPXeulOtjEch2BkGQBzb
HNBOSlVyxyl7e2_ZuFXYJaSX5DCzo007EsUtI
pjipKv6OlbU3DA6dcbsxy4L3mzobNZp92ivN60
wtGPE48KaXb33S"))

```
    {
      var message = new Message
      {
        RegistrationIds = new
List<string>{token},
        Notification = new Notification
        {
          Title = "REAHCED",
          Body = "DONER
"+name+"REACHED",
          ClickAction =
"com.example.hamzaa.bloodbank.getinfo",
          Sound =
"TYPE_NOTIFICATION"
        }
      };
      var result = await
sender.SendAsync(message);
      string response =
result.MessageResponse.Success.ToString();
      return response;
    }
  }


package com.example.hamzaa.bloodbank.FCM;

import android.app.NotificationManager;
import android.app.PendingIntent;
import android.content.Context;
import android.content.Intent;
import android.graphics.BitmapFactory;
import android.media.RingtoneManager;
import android.net.Uri;
import android.os.Vibrator;
import
android.support.v4.app.NotificationCompat;
import android.util.Log;

import com.example.hamzaa.bloodbank.R;
import
com.example.hamzaa.bloodbank.navigationdraw
er;
import
com.google.firebase.messaging.FirebaseMessagi
ngService;
import
com.google.firebase.messaging.RemoteMessage;

import org.json.JSONException;
```

```
import org.json.JSONObject;
/**
 * Created by hamzaa on 11/25/2018.
 */

public class FcmMessageService extends
FirebaseMessagingService {
  String type="";
  @Override
  public void
onMessageReceived(RemoteMessage
remoteMessage) {
    super.onMessageReceived(remoteMessage);
    type=remoteMessage.getData().toString();
sendNotification(remoteMessage.getNotification(
).getBody(),remoteMessage.getNotification().get
ClickAction(),type);
  }
  private void sendNotification(String s,String
action,String type) {
    String Hospitalid="",Historyid="";
    if(type!=null) {
      try {
        JSONObject jsonObject = new
JSONObject(type);
        Hospitalid =
jsonObject.getString("Hospitalid");
        Historyid =
jsonObject.getString("Historyid");
      } catch (Exception e) {
        e.printStackTrace();
      }
    }
    Intent intent = new Intent(action);
    if(Hospitalid!=""&&Historyid!="") {
      intent.putExtra("Hospitalid", Hospitalid);
      intent.putExtra("Historyid", Historyid);
    }
intent.addFlags(Intent.FLAG_ACTIVITY_CLEA
R_TOP);
    PendingIntent
pendingIntent=PendingIntent.getActivities(this,0,
new
Intent[]{intent},PendingIntent.FLAG_ONE_SH
OT);
    NotificationCompat.Builder builder=new
NotificationCompat.Builder(this);
builder.setContentTitle(getString(R.string.app_na
me));
    builder.setContentText(s);
    Uri sounduri =
RingtoneManager.getDefaultUri(RingtoneManag
er.TYPE_NOTIFICATION);
```

```
      builder.setSound(sounduri);

builder.setSmallIcon(R.mipmap.ic_launcher);
      //
BitmapFactory.decodeResource(this.getResource
s(), R.drawable.logo);
builder.setLargeIcon(BitmapFactory.decodeReso
urce(this.getResources(),R.drawable.ic_launcher_
foreground));
      builder.setAutoCancel(true);
      Vibrator
v=(Vibrator)this.getSystemService(Context.VIB
RATOR_SERVICE);
      v.vibrate(1000);
      builder.setContentIntent(pendingIntent);
      NotificationManager
notificationManager=(NotificationManager)
getSystemService(Context.NOTIFICATION_SE
RVICE);

notificationManager.notify(0,builder.build());
   }
}
```

6. Results and Discussions

The android application developed is aimed to change the way how blood donation is done using the mobile application. This application is the solution to overcome all the difficulties faced by donors or needy people in regard to a mobile application. This will make it easy for collectors and donors since there is a certain level of trust developed by introducing some new and innovative features.

This application serves a good purpose to both the hospitals and donors. Hospitals can manage donors' history, donors' information, track their location in real-time, and generate requests in the form of notifications and SMS. For donors, this application is a factor of authenticity. We have seen that donors certainly not trust needy individuals on the basis that they are strangers and they cannot be trusted. By introducing a hospital-end module donor can trust where they are going to donate and to whom. Similarly, from the point of needy individuals, it provides a guarantee for them if the donors are approaching the hospital or not with the feature of real-time tracking. We also have included a finance factor by the hospital end which is a motivational factor for the donor to really approach to the needy individual

References

[1] Oborne, D.J., Bradley, S., and Lloyd-Griffiths, M., 1978. The anatomy of a volunteer blood donation system. Transfusion, 18(4), pp.458-465.

[2] Wiwanitkit, V., 2000. A study on attitude towards blood donation among people in a rural district, Thailand. Age (years), 11(20), pp.21-30.

[3] Buciuniene, I., Stonienë, L., Blazeviciene, A., Kazlauskaite, R., and Skudiene, V., 2006. Blood donors' motivation and attitude to non-remunerated blood donation in Lithuania. BMC Public Health, 6(1), p.166.

[4] Shenga, N., Pal, R., and Sengupta, S., 2008. Behavior disparities towards blood donation in Sikkim, India. Asian journal of transfusion science, 2(2), p.56.

[5] Oborne, D. J., S. Bradley, and M. Lloyd-Griffiths. "The anatomy of a volunteer blood donation system." Transfusion 18.4 (1978): 458-465.

[6] Sahinyazan, Fevza Güliz, Bahar Y. Kara, and Mehmet Rüstü Taner. "Selective vehicle routing for a mobile blood donation system." European Journal of Operational Research 245.1 (2015): 22-34.

[7] Buciuniene, Ilona, et al. "Blood donors' motivation and attitude to non-remunerated blood donation in Lithuania." BMC Public Health 6.1 (2006): 166.

[8] Shenga, Namgay, Ranabir Pal, and Subhabrata Sengupta. "Behavior disparities towards blood donation in Sikkim, India." Asian journal of transfusion science 2.2 (2008): 56.

[9] Gillespie, Theresa W., and Christopher D. Hillyer. "Blood donors and factors impacting the blood donation decision." Transfusion Medicine Reviews 16.2 (2002): 115-130.

[10] Mostafa, A.M., Youssef, A.E. and Alshorbagy, G., 2014. A framework for a smart social blood donation system based on mobile cloud computing. arXiv preprint arXiv:1412.7276.

[11] Marantidou, O., Loukopoulou, L., Zervou, E., Martinis, G., Egglezou, A., Fountouli, P., Dimoxenous, P., Parara, M., Gavalaki, M. and Maniatis, A., 2007. Factors that motivate and hinder blood donation in Greece. Transfusion Medicine, 17(6), pp.443-450.

[12] Bas, S., Carello, G., Lanzarone, E., Ocak, Z. and Yalçındağ, S. 2016. Management of blood donation system: literature review and research perspectives. In Health Care Systems Engineering for Scientists and Practitioners (pp. 121-132). Springer, Cham.

[13] Buyx, A.M., 2009. Blood donation, payment, and non-cash incentives: classical questions drawing renewed interest. Transfusion Medicine and Hemotherapy, 36(5), pp.329-339.

[14] Alfouzan, N., 2014. Knowledge, attitudes, and motivations towards blood donation among King Abdulaziz Medical City population. International journal of family medicine, 2014.

[15] Papagiannis, D., Rachiotis, G., Symvoulakis, E.K., Anyfantakis, D., Douvlataniotis, K., Zilidis, C., Markaki, A. and Hadjichristodoulou, C., 2016. Blood donation knowledge and attitudes among undergraduate health science students: A cross-sectional study. Transfusion and Apheresis Science, 54(2), pp.303-308.

[16] World Health Organization, 2012. Blood donor selection: guidelines on assessing donor suitability for blood donation. World Health Organization.

[17] Ouhbi, S., Fernández-Alemán, J.L., Toval, A., Idri, A. and Pozo, J.R., 2015. Free blood donation mobile applications. Journal of medical systems, 39(5), p.52.

[18] BalaSenthilMurugan, L. and Julian, A., 2015, March. Design and implementation of Automated Blood Bank using embedded systems. In 2015 International Conference on Innovations in Information, Embedded and Communication Systems (ICIIECS) (pp. 1-6). IEEE.

[19] Adsul, A.C., Bhosale, V.K. and Autee, R.M., 2018, January. Automated blood bank system using Raspberry PI. In 2018 2nd International Conference on Inventive Systems and Control (ICISC) (pp. 252-255). IEEE.

[20] Esmail, M.Y. and Osman, Y.S.H., 2018, August. Computerized Central Blood Bank Management System (CCBBMS). In 2018 International Conference on Computer, Control, Electrical, and Electronics Engineering (ICCCEEE) (pp. 1-5). IEEE.

[21] Cheema, A.S., Srivastava, S., Srivastava, P.K. and Murthy, B.K., 2015, December. A standard compliant blood bank management system with enforcing mechanism. In 2015 International Conference on Computing, Communication and Security (ICCCS) (pp. 1-7). IEEE.

[22] Kumari, D.M.S. and Wijayanayake, A.N., 2016, October. An efficient inventory model to reduce the wastage of blood in the national blood transfusion service. In 2016 Manufacturing & Industrial Engineering Symposium (MIES) (pp. 1-4). IEEE

Static Analysis of Six Bar Tensegrity Ball Structure Robot

Muhammad Basit Chandio[1], Ani Luo[1], Asif Raza[1], Sanaullah Khushak[1],
Muhammad Nazim Lakhan[2], Altaf Hussain Shar[2], Kishore Chand[2], Fahad
Hussain[3], Zubair Ali Shah[4]

Abstract:

All pre-stressed structures called as tensegrity structures have been introducing into robotics, modern architectural designs, and medical necessities called bio-tensegrity, space structure alternates, and many other emerging technologies because of its numerous useful properties. Six bar tensegrity ball robot structure has an essential importance in the field of robotics due to its deployable, movable, deformable, and easily controllable capabilities. This structure has 6 rigid bars (in compression) and 24 flexible strings (in tension) that are connected in such a 12 nodes arrangement that provides the highest spatial symmetrical shape to this structure among most of the tensegrity structure. In this paper, the internal forces of bars and strings on each node have been studied, and the force equation on every node has been developed. Furthermore, the balance of all bars and strings forces on the whole structure has been analytically verified to assure the structure remains statically pre-stressed under the zero net effect of all internal forces applied by bars and strings.

Keywords: *static analysis; force equations; equilibrium*

1. Introduction

Tensegrity structures are formed by a combination of rigid elements (the bars) and elastic elements (the strings) [1-4]. The bars are always in compression and the strings in tension. The entire structure stands by itself and maintains its form solely because of the internal arrangement of the strings and the bars [5-8]. Tensegrity structures were used only in arts and architecture in the early1960s when fuller coined this tensegrity idea [9-12]. Orthopedic surgeon Stephen Levin found a tensegrity structure could be a new biomechanical approach and coined a bio-tensegrity term in the medical field in the 1970s[13], later these structures have been remaining a vital part in medical researches[14-17]. Tensegrity structures are also used in robotics because of implement flexibility, dynamism, and light-weighting

[1]College of Mechanical & Electrical Engineering, Harbin Engineering University, Harbin, China

[2]College of Material Science and Chemical Engineering, Harbin Engineering University, Harbin, China

[3]Department of Mechanical Engineering MUET SZAB Campus Khairpur Mir's, Pakistan

[4]College of Power & Energy Engineering, Harbin Engineering University, Harbin, China

Corresponding Author: basitchandio47@gmail.com

[18-21]. These structures are also used in space applications due to super deplorability [22, 23].

Louani modeled the mathematics of the six-bar tensegrity ball structure robot[24] and analyzed the possible and feasible ways to drive this structure [25-27]. NASA proposed a six-bar tensegrity ball robot structure as workable in landing on different surfaces for planetary exploration missions and easy to move and control the structure [28, 29].

It is vital to recognize the all internal forces exerted by all bars and strings on each node of six-bar tensegrity ball structure robot in a static position in order to move it by servomotors or to land it for planetary exploring mission to protect the payload. Skelton in his book and Julio in his paper have mentioned basic general methods to analyze the static tensegrity structures [30, 31]. But, there is a gap of static analysis of the six-bar tensegrity ball structure robot in research. Here, a static study of the six-bar tensegrity ball structure has been done to analyze the position and forces exerted by all bars and strings on each node and the overall net effect of all internal forces of the structure has been observed to verify the static mode of structure.

In this paper, a six-bar tensegrity ball structure robot has been defined and a node matrix has been developed. Later, Individual force equations for all nodes have been established. In the last, all individual force equations on each node have been examined to validate the static position of the structure by balancing the bars forces and strings forces.

2. Introduction of the Six Bar Tensegrity Ball Robot Structure

Six bar tensegrity ball robot structure has 6 rigid bars in compression and 24 flexible strings in tension. All bars are shown by blue color and strings are shown by red color and

are connected by 12 nodes. Each node is connected with one bar and four strings. In this structure, all six bars are lying along three different planes. Each plane has two parallel bars. Bars b_1 & b_2 lay along *XY* plane, bars b_3 & b_4 lay along *YZ* plane and bars b_5 & b_6 lay along *XZ* plane. Similarly nodes1,2,3 & 4 are in *XY* plane, nodes 5,6,7 & 8 are in *YZ* plane and nodes 9,10,11 & 12 are in *XZ* plane as illustrated in Fig.1.
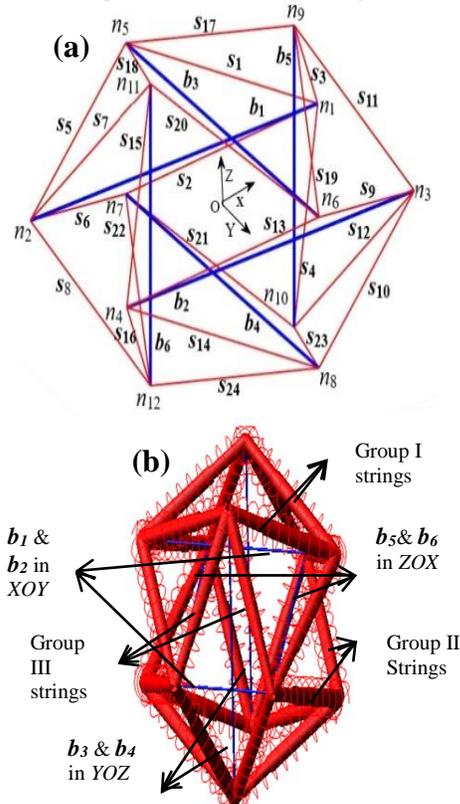

Fig. 1. Six bar tensegrity ball structure robot illustrated (a) in MATLAB & (b) in ADAMS

All members of six-bar tensegrity structure are connected by 12 nodes and a node n_i can be represented in Cartesian coordinates as

$$n_i = \begin{bmatrix} n_{ix} & n_{iy} & n_{iz} \end{bmatrix}, i \in \begin{bmatrix} 1, 12 \end{bmatrix}$$

Node matrix (N) can be obtained by putting all nodes in a column of the matrix.

$$N = \begin{bmatrix} n_1, n_2, n_3 \dots n_{12} \end{bmatrix}_{3 \times 12}$$

Coordinates of all 12 nodes along three axes can be rearranged as displayed in Eq. (1) [24].

$$N = \begin{bmatrix} 0.5L_b & -0.5L_b & 0.5L_b & -0.5L_b & 0 & 0 & 0 & 0 & 0.5L_d & 0.5L_d & -0.5L_d & -0.5L_d \\ 0.5L_d & 0.5L_d & -0.5L_d & -0.5L_d & 0.5L_b & -0.5L_b & 0.5L_b & -0.5L_b & 0 & 0 & 0 & 0 \\ 0 & 0 & 0 & 0 & 0.5L_d & 0.5L_d & -0.5L_d & -0.5L_d & 0.5L_b & -0.5L_b & 0.5L_b & -0.5L_b \end{bmatrix} \in R^{3 \times 12} \quad (1)$$

3. Internal Forces on Structure

Every node of the six-bar tensegrity ball structure is acted by four strings forces and one bar force. We have modeled separate equations of forces for each node in all three axes. Force density in strings is the tension applied string per unit its length (i-e: $\gamma = T_s/L_s$) and force density by the bar is the force applied by bar per unit its length (i-e: $\lambda = F_b/L_b$) [24, 30]. Six bar tensegrity structure is spatial structure and lies along three space axes. Each plane contains four nodes.

3.1. Internal Forces on Nodes laying along *XY* Plane

Plane *XY* contains four nodes 1, 2, 3 & 4. We find the force equations of each node. Here, node 1 is connected with strings *s₁*, *s₂*, *s₃*, *s₄* & bar *b₁* in such an arrangement that strings pull the node inwards and bar pushes it back by the forces *Ts₁*, *Ts₂*, *Ts₃*, *Ts₄* & *Fb₁* respectively, but the node does not move in any direction as shown in Fig.2.
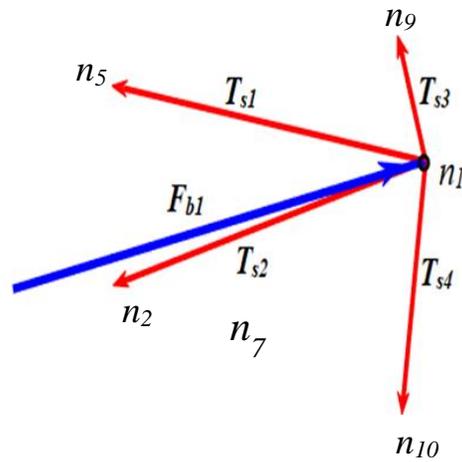
Fig. 2. Forces on node 1

$$F_{b_1} + T_{s_1} + T_{s_2} + T_{s_3} + T_{s_4} = 0 \quad (2)$$

As we already mentioned $\lambda = F_b/L_b$ & $\gamma = T_s/L_s$ in section 3, therefore, by putting substitutes of bar force and all string forces in terms of force densities in eq. (2), we achieve

$$\lambda_1(n_1 - n_2) + \gamma_1(n_5 - n_1) + \gamma_2(n_7 - n_1) + \gamma_3(n_9 - n_1) + \gamma_4(n_{10} - n_1) = 0$$

All bars have the same force density as λ, and all strings have the same force density as γ when no external force acts on the structure.

$$\lambda_1(n_2 - n_1) + \gamma_5(n_5 - n_2) + \gamma_6(n_7 - n_2) + \gamma_7(n_{11} - n_2) + \gamma_8(n_{12} - n_2) = 0$$

$$\lambda \begin{bmatrix} n_{1x} - n_{2x} \\ n_{1y} - n_{2y} \\ n_{1z} - n_{2z} \end{bmatrix} + \gamma \begin{bmatrix} n_{5x} + n_{7x} + n_{9x} + n_{10x} - 4n_{1x} \\ n_{5y} + n_{7y} + n_{9y} + n_{10y} - 4n_{1y} \\ n_{5z} + n_{7z} + n_{9z} + n_{10z} - 4n_{1z} \end{bmatrix} = 0 \qquad (3)$$

We get Eq. (4) by putting coordinates of nodes in Eq. (3)

$$\lambda \begin{bmatrix} 0.5L_b - (-0.5L_b) \\ 0.5L_d - 0.5L_d \\ 0 - 0 \end{bmatrix} + \gamma \begin{bmatrix} 0 + 0 + 0.5L_d + 0.5L_d - 4 \times 0.5L_b \\ 0.5L_b + 0.5L_b + 0 + 0 - 4 \times 0.5L_d \\ 0.5L_d + (-0.5L_d) + 0.5L_b + (-0.5L_b) - 4 \times 0 \end{bmatrix} = 0 \qquad (4)$$

Force equations along the x-axis and y-axis on node 1 are Eq. (5) & Eq. (6) respectively and force equation along the z-axis is zero.

$$\lambda(L_b) + \gamma(L_d - 2L_b) = 0 \quad (5)$$

$$\gamma(L_b - 2L_d) = 0 \qquad (6)$$

Eq. (5) & Eq. (6) are force equations in terms of force densities, bars length, and the perpendicular distance between two parallel bars.

Similarly, we find force equations on node 2. this node is connected with strings s_5, s_6, s_7, s_8 & bar b_1 in such an arrangement that strings pull the node inwards and bar pushes it back by forces T_{s5}, T_{s6}, T_{s7}, T_{s8} & F_{b1}

respectively, but this node does not move in any direction also as illustrated in Fig. 3.
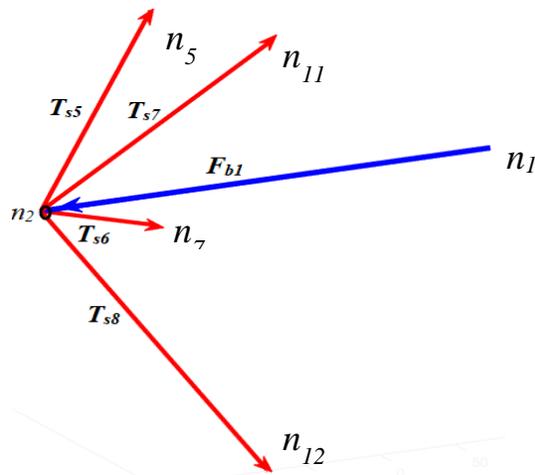

Fig 3. Forces on node 2

$$F_{b_1} + T_{s_5} + T_{s_6} + T_{s_7} + T_{s_8} = 0 \quad (7)$$

Similarly, by putting substitutes of bar force and all string forces in terms of force densities eq. (7), we achieve

$$\lambda_1(n_2 - n_1) + \gamma_5(n_5 - n_2) + \gamma_6(n_7 - n_2) + \gamma_7(n_{11} - n_2) + \gamma_8(n_{12} - n_2) = 0$$

All bars have the same force density as λ, and all strings have the same force density as γ when no external force acts on structure, therefore

$$\lambda(n_2 - n_1) + \gamma(n_5 + n_7 + n_{11} + n_{12} - 4n_2) = 0$$

$$\lambda \begin{bmatrix} n_{2x} - n_{1x} \\ n_{2y} - n_{1y} \\ n_{2z} - n_{1z} \end{bmatrix} + \gamma \begin{bmatrix} n_{5x} + n_{7x} + n_{11x} + n_{12x} - 4n_{2x} \\ n_{5y} + n_{7y} + n_{11y} + n_{12y} - 4n_{2y} \\ n_{5z} + n_{7z} + n_{11z} + n_{12z} - 4n_{2z} \end{bmatrix} = 0 \quad (8)$$

We get Eq. (9) by putting coordinates of nodes in Eq. (8)

$$\lambda \begin{bmatrix} (-0.5L_b) - 0.5L_b \\ 0.5L_d - 0.5L_d \\ 0 - 0 \end{bmatrix} + \gamma \begin{bmatrix} 0 + 0 + (-0.5L_d) + (-0.5L_d) - 4 \times (-0.5L_b) \\ 0.5L_b + 0.5L_b + 0 + 0 - 4 \times 0.5L_d \\ 0.5L_d + (-0.5L_d) + 0.5L_b + (-0.5L_b) - 4 \times 0 \end{bmatrix} = 0 \quad (9)$$

Force equations along the x-axis and y-axis on node 2 are in Eq. (10) & Eq. (11) respectively and force equation along the z-axis is zero

$$\lambda(-L_b) + \gamma(-L_d + 2L_b) = 0 \quad (10)$$

$$\gamma(L_b - 2L_d) = 0 \quad (11)$$

Eq. (10) & Eq. (11) are force equations in terms of force densities, bars length, and the perpendicular distance between two parallel bars. Again, node 3 is connected with strings $s_9, s_{10}, s_{11}, s_{12}$ & bar b_2 in such an arrangement that strings pull the node inwards and bar pushes it back by forces $T_{s9}, T_{s10}, T_{s11}, T_{s12}$ &

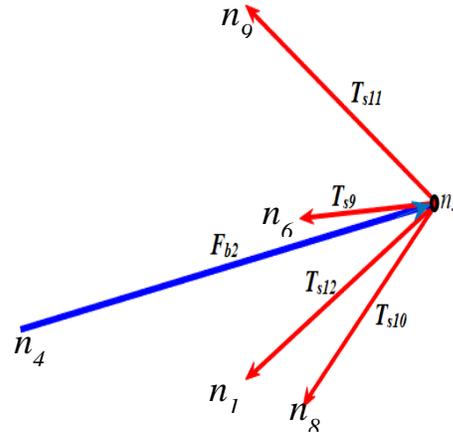F_{b2} respectively, but this node also does not move in any direction as shown in Fig. 4.

Fig. 4. Forces on node 3

$$F_{b_2} + T_{s_9} + T_{s_{10}} + T_{s_{11}} + T_{s_{12}} = 0 \quad (12)$$

Similarly, by putting substitutes of bar force and all string forces in terms of force densities eq. (12), we achieve

$$\lambda_2(n_3 - n_4) + \gamma_9(n_6 - n_3) + \gamma_{10}(n_8 - n_3) + \gamma_{11}(n_9 - n_3) + \gamma_{12}(n_{10} - n_3) = 0$$

All bars have the same force density as λ and all strings have the same force density as γ when no external force acts on structure, therefore

$$\lambda(n_3 - n_4) + \gamma(n_6 + n_8 + n_9 + n_{10} - 4n_3) = 0$$

$$\lambda \begin{bmatrix} n_{3x} - n_{4x} \\ n_{3y} - n_{4y} \\ n_{3z} - n_{4z} \end{bmatrix} + \gamma \begin{bmatrix} n_{6x} + n_{8x} + n_{9x} + n_{10x} - 4n_{3x} \\ n_{6y} + n_{8y} + n_{9y} + n_{10y} - 4n_{3y} \\ n_{6z} + n_{8z} + n_{9z} + n_{10z} - 4n_{3z} \end{bmatrix} = 0 \quad (13)$$

We get Eq. (14) by putting coordinates of nodes in Eq. (13)

$$\lambda \begin{bmatrix} 0.5L_b - (-0.5L_b) \\ -0.5L_d - (-0.5L_d) \\ 0 - 0 \end{bmatrix} + \gamma \begin{bmatrix} 0 + 0 + 0.5L_d + 0.5L_d - 4 \times (0.5L_b) \\ -0.5L_b + (-0.5L_b) + 0 + 0 - 4 \times (-0.5L_d) \\ 0.5L_d + (-0.5L_d) + 0.5L_b + (-0.5L_b) - 4 \times 0 \end{bmatrix} = 0 \quad (14)$$

Force equations along the x-axis and y-axis on node 3 are in Eq. (15) & Eq. (16) respectively and force equation along the z-axis is zero

$$\lambda(L_b) + \gamma(L_d - 2L_b) = 0 \quad (15)$$

$$\gamma(-L_b + 2L_d) = 0 \quad (16)$$

Eq. (15) & Eq. (16) are force equations in terms of force densities, bars length, and the perpendicular distance between two parallel bars.

Likewise, node 4 is connected with strings s_{13}, s_{14}, s_{15}, s_{16} & bar b_2 in such an arrangement that strings pull the node inwards and bar pushes it back by forces T_{s13}, T_{s14}, T_{s15}, T_{s16} & F_{b2} respectively, but the node does not move in any direction as illustrated in Fig. 5.
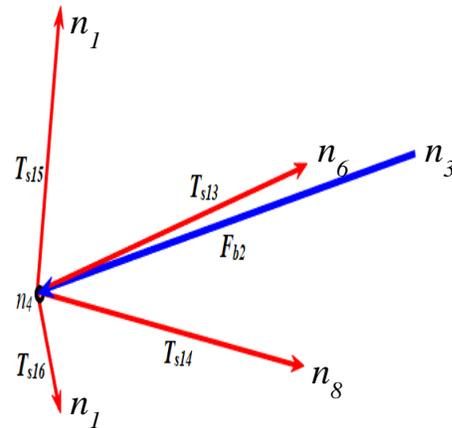

Fig 5. Forces on node 4

$$F_{b_2} + T_{s_{13}} + T_{s_{14}} + T_{s_{15}} + T_{s_{16}} = 0 \quad (17)$$

Similarly, by putting substitutes of bar force and all string forces in terms of force densities eq. (17), we achieve

$$\lambda_2(n_4 - n_3) + \gamma_{13}(n_6 - n_4) + \gamma_{14}(n_8 - n_4) + \gamma_{14}(n_{11} - n_4) + \gamma_{15}(n_{12} - n_4) = 0$$

All bars have the same force density as λ, and all strings have the same force density as γ when no external force acts on structure, therefore

$$\lambda(n_4 - n_3) + \gamma(n_6 + n_8 + n_{11} + n_{12} - 4n_4) = 0$$

$$\lambda \begin{bmatrix} n_{4x} - n_{3x} \\ n_{4y} - n_{3y} \\ n_{4z} - n_{3z} \end{bmatrix} + \gamma \begin{bmatrix} n_{6x} + n_{8x} + n_{11x} + n_{12x} - 4n_{4x} \\ n_{6y} + n_{8y} + n_{11y} + n_{12y} - 4n_{4y} \\ n_{6z} + n_{8z} + n_{11z} + n_{12z} - 4n_{4z} \end{bmatrix} = 0 \quad (18)$$

We get Eq. (19) by putting coordinates of nodes in Eq. (18)

$$\lambda \begin{bmatrix} -0.5L_b - 0.5L_b \\ -0.5L_d - (-0.5L_d) \\ 0 - 0 \end{bmatrix} + \gamma \begin{bmatrix} 0 + 0 - 0.5L_d - 0.5L_d - 4 \times (-0.5L_b) \\ -0.5L_b + (-0.5L_b) + 0 + 0 - 4 \times (-0.5L_d) \\ 0.5L_d + (-0.5L_d) + 0.5L_b + (-0.5L_b) - 4 \times 0 \end{bmatrix} = 0 \quad (19)$$

Force equations along the x-axis and y-axis on node 4 are in Eq. (20) & Eq. (21) respectively and force equation along the z-axis is zero

$$\lambda(-L_b) + \gamma(-L_d + 2L_b) = 0 \quad (20)$$

$$\gamma(-L_b + 2L_d) = 0 \quad (21)$$

Eq. (20) & Eq. (21) are force equations in terms of force densities, bars length, and the perpendicular distance between two parallel bars.

3.2. Internal Forces on Nodes laying along *YZ* Plane

Plane *YZ* also contains four nodes 5, 6, 7 & 8. Here in this section, we just put the force equations on each node lying in the *YZ* plane,

and these equations can be found with the same method used in section 3.1.

Here, node 5 is connected with four strings *s₁, s₅, s₁₇, s₁₈* & one bar *b₃* in such an arrangement that strings pull the node inwards and bar pushes it back by forces *T_{s1}, T_{s5}, Ts17, Ts18* & *F_{b3}* respectively, but the node does not move in any direction as shown in Fig. 6

$$F_{b_3} + T_{s_1} + T_{s_5} + T_{s_{17}} + T_{s_{18}} = 0 \quad (22)$$

We found force equations in terms of force densities, bars length, and the perpendicular distance between two parallel bars along the y-axis and z-axis on node 5 in

Eq. (23) & Eq. (24) respectively and force equation along the x-axis as zero.

$$\lambda(L_b) + \gamma(L_d - 2L_b) = 0 \qquad (23)$$
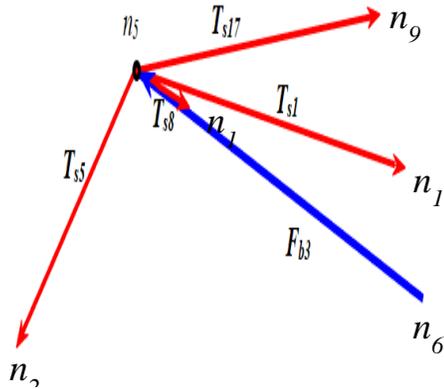
$$\gamma(L_b - 2L_d) = 0 \qquad (24)$$

respectively one node 7 in such manner that this node has no movement in any direction as shown in Fig. 8.

Fig. 6. Forces on node 5
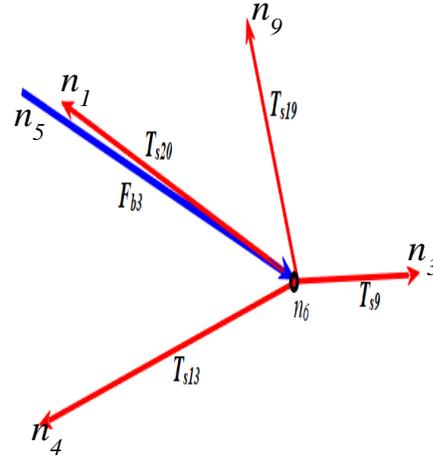

Fig. 7. Forces on node 6

Similarly, T_{s9}, T_{s13}, T_{s19}, T_{s20} & F_{b3} are forces exerted by four strings s_9, s_{13}, s_{19}, s_{20} & one bar b_3 on node 6 in such manner that strings pull the node inwards and bar pushes it back and the node does not move in any direction as shown in Fig. 7.

$$F_{b_3} + T_{s_9} + T_{s_{13}} + T_{s_{19}} + T_{s_{20}} = 0 \qquad (25)$$

We found force equations in terms of force densities, bars length, and the perpendicular distance between two parallel bars along the y-axis and z-axis on node 6 as in Eq. (26) & Eq. (27) respectively and force equation along the x-axis as zero.

$$\lambda(-L_b) + \gamma(-L_d + 2L_b) = 0 \qquad (26)$$

$$\gamma(L_b - 2L_d) = 0 \qquad (27)$$

Four strings s_2, s_6, s_{21}, s_{22} & one bar b_4 exert forces T_{s2}, T_{s6}, T_{s21}, T_{s22} & F_{b4}
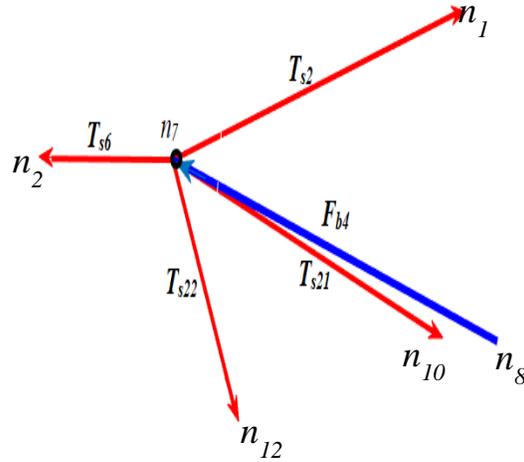

Fig. 8. Forces on node 7

$$F_{b_4} + T_{s_2} + T_{s_6} + T_{s_{21}} + T_{s_{22}} = 0 \qquad (28)$$

We found force equations in terms of force densities, bars length, and the perpendicular distance between two parallel bars along the y-axis and z-axis on node 7 as in Eq. (29) & Eq. (30). Moreover, the force equation along the x-axis is zero.

$$\lambda(L_b) + \gamma(L_d - 2L_b) = 0 \qquad (29)$$

$$\gamma(-L_b + 2L_d) = 0 \qquad (30)$$

Similarly, node 8 is balanced by forces T_{s10}, T_{s14}, T_{s23}, T_{s24} & F_{b4} applied by four strings s_{10}, s_{14}, s_{23}, s_{24} & one bar b_4 as shown in Fig.9.
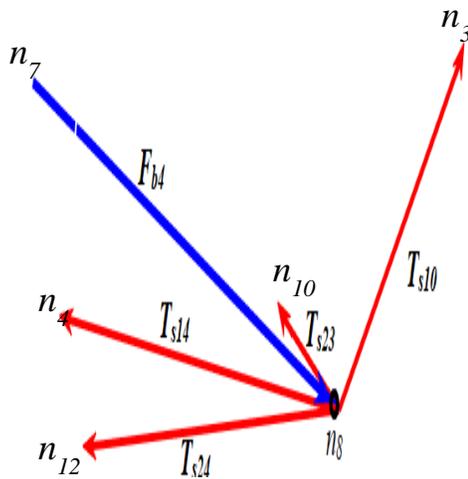

Fig. 9. Forces on node 8

$$F_{b_4} + T_{s_{10}} + T_{s_{14}} + T_{s_{23}} + T_{s_{24}} = 0 \qquad (31)$$

We found force equations in terms of force densities, bars length, and the perpendicular distance between two parallel bars along the y-axis and z-axis on node 8 as in Eq. (32) & Eq. (33) respectively and force equation along the x-axis is zero.

$$\lambda(-L_b) + \gamma(-L_d + 2L_b) = 0 \qquad (32)$$

$$\gamma(-L_b + 2L_d) = 0 \qquad (33)$$

3.3. Internal Forces on Nodes laying along *XZ* Plane

Plane *XZ* also contains four nodes 9, 10, 11 & 12. Here in this section, we just put the force equations on each node lying in the *XZ* plane, and these equations can be found with the same method used in section 3.1.

So, node 9 is connected with four strings s_{10}, s_{14}, s_{23}, s_{24} & one bar b_5 in such an arrangement that strings pull the node inwards and bar pushes it back by the forces T_{s10}, T_{s14}, T_{s23}, T_{s24} & F_{b5} respectively but node remains in the same position as shown in Fig.10.
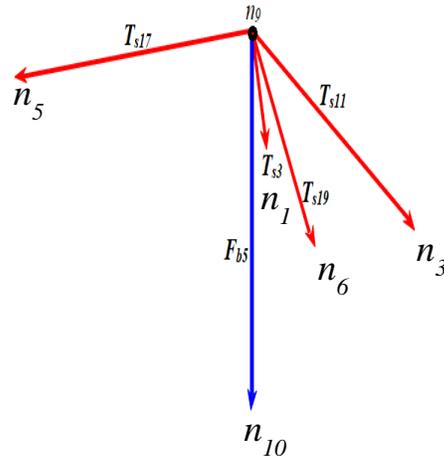

Fig 10. Forces on node 9

$$F_{b_5} + T_{s_3} + T_{s_{11}} + T_{s_{17}} + T_{s_{19}} = 0 \qquad (34)$$

We found force equations in terms of force densities, bars length, and the perpendicular distance between two parallel bars along the x-axis and z-axis on node 9 as

in Eq. (35) & Eq. (36) respectively and force equation along the y-axis as zero.

$$\gamma(L_b - 2L_d) = 0 \qquad (35)$$

$$\lambda(L_b) + \gamma(L_d - 2L_b) = 0 \qquad (36)$$

Similarly, four strings s_4, s_{12}, s_{21}, s_{23}, & one bar b_5 apply forces T_{s4}, T_{s12}, T_{s21}, T_{s23} & F_{b5} respectively on node 10 in such manner that node does not move in any direction as shown in Fig. 11.
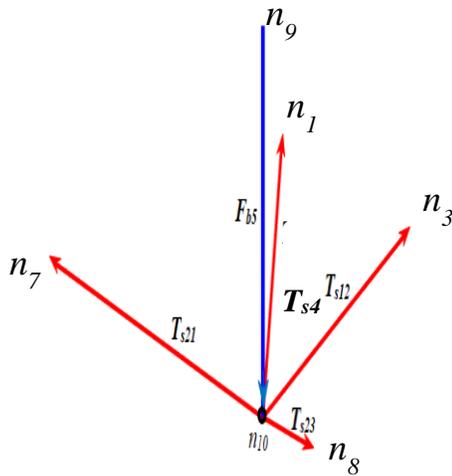

Fig. 11. Forces on node 10

$$F_{b_5} + T_{s_4} + T_{s_{12}} + T_{s_{21}} + T_{s_{23}} = 0 \qquad (37)$$

We found force equations in terms of force densities, bars length, and the perpendicular distance between two parallel bars along the x-axis and z-axis on node 10 as in Eq. (38) & Eq. (39) respectively and force equation along the y-axis as zero.

$$\gamma(L_b - 2L_d) = 0 \qquad (38)$$

$$\lambda(-L_b) + \gamma(-L_d + 2L_b) = 0 \qquad (39)$$

Node 11 is connected with strings s_7, s_{15}, s_{18}, s_{20}, & b_6 in such an arrangement that strings pull the node inwards and bar pushes it back T_{s7}, T_{s15}, T_{s18}, T_{s20} & F_{b6} respectively, but the node does not move in any direction as illustrated in Fig.12.
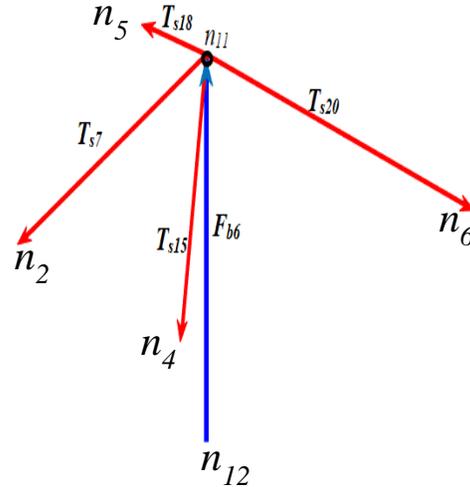

Fig. 12. Forces on node 11

$$F_{b_6} + T_{s_7} + T_{s_{15}} + T_{s_{18}} + T_{s_{20}} = 0 \qquad (40)$$

We found force equations in terms of force densities, bars length, and the perpendicular distance between two parallel bars along the x-axis and z-axis on node 11 as in Eq. (41) & Eq. (42) respectively and force equation along the y-axis as zero.

$$\gamma(-L_b + 2L_d) = 0 \qquad (41)$$

$$\lambda(L_b) + \gamma(L_d - 2L_b) = 0 \qquad (42)$$

Finally, node 12 is pulled by forces T_{s8}, T_{s16}, T_{s22}, T_{s24} applied by four strings s_8, s_{16}, s_{22}, s_{24}, and pushed back by force F_{b6} applied

by bar b_6, but the node does not experience any movement in any direction as shown in Fig.13.
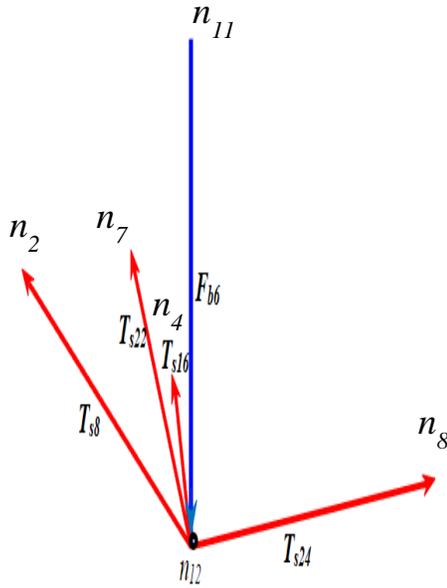

Fig. 13. Forces on node 12

$$F_{b_6} + T_{s_8} + T_{s_{16}} + T_{s_{22}} + T_{s_{24}} = 0 \qquad (43)$$

We found force equations in terms of force densities, bars length, and the perpendicular distance between two parallel bars along the x-axis and z-axis on node 12, as in Eq. (44) & Eq. (45) respectively and force equation along the y-axis as zero.

$$\gamma(-L_b + 2L_d) = 0 \qquad (44)$$

$$\lambda(-L_b) + \gamma(-L_d + 2L_b) = 0 \qquad (45)$$

3.4. Internal force on the whole structure

We have found force equations of all 12 nodes along three axes individually. Here, we add all these force equations to analyze overall force along each axis on the whole structure. We got net force as zero by adding all force components along the x-axis of all nodes as follows:

$$\lambda(L_b) + \gamma(L_d - 2L_b) + \lambda(-L_b) + \gamma(-L_d + 2L_b) + \lambda(L_b) + \gamma(L_d - 2L_b) + \lambda(-L_b) \\ + \gamma(-L_d + 2L_b) + \gamma(L_b - 2L_d) + \gamma(L_b - 2L_d) + \gamma(-L_b + 2L_d) + \gamma(-L_b + 2L_d) = 0 \qquad (46)$$

Similarly, we get net force as zero by adding all force components along the y-axis of all nodes as follows

$$\gamma(L_b - 2L_d) + \gamma(L_b - 2L_d) + \gamma(-L_b + 2L_d) + \gamma(-L_b + 2L_d) + \lambda(L_b) + \gamma(L_d - 2L_b) + \\ \lambda(-L_b) + \gamma(-L_d + 2L_b) + \lambda(L_b) + \gamma(L_d - 2L_b) + \lambda(-L_b) + \gamma(-L_d + 2L_b) = 0 \qquad (47)$$

Again, we get net force as zero by adding all force components along the z-axis of all nodes as follows

$$\gamma(L_b - 2L_d) + \gamma(L_b - 2L_d) + \gamma(-L_b + 2L_d) + \gamma(-L_b + 2L_d) + \lambda(L_b) + \gamma(L_d - 2L_b) +$$
$$\lambda(-L_b) + \gamma(-L_d + 2L_b) + \lambda(L_b) + \gamma(L_d - 2L_b) + \lambda(-L_b) + \gamma(-L_d + 2L_b) = 0 \tag{48}$$

It can be analyzed by the above calculations that all internal forces exerted by rigid bars and flexible strings acting on the whole structure have no net effect along any axis, which results in the structure to remain in equilibrium, this null result of all internal forces of members on whole structure shows the all force equations developed for each node are valid.

4. Conclusion

We defined the structure of the six-bar tensegrity ball structure robot and developed its nodes matrix. Force equations for each node were developed individually. The overall net effect of forces applied by strings and bars of the structure was investigated, and it was observed that forces applied by all strings and bars on the whole structure balance each node and form a whole spatial balanced structure.

NOMENCLATURE

L_b Length of each bar

L_d Distance between each couple of parallel bars

F_b internal force of bars

T_s Internal force of strings

λ Bar force density

γ String force density in group I strings after

References

[1] J. Yin, J. Duffy, and R. Crane ," An analysis for the design of self-deployable tensegrity and reinforced tensegrity prisms with elastic ties". 2002. 17(1): p. 38-45.

[2] Fuller R B, Tensile integrity structures, U.S.P. Office, Editor. 1959: United States.

[3] Otto F, Tensile structures. 1967, Cambridge: MIT Press.

[4] Fuller R B and Applewhite E J, Synergetics : explorations in the geometry of thinking. 1975, New York: Macmillan.

[5] R. Tobie, Pratt Institute, NY, A report on an inquiry into the existence, formation and representation of tensile structures. 1976.

[6] R. Motro, Tensegrity : from Art to Structural Engineering. 2011.

[7] Sultan C, Chapter 2 Tensegrity: 60 Years of Art, Science, and Engineering, in Advances in Applied Mechanics. 2009, Elsevier. p. 69-145.

[8] J. Cai and J. Feng, Form-finding of tensegrity structures using an optimization method. Engineering Structures, 2015. 104: p. 126-132.

[9] B. Fuller, "Tensegrity" Portfolio Art News Annual. 1961. 4: p. 112-127.

[10] K. Snelson, Continuous tension, discontinuous compression structures, U.S.P. 611, Editor. 1965: U.S.A.

[11] K.Snelson, " Kenneth Snelson, Art and Ideas." Kenneth Snelson, Marlborough Gallery, ,New York. 2013.

[12] C.R. Calladine, Buckminster Fuller's "Tensegrity" structures and Clerk Maxwell's rules for the construction of stiff frames. International Journal of Solids and Structures, 1978. 14(2): p. 161-172.

[13] D.S. Levin, http://biotensegrity.com

[14] G. Scarr, Biotensegrity. 2014: Handspring Publishing, United Kingdom.

[15] S. Levin, "The tensegrity-truss as a model for spine mechanics: biotensegrity". Journal of

mechanics in medicine biology, 2002. 2(03n04): p. 375-388.

[16] R. Noguera, O.A. Nieto, and I. Tadeo, Extracellular matrix, biotensegrity and tumor microenvironment. An update and overview. 2012.

[17] Scarr. G, Biotensegrity: What is the big deal? Journal of Bodywork and Movement Therapies, 2020. 24(1): p. 134-137.

[18] S.H. Juan, and R.E. Skelton. "Dynamically stable collision avoidance for tensegrity based robots". in 2009 ASME/IFToMM International Conference on Reconfigurable Mechanisms and Robots. 2009. IEEE.

[19] M. Azadi, S. Behzadipour, and M. Faulkner, "Variable Stiffness Spring Using Tensegrity Prisms". 2010. 2(4): p. 041001.

[20] Y. Sugiyama and R. Hirai," Crawling and jumping by a deformable robot". 2006. 25(5-6): p. 603-620.

[21] K. Kim , A.K. Agogino and A.M. Agogino, Rolling Locomotion of Cable-Driven Soft Spherical Tensegrity Robots. Soft Robotics, 2020.

[22] Tibert G, "Deployable tensegrity structures for space applications", in Department of Mechanics. 2002, KTH Royal Institute of Technology: Sockholm, Sweden.

[23] K.Garanger, R. Miriam ,K.Matthew, Soft Tensegrity Systems for Planetary Landing and Exploration. arXiv preprint:2003.10999, 2020.

[24] A. Luo, R. E. Skelton and H. Liu. "Structure of the ball tensegrity robot." in 2014 IEEE International Conference on Robotics and Biomimetics (ROBIO 2014). 2014. IEEE.

[25] A. Luo and H. Liu, "Analysis for Feasibility of the Method for Bars Driving the Ball Tensegrity Robot". Journal of Mechanisms and Robotics, 2017. 9(5): p. 051010-051010-6.

[26] A. Luo, H. Liu and Y. Liu. "Analyzing the driving method for the ball tensegrity robot". in 2016 IEEE International Conference on Robotics and Biomimetics (ROBIO). 2016.

[27] A. Luo, H. Xin, P. Cao, "Motion simulation of six-bar tensegrity robot based on adams. in 2016" IEEE International Conference on Mechatronics and Automation. 2016. IEEE.

[28] SunSpiral V, George G, Bruce J , "Tensegrity based probes for planetary exploration: Entry, descent and landing (EDL) and surface mobility analysis". International Journal of Planetary Probes, 2013. 7: p. 13.

[29] Vespignani M, and Friesen J," Design of SUPERball v2, a Compliant Tensegrity Robot for Absorbing Large Impacts". 2018 Ieee/Rsj International Conference on Intelligent Robots and Systems, ed. A.A. Maciejewski, et al. 2018, New York: IEEE. 2865-2871.

[30] R.E. Skelton and M.C. de Oliveira, Tensegrity systems. Vol. 1. 2009: Springer.

[31] C.D.Crane , J. Duffy, and J.C. Correa, Static Analysis of Tensegrity Structures. Journal of Mechanical Design, 2005. 127(2): p. 257-268.

0.7''   Margin Top

Paper Formatting Guidelines

Title: 14pts Bold

Author Name: 11pts Bold

Affiliation: 11pts Italic

Abstract: Single Paragraph (Min: 150 – Max: 250 words)

Paper Length: Formatted as guided (Min: 4,000 – Max: 8,000 words)

Font: Times New Roman 10pts

Font Color: Black

Line Spacing: 1.0 (single line space throughout the paper)

Indentation: Justify

References & In-text Citations: Follow the IEEE & Use EndNote X7 for In-text citations and Bibliography.

Headings: 12pts Bold

1. **12pts Bold**
   1.1. **11pts Bold**
      1.1.1.   ***11pts Bold Italic***

Margin Left
0.8''

Margin Right
0.5''

6.5''x10''

Page Size: 6.5'' (Width) x 10'' (Height)

Submission: Formatted paper as guided can be submitted through our online submission system at http://sjet.iba-suk.edu.pk

1.9''   **Margin Bottom**

Sukkur IBA
Journal of
Emerging Technologies

SUKKUR IBA UNIVERSITY
Merit - Quality - Excellence